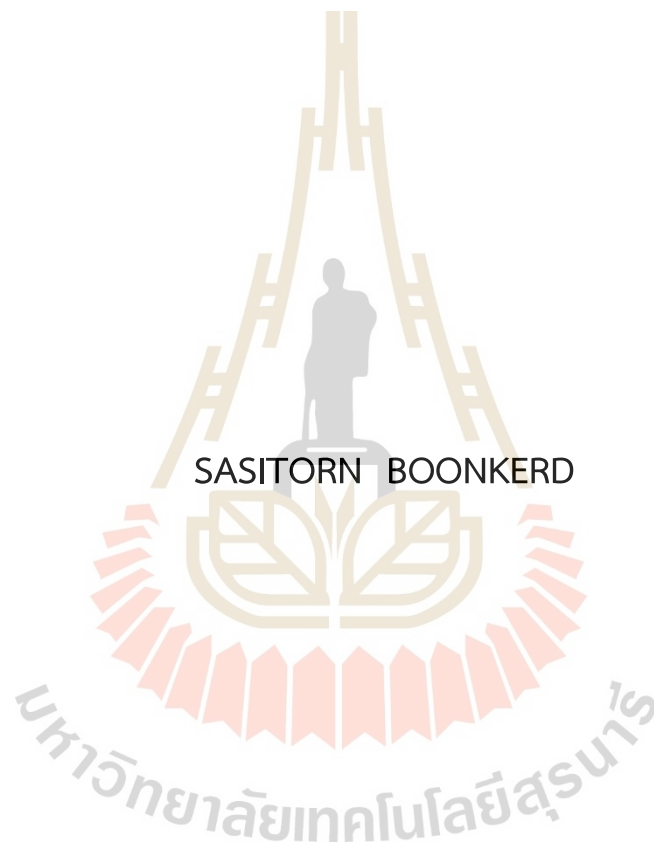


PAPAIN ENCAPSULATION WITHIN STARCH BY ANTI-SOLVENT
PRECIPITATION



A Thesis Submitted in Partial Fulfillment of the Requirements for the
Degree of Master of Engineering in Mechanical and Process System Engineering
Suranaree University of Technology
Academic Year 2023

การห่อหุ้มปาเปนด้วยแป้งโดยใช้วิธีการตกตะกอนด้วยตัวต้านการละลาย



นางสาวศศิธร บุญเกิด

วิทยานิพนธ์นี้เป็นส่วนหนึ่งของการศึกษาตามหลักสูตรปริญญาวิศวกรรมศาสตรมหาบัณฑิต
สาขาวิชาวิศวกรรมเครื่องกลและระบบกระบวนการ
มหาวิทยาลัยเทคโนโลยีสุรนารี
ปีการศึกษา 2566

PAPAIN ENCAPSULATION WITHIN STARCH BY ANTI-SOLVENT
PRECIPITATION

Suranaree University of Technology has approved this thesis submitted in partial fulfillment of the requirements for a Master's degree.

Thesis Examining Committee

Nikom Klomkliang

(Assoc. Prof. Dr. Nikom Klomkliang)
Chairperson

Lek Wantha

(Assoc. Prof. Dr. Lek Wantha)
Member (Thesis Advisor)

Adrian Flood

(Professor Dr. Adrian Flood)
Member

Atthaphon Maneedaeng

(Asst. Prof. Dr. Atthaphon Maneedaeng)
Member

Yupaporn Ruksakulpiwat

(Assoc. Prof. Dr. Yupaporn Ruksakulpiwat)
Vice Rector for Academic Affairs and
Quality Assurance

Pornsiri Jongkol

(Assoc. Prof. Dr. Pornsiri Jongkol)
Dean of Institute of Engineering

ศศิธร บุญเกิด: การห่อหุ้มปาเปนด้วยแป้งโดยใช้วิธีการตกตะกอนด้วยตัวทำละลาย
(PAPAIN ENCAPSULATION WITHIN STARCH BY ANTI-SOLVENT PRECIPITATION)
อาจารย์ที่ปรึกษา: รองศาสตราจารย์ ดร. เล็ก วันทา, 141 หน้า.

คำสำคัญ: เอนไซม์ปาเปน/การห่อหุ้ม/การตกตะกอนด้วยตัวทำละลาย

ปัจจุบันมีการใช้ปาเปนในหลากหลายอุตสาหกรรม อย่างไรก็ตาม ปาเปนมีความไวและเสถียรภาพต่ำในสภาวะแวดล้อมที่ไม่พึงประสงค์ ดังนั้นจึงจำเป็นต้องห่อหุ้มปาเปนด้วยวัสดุเคลือบเพื่อปกป้องมันจากสภาวะที่ไม่พึงประสงค์และเพื่อเพิ่มความเสถียร ในงานวิจัยนี้เลือกใช้วัสดุเคลือบเป็นไบโอโพลีเมอร์คือแป้งดัดแปลงที่มีชื่อว่า “แป้งมันสำปะหลังแอซิติลเลต (Acetylated cassava starch: ACS)” ซึ่งมีค่าระดับการแทนที่ (Degree of Substitution: DS) เท่ากับ 0.037 ซึ่งเป็นค่าที่โรงงานส่วนใหญ่ในประเทศไทยสามารถผลิตได้ สำหรับกระบวนการห่อหุ้มใช้วิธีการตกตะกอนด้วยตัวทำละลายแบบขั้นตอน (Stepwise anti-solvent precipitation method) โดยปาเปนจะตกตะกอนก่อนแล้วจึงถูกห่อหุ้มด้วยแป้ง การศึกษานี้มีเป้าหมายเพื่อหาสภาวะที่เหมาะสมโดยการตรวจสอบผลของประเภทของตัวทำละลาย ความเข้มข้นของปาเปน และอัตราส่วนปริมาตรของตัวทำละลายต่อตัวทำละลายสำหรับกระบวนการตกตะกอนของปาเปน นอกจากนี้ยังตรวจสอบผลของความเข้มข้นของแป้ง ปริมาตรของสารละลายแป้ง และประเภทและความเข้มข้นของสารลดแรงตึงผิวสำหรับกระบวนการห่อหุ้มปาเปน

จากการศึกษาการตกตะกอนปาเปนเพื่อสร้างอนุภาคนาโนของปาเปน พบว่าเอทานอลเป็นตัวทำละลายที่เหมาะสมที่สุดสำหรับการเตรียมอนุภาคนาโนของปาเปน เนื่องจากเอทานอลส่งผลต่อกิจกรรมของปาเปนน้อยที่สุด นอกจากนี้ยังทำให้เกิดตะกอนเหนียวของปาเปนเกิดขึ้นน้อยกว่าอะซิโตนและอะซิโตนไตรัล สำหรับผลของอัตราส่วนตัวทำละลายต่อตัวทำละลายและความเข้มข้นของปาเปน พบว่าอัตราส่วนตัวทำละลายต่อตัวทำละลายมีผลต่อขนาดของอนุภาค การกระจายขนาด ศักยภาพของซีตา และผลได้การตกตะกอน ซึ่งสภาวะที่เหมาะสมและเพียงพอต่อการสร้างอนุภาคนาโนโดยไม่จำเป็นต้องใช้ตัวทำละลายที่มากเกินไปอยู่ที่ 1:4 เนื่องจากสภาวะนี้ให้อนุภาคที่มีขนาดเล็กที่สุดและการกระจายขนาดแคบที่สุด อีกทั้งอนุภาคที่ได้อังมีความเสถียรที่ดีอีกด้วย และความเข้มข้นของปาเปนส่งผลต่อขนาดของอนุภาคและศักยภาพของซีตา ในขณะที่ส่งผลต่อผลได้เฉพาะในช่วงความเข้มข้นต่ำคือ 10 ถึง 15 mg/ml แต่ไม่ส่งผลต่อการกระจายขนาดของอนุภาค สภาวะที่เหมาะสมที่สุดที่ได้จากงานวิจัยนี้อยู่ที่ 30 mg/ml เนื่องจากเป็นสภาวะที่ให้อนุภาคมีความเสถียรที่สุดและยังคงสามารถกักกิจกรรมไว้ได้ 100% ดังนั้น ณ จุดที่กล่าวไปนี้ให้อนุภาคปาเปนที่มีขนาด 207.6 nm และการกระจายขนาดที่แคบ ผลได้การตกตะกอนอยู่ที่ 80.89% ซึ่งเพียงพอต่อการสร้างอนุภาคนาโนของปาเปนที่เสถียรและยังคงกักกิจกรรมไว้ได้ ในขณะที่ถ้าหากนำไปใช้งานต่อในกระบวนการห่อหุ้มโดยวิธีการตกตะกอนด้วยตัวทำละลายแบบขั้นตอนแล้วนั้น การเพิ่มปริมาตรของเอทานอลเป็น 1:8 จะทำให้ตะกอนมีความเสถียรและมีตะกอนขนาดเล็กมากขึ้น

รวมทั้งลดการเกาะตัวกันของอนุภาคได้ดีขึ้น บ่งบอกว่าตะกอนมีความเสถียรและเหมาะสมสำหรับการห่อหุ้มด้วยแป้ง ดังนั้นในการทดลองการห่อหุ้มได้เลือกใช้ความเข้มข้นของสารละลายปาเปนที่ 30 mg/ml และอัตราส่วนปริมาตรของตัวทำละลายต่อตัวต้านการละลายที่ 1:8 ในการตกตะกอนปาเปนในขั้นต้นแรก

จากการศึกษาการห่อหุ้มตะกอนปาเปนด้วยแป้งเพื่อสร้างคอมโพสิตของปาเปนและแป้ง (ACS/Papain composites) พบว่าความเข้มข้นของแป้งที่สูงขึ้นโดยทั่วไปจะช่วยปรับปรุงประสิทธิภาพการห่อหุ้มและความสามารถในการบรรจุ แต่ความเข้มข้นที่มากเกินไปจะทำให้ประสิทธิภาพลดลงเนื่องจากการจับตัวของแป้ง ในขณะที่ปริมาตรของสารละลายแป้งมีผลต่อความสามารถในการบรรจุ การใช้สารลดแรงตึงผิวช่วยกระจายอนุภาคเพื่อป้องกันการเกาะตัวกันระหว่างการห่อหุ้ม แต่ความเข้มข้นของสารลดแรงตึงผิวที่สูงขึ้น โดยเฉพาะ Tween 80 ช่วยปรับปรุงประสิทธิภาพการห่อหุ้มและความสามารถในการบรรจุ แต่ลดกิจกรรมของปาเปน สภาวะที่เหมาะสมที่สุดที่ได้จากงานวิจัยนี้คือความเข้มข้นของแป้ง 30 mg/ml ปริมาตรแป้ง 7 ml และความเข้มข้นของ Tween 80 ที่ 3% v/v ให้ประสิทธิภาพการห่อหุ้มที่ 96.23% และความสามารถในการบรรจุที่ 12.40% อย่างไรก็ตามภายใต้เงื่อนไขเหล่านี้กิจกรรมของปาเปนลดลงเหลือประมาณ 56% ในขณะที่ Tween 20 ที่ความเข้มข้น 1%v/v สามารถคงกิจกรรมของปาเปนได้สูงกว่า (ประมาณ 87%) แต่ให้ประสิทธิภาพการห่อหุ้มและความสามารถในการบรรจุเพียง 69.87% และ 9.32% ตามลำดับ การวิเคราะห์ยืนยันด้วยสเปกตรัมฟลูออเรสเซนส์และ FTIR ยืนยันได้ว่าปาเปนถูกห่อหุ้มภายในแป้งแอสซิทิลเลตที่มีค่าดีกรีของการแทนที่ต่ำได้

สาขาวิชา วิศวกรรมเคมี
ปีการศึกษา 2566

ลายชื่อนักศึกษา พิศิธร
ลายชื่ออาจารย์ที่ปรึกษา อ. อ.
.....

SASITORN BOONKRD: PAPAINE ENCAPSULATION WITHIN STARCH BY ANTI-SOLVENT PRECIPITATION

THESIS ADVISOR: ASSOC. PROF. LEK WANTHA, Ph.D., 141 PP.

Keyword: PAPAINE/ENCAPSULATION/ANTI-SOLVENT PRECIPITATION


Currently, papain is utilized across a wide range of industries. However, it is sensitive and destabilizes in adverse environmental conditions. Therefore, it is necessary to encapsulate papain with a coating material to protect it from these harsh conditions and improve its stability. In this research, acetylated cassava starch (ACS), a biopolymer, was chosen as the coating material. Acetylated cassava starch with Degree of Substitution (DS) of 0.037 was used, a value that is commonly produced by factories in Thailand. For the encapsulation process, a stepwise anti-solvent precipitation method was employed, where papain was first precipitated and then encapsulated with the starch. The study aims to determine the optimal conditions by investigating the effects of the type of anti-solvent, papain concentration, and solvent to anti-solvent volume ratios on the papain precipitation process. Additionally, it examines the impact of starch concentration, volume of the starch solution, and the type and concentration of surfactant on the papain encapsulation process.

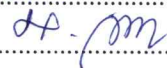
From the investigation of the precipitation of papain to create nanoparticles, the results showed that ethanol was the most suitable anti-solvent for preparing papain nanoparticles. Ethanol had the least impact on papain activity and produced fewer sticky precipitates compared to acetone and acetonitrile (ACN). Regarding the effects of solvent-to-anti-solvent volume ratios and papain concentration, it was observed that these ratios influenced particle size, size distribution, zeta potential, and precipitation yield. An optimal solvent-to-anti-solvent ratio of 1:4 was sufficient for nanoparticle formation without excessive use of anti-solvent and can produce particles with the smallest average size and narrowest size distribution. Moreover, the resulting particles have good stability. Papain concentration affected particle size and zeta potential, with a significant impact on yield only at low concentrations (10 to 15 mg/ml) but did not affect size distribution. The ideal concentration was found to be 30 mg/ml, which produced the most stable particles while retaining 100% activity. Under these conditions, the papain nanoparticles had an average size of 207.6 nm and a narrow size distribution, with a precipitation yield of 80.89%, ensuring stable and active

nanoparticles. For further encapsulation using the stepwise anti-solvent precipitation method, increasing the ethanol volume ratio to 1:8 produced smaller size, more stable precipitates with reduced aggregation, indicating suitability for encapsulation with starch. Thus, for encapsulation experiments, a papain solution concentration of 30 mg/ml and a solvent-to-anti-solvent volume ratio of 1:8 were selected for the initial precipitation step.

In the encapsulation study of papain precipitates with starch to create ACS/Papain composites, higher starch concentrations generally improved encapsulation efficiency and loading capacity, but excessive concentrations led to decrease performance due to starch aggregation, while starch solution volume primarily influenced loading capacity. Employing surfactants aided in dispersing particles to prevent aggregation during encapsulation. However, higher surfactant concentrations, particularly Tween 80, improved encapsulation efficiency and loading capacity but reduced papain activity. The optimal conditions achieved were a starch concentration of 30 mg/ml, a starch volume of 7 ml, and a 3% v/v Tween 80 concentration, yielding an encapsulation efficiency of 96.23% and a loading capacity of 12.40%. However, residual papain activity under these conditions dropped to approximately 56%. In contrast, Tween 20 at 1% v/v preserved higher papain activity (~87%), although it yielded a lower encapsulation efficiency of 69.87% and loading capacity of 9.32%. Confirmatory analyses via fluorescent spectra and FTIR confirmed successful papain entrapment within acetylated starch with a lower degree of substitution.

School of Chemical Engineering
Academic Year 2023

Student's Signature 

Advisor's Signature 

ACKNOWLEDGEMENT

This thesis was successfully completed with invaluable support and assistance from many individuals, both academically and in the research process, as well as emotionally. I would like to express my deepest gratitude to the following people:

Assoc. Prof. Dr. Lek Wanta, my thesis advisor from the School of Chemical Engineering at Suranaree University of Technology, provided me with educational opportunities, offered invaluable guidance in my research, and assisted in every aspect of my academic and personal life. He consistently supported various research endeavors, meticulously reviewed, and corrected this thesis, ensuring its successful completion.

I would like to thank my thesis committee members, Assoc. Prof. Dr. Nikom Klomkliang, Professor Dr. Adrian Flood and Asst. Prof. Dr. Atthaphon Maneedaeng for agreement to the part of my committee for my thesis defense. Thank you for your valuable comments and recommendations.

I extend my sincere thanks to all faculty members of the School of Chemical Engineering at Suranaree University of Technology for their dedicated teaching, guidance, and support throughout my academic journey.

Special thanks to Mr. Saran Dokmaikun, a staff member at the Center for Scientific and Technological Equipment, for facilitating the finding of instruments and providing essential guidance during the research process.

Thank you to Mrs. Amphorn Ladnongkhun for her assistance, coordination, and advice on documentation throughout my studies.

I am grateful to Sanguan Wongse Industries Co., Ltd. (SWI) for generously providing the raw materials necessary for this research.

Thank you to Suranaree University of Technology for the financial support and the opportunity to pursue and conduct this research.

Finally, I would like to extend my heartfelt thanks to my parents and my beloved sister for their unwavering support, encouragement, and financial assistance throughout my studies. Additionally, I am grateful to my fellow graduate students and my love for their continuous support, motivation, and advice, which has been vital to the completion of this thesis. I am profoundly appreciative and would like to express my highest gratitude to everyone mentioned here.

Sasitorn Boonkerd

TABLE OF CONTENTS

	Page
ABSTRACT (THAI).....	I
ABSTRACT (ENGLISH).....	III
ACKNOWLEDGEMENT.....	V
TABLE OF CONTENTS.....	VI
LIST OF TABLES.....	IX
LIST OF FIGURES.....	X
CHAPTER	
I INTRODUCTION.....	1
1.1 Background.....	1
1.2 Research Objective.....	3
1.3 Scope and Limitations of the Study.....	3
1.4 Expected Benefit of Research.....	3
II LITERATURE REVIEWS.....	4
2.1 Papain.....	4
2.1.1 Advantage of papain.....	4
2.1.2 Research of encapsulation of papain.....	6
2.2 Starch.....	9
2.2.1 Modified starch.....	11
2.2.1.1 Starch hydrolysis.....	12
2.2.1.2 Chemical modification.....	12
2.2.1.3 Physical modification.....	17
2.2.2 Research of starch as coat material.....	17
2.3 Encapsulation.....	21
2.3.1 Benefit of encapsulation.....	22
2.3.2 Classification of micro/nano capsules.....	22
2.3.3 Encapsulation technique.....	23
2.3.3.1 Chemical methods.....	23
2.3.3.2 Physical methods.....	23

TABLE OF CONTENTS (Continued)

	Page
2.3.3.3 Physico-chemical methods.....	24
2.4 Anti-solvent Precipitation.....	24
2.4.1 One-step liquid anti-solvent precipitation.	26
2.4.2 Two-step liquid anti-solvent precipitation.	26
2.4.3 Stepwise liquid anti-solvent precipitation.....	27
2.4.4 Anti-solvent precipitation mechanism	29
2.4.5 Important parameters	32
2.4.6 Nanoparticle structure	36
2.5 Oral Administration	38
2.6 Conclusion.....	41
III RESEARCH METHODOLOGY	42
3.1 Research Methodology.....	42
3.2 Location of Research	42
3.3 Chemicals and Instruments.....	43
3.3.1 Materials	43
3.3.2 Chemicals.....	43
3.3.3 Equipment and tools	43
3.3.4 Measuring and analytical instruments.....	44
3.4 Solubility Measurement	44
3.5 Preparation of Standard Curve of Papain	45
3.6 Preparation of ACS Solution.....	45
3.7 Papain Precipitation	46
3.8 Papain Encapsulation.....	47
3.9 Papain Precipitate Characteristics	47
3.9.1 Precipitation yield (%).....	47
3.9.2 Dynamic light scattering.....	48
3.9.3 Morphology	49
3.10 ACS/Papain Composites Characteristics	51
3.10.1 Encapsulation efficiency (EE) and loading capacity (LC)51	
3.10.2 Fluorescence analysis	51
3.10.3 Fourier transform infrared (FTIR) analysis.	52

TABLE OF CONTENTS (Continued)

	Page
3.10.4 Morphology	53
3.11 Residual Activity (%).....	53
3.11.1 α -N-benzoyl-L-arginine ethyl ester hydrochloride (BAEE) method.....	53
3.11.2 N α -benzoyl-DL-arginine 4-nitroanilide (BAPNA) method (Amidase method).....	55
IV RESULTS AND DISCUSSION	56
4.1 Papain Precipitation	56
4.1.1 The effect of anti-solvent types	56
4.1.2 The effect of solvent-to-anti-solvent volume ratios	58
4.1.3 The effect of papain concentrations.....	61
4.1.4 Scanning electron microscopy (SEM) Analysis.....	63
4.2 Papain Encapsulation.....	63
4.2.1 The effect of starch concentrations	65
4.2.2 The effect of starch solution volumes.....	67
4.2.3 The effect of surfactant types and concentrations	68
4.2.4 Fluorescent spectrum	71
4.2.5 FTIR analysis	73
4.2.6 Scanning electron microscopy (SEM) Analysis.....	81
V CONCLUSIONS AND RECOMMENDATIONS.....	82
5.1 Conclusions.....	82
5.2 Recommendations	83
REFERENCES	84
APPENDIX A.....	92
APPENDIX B	98
BIOGRAPHY	125

LIST OF TABLES

Table	Page
2.1	Research of encapsulation of papain. 7
2.2	A list of different starch sources. 11
2.3	Comparison of Amylose and Amylopectin..... 11
2.4	Research of starch as coat material..... 18
2.5	Segments of the GI tract and their corresponding functions 40
4.1	Residual activity of papain precipitate and crystallization yield (%) at different anti-solvent types 58
4.2	Residual activity of papain precipitate at different papain concentration..... 63
4.3	The FTIR spectrum of Papain and ACS/Papain composite 76
4.4	The FTIR spectrum of ACS, ACS composites and ACS/Papain composite 78

LIST OF FIGURES

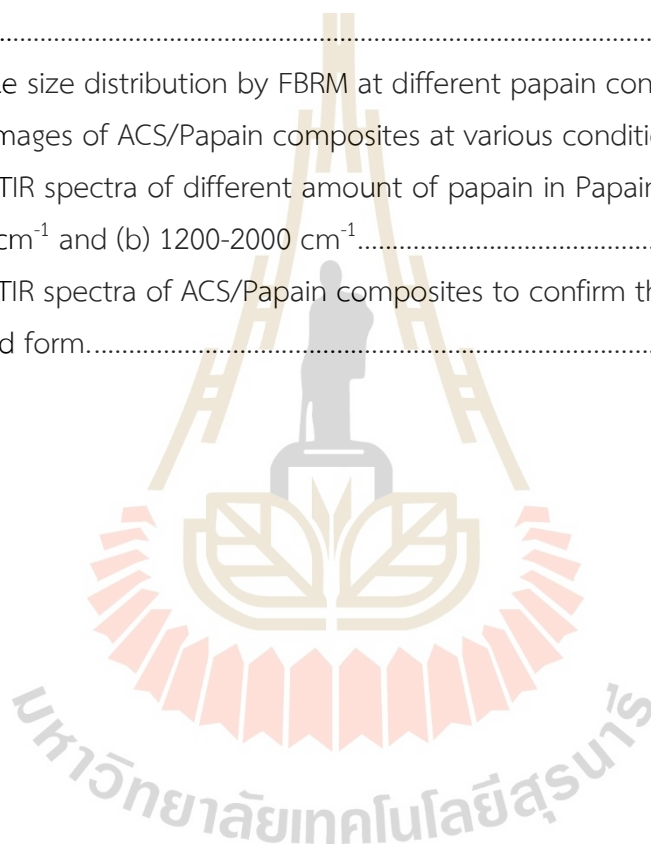
Figure	Page
2.1	Molecular structures of (a) amylose and (b) amylopectin 10
2.2	Fundamental consideration of encapsulation..... 21
2.3	Structure of the Capsule..... 22
2.4	Main morphologies of loaded microcapsules. (a) multi-wall with single core; (b) single-wall with multi-core; (c) single-wall with single core; (d) irregular shape with single core and wall..... 23
2.5	Schematic representation of the anti-solvent process..... 25
2.6	Schematic overview of an anti-solvent precipitation process. 25
2.7	Schematic representation of a One-step anti-solvent precipitation process... 26
2.8	Schematic representation of a Two-step anti-solvent precipitation process... 27
2.9	Schematic representation of a stepwise anti-solvent precipitation process (a) type 1 and (b) type 2..... 28
2.10	An illustration of formation mechanisms and possible structures by stepwise anti-solvent precipitation..... 28
2.11	Cross sections of different nanoparticle structure..... 38
2.12	Schematic representation of the processes involved in the dissolution and absorption process of a drug after oral administration. 39
2.13	Anatomy of the human GI-tract relevant for oral drug absorption 40
3.1	Calibration curve of papain..... 45
3.2	Cuvette for Zetasizer (Nano ZS, Malvern Instruments, Worcestershire, U.K.) (a) plastic cuvette and (b) U-shaped cuvette..... 48
3.3	Zetasizer (Nano ZS, Malvern Instruments, Worcestershire, U.K.) 49
3.4	Equipment for sample preparation before SEM analysis. (a) Carbon Tape, (b) Rubber Dust Blower and (c) Stub. 50
3.5	JSM-7800F Schottky Field Emission Scanning Electron Microscope..... 50
3.6	FP-8300 Spectrofluorometer..... 52
3.7	Bruker Tensor 27 with an Attenuated Total Reflectance (ATR) accessory..... 52

LIST OF FIGURES (Continued)

Figure		Page
3.8	JEOL JSM-6010LV Scanning Electron Microscope	53
4.1	Photomicrographs of papain crystals obtained using different anti-solvent types: (a) ethanol, (b) acetonitrile, and (c) acetone.....	58
4.2	Solubility of papain in water/ethanol mixture at 25 °C.....	59
4.3	The effect of S:AS volume ratios: (a) particle size distribution, (b) photograph of the suspensions formed after mixing ethanol with papain solution, (c) particle size (back line) and polydispersity index (PDI) (red line), (d) precipitation yield (red line) and zeta potential (back line) of particles with papain concentration of 25 mg/ml at different S:AS ratios.....	60
4.4	The effect of papain concentrations: (a) particle size (back line) and polydispersity index (PDI) (red line), (b) precipitation yield (red line) and zeta potential (back line), and (c) particle size distribution of particles with papain concentration of 25 mg/ml at different AS:S ratios.....	62
4.5	SEM photomicrographs of native papain and papain particles prepared by anti-solvent precipitation process under different operation parameters.....	65
4.6	Encapsulation efficiency and loading capacity of ACS/papain composites as functions of (a) starch concentration with fixed volume of starch solution of 1 ml and Tween 20 concentration of 3%v/v, and (b) starch volume with fixed starch concentration of 30 mg/ml and Tween 20 concentration of 3%v/v.....	67
4.7	Effect of surfactants on starch particle dispersion: (a) Without surfactant and (b) With surfactant.....	70
4.8	Encapsulation efficiency (a) and loading capacity (b) with fixed starch concentration of 30 mg/ml and starch solution volume of 7 ml, (c) residual activity after papain precipitation as functions of surfactant concentration (%v/v) and surfactant types.....	70
4.9	Fluorescence spectra of ACS/papain composites.....	72
4.10	The FTIR spectra of (a) ACS, ACS composites and (b) papain and ACS/papain composites.....	74

LIST OF FIGURES (Continued)

Figure	Page
4.11 SEM photomicrographs of (a) native ACS particles, (b) ACS composites, and (c), and (d) ACS/papain composites.....	75
A1 Particle size distribution by FBRM at different solvent-to-anti-solvent volume ratios.....	93
A2 Particle size distribution by FBRM at different papain concentrations.	94
A3 SEM images of ACS/Papain composites at various conditions.....	95
A4 The FTIR spectra of different amount of papain in Papain/ACS mixture (a) 400-4000 cm^{-1} and (b) 1200-2000 cm^{-1}	96
A5 The FTIR spectra of ACS/Papain composites to confirm the presence of papain in solid form.....	96



CHAPTER I

INTRODUCTION

1.1 Background

Nowadays, many proteins or peptides are increasingly being used for therapeutic purposes (Hassani et al., 2013; Kwon & Daniell, 2016). Usually, they are administered via intravenous, subcutaneous, or intramuscular injections. However, these routes can reduce drug efficacy, cause complications such as thrombophlebitis or tissue necrosis (Arisanti, Rachmawati, Pamudji, & Sumirtapura, 2012; Robertson, Broers, & Harris, 2021), and be inconvenient for patients due to repeated injections or hospital visits (Kwon & Daniell, 2016; Shaji & Patole, 2008). Therefore, it is necessary to explore alternative routes that do not involve blood vessels for drug delivery. The most convenient non-vascular route for patients is the oral route, which reduces the frequency of drug exposure, is painless, and helps in better disease management (Arisanti et al., 2012; Shaji & Patole, 2008).

Papain or papaya proteinase I (EC 3.4.22.2), an enzyme that is extracted from papaya (*Carica papaya*), is used in various industries, including food processing, cosmetics, detergents, leather processing, and pharmaceuticals (Shouket et al., 2020). In the pharmaceutical industry, papain is valued for its wound healing (Moreira Filho, Vasconcelos, Andrade, Rosa, & Vieira, 2020), anti-inflammatory formulations (Ezekiel & Florence, 2012), antibacterial treatments (dos Anjos et al., 2016), and even exhibits antioxidant properties (da Silva et al., 2010). Furthermore, papain has shown promise in cancer therapy (Chandran, Nachinmuthu, Natarajan, Inamdar, & Shahimi, 2018) and its role in aiding digestion (Muss, Mosgoeller, & Endler, 2013). With its various benefits and versatile properties, papain is highly valued in the medical field and other industries. Despite its benefits, papain's low chemical stability limits its effectiveness during processing, storage, and oral drug delivery. It usually needs to be stored at low temperatures and can degrade in the gastrointestinal tract due to instability in high temperatures and acidic conditions (Chankhampan et al., 2012). Therefore, encapsulation is a method that can help improve the chemical stability of papain for various applications.

Materials for coatings come in various forms, including synthetic polymers, biopolymers, and inorganic porous materials among others (Chankhampan et al., 2012;

Hassani et al., 2013; Mahmoudi Najafi, Baghaie, & Ashori, 2016). The choice depends on the protein's application. For oral drug delivery, biodegradable coatings are preferred as they are safe for the human body and can withstand acidic conditions and digestive enzymes (Klein, 2009; Shaji & Patole, 2008).

Starch is popular for encapsulating bioactive compounds in food and biomedical fields due to its natural, renewable, biodegradable, and biocompatible properties (Li, Feng, Li, & Gilbert, 2023; Zhu, 2017). It effectively protects and delivers bioactive compounds, maintaining their stability and functionality. Various starch types are used for encapsulation, including native starch granules, microporous starch, starch nanoparticles, substituted starch, cross-linked starch, hydrolyzed starch, amylose inclusion complexes, and other modified starches (Zhu, 2017). Native starch is environmentally friendly, biocompatible, and non-toxic (Li et al., 2023; Zhu, 2017). However, it may not control drug release well due to rapid drug release caused by high swelling and enzymatic digestion in biological fluids (Mahmoudi Najafi et al., 2016; Tuovinen, Peltonen, & Jarvinen, 2003; Xiao et al., 2019). Modified starches, like acetylated starch, offer better drug release control by reducing swelling and improving resistance to enzymatic digestion (Acevedo-Guevara, Nieto-Suaza, Sanchez, Pinzon, & Villa, 2018; Xiao et al., 2019). The effectiveness of acetylated starch depends on the degree of substitution (DS); higher DS values improve its properties (Mahmoudi Najafi et al., 2016; Xiao et al., 2019). This study focuses on acetylated starch with low DS values to enhance the production capabilities of general factories in Thailand.

Protein encapsulation into coating materials can be achieved using various methods. These include emulsion evaporation/extraction, solvent evaporation, interfacial methods, physical absorption, anti-solvent precipitation, and supercritical fluid anti-solvent precipitation (McClements, 2018; Mishra, Patel, & Tiwari, 2010; Ye & Chi, 2018). This study, the anti-solvent precipitation will be used to encapsulate papain with modified starches as this method is straightforward, quick, and easy to operate, it does not require long shear or stirring rates, sonication, or very high temperatures. It also provides very high encapsulate efficiency and low power consumption (de Boer, Imhof, & Velikov, 2019).

This research focuses on studying the encapsulation of papain using acetylated cassava starch (ACS) through a stepwise anti-solvent precipitation method, which consists of two main parts: first, the precipitation of papain, followed by its encapsulation with starch. The study aims to determine the optimal conditions by investigating the effects of the type of anti-solvent, papain concentration, and solvent to anti-solvent volume ratios on the papain precipitation process. Additionally, it

examines the impact of starch concentration, volume of the starch solution, and the type and concentration of surfactant on the papain encapsulation process.

1.2 Research Objective

1.2.1 To encapsulate papain within starch.

1.2.2 To study the optimum conditions for papain encapsulation.

1.3 Scope and Limitations of the Study

This research utilized papain as the protein for encapsulated material and acetylated cassava starch (ACS) with a degree of substitution (DS) of 0.037, provided by Sanguan Wongse Industries Co., Ltd. (SWI), as the carrier for encapsulating papain using the stepwise anti-solvent precipitation process. The experiments were conducted exclusively at the laboratory scale. This research is divided into two sections as follows:

1.3.1 Papain precipitation process

Examining the influence of different parameters on the papain precipitation process, including the type of anti-solvent, papain concentrations, solvent to anti-solvent volume ratios, and the type and concentration of surfactants.

1.3.2 Papain encapsulation process

Investigating various parameters affecting the papain encapsulation process, such as starch concentration, starch solution volume, and the type and concentration of surfactant.

1.4 Expected Benefits of Research

1.4.1 The understanding of the process of protein encapsulation with acetylated cassava starch by stepwise anti-solvent precipitation will be achieved.

1.4.2 Optimum conditions for papain encapsulation into acetylated cassava starch will be obtained.

1.4.3 The production of papain particles that are encapsulated in biological materials from Thailand will be achieved.

CHAPTER II

LITERATURE REVIEWS

2.1 Papain

Papain is one of the four enzymes produced from *Carica papaya* whose quantity is less than 10% (Department of Industrial Promotion, 2008) and is a protease with EC Number: EC 3.4.22.2 (Tacias-Pascacio et al., 2021), consisting of 212 amino acids and a molecular mass of 23.5 kDa. Papain is poorly stable as it is unstable at high temperatures and under pH conditions below 2.8, where papain activity is greatly lost (Chankhampan et al., 2012), but is stable at low temperatures and pH range 3 to 9 varies with different substrates. However, papain is almost inactive at a gastric acid pH of 1.2, so the ideal location for papain delivery is the small intestine with a pH in the range of 7 to 8 (Deulgaonkar & Thorat, 2008).

The production or purification of papain is generally used by precipitation yielding up to 53 g of coarse enzyme per kg of latex but still yielding only 39 % of papain. Different types of chromatography are a better alternative to precipitation because they provide more purity and efficiency (Fernández-Lucas, Castañeda, & Hormigo, 2017).

2.1.1 Advantage of papain

Papain can be used widely in various industries such as:

2.1.1.1 Pharmaceutical industry

Papain is a crucial ingredient in various pharmaceutical formulations. It is used in wound healing products to promote faster recovery by breaking down dead tissue and facilitating the growth of new tissue (Moreira Filho et al., 2020). Additionally, papain is incorporated into anti-inflammatory formulations (Ezekiel & Florence, 2012), antibacterial treatments (dos Anjos et al., 2016), and even exhibits antioxidant properties (da Silva et al., 2010) and digestive aid formulations (Muss et al., 2013), and it shows potential in cancer therapy due to its ability to modulate the immune response and induce apoptosis in cancer cells (Chandran et al., 2018).

2.1.1.2 Food industry

Papain is extensively used as a meat tenderizer, helping to break down tough muscle fibers and enhance the texture of meats. It is also employed in brewing to prevent chill haze in beer, and in the dairy industry to modify proteins for improved solubility and digestibility (Department of Industrial Promotion, 2008; Fernández-Lucas et al., 2017).

2.1.1.3 Cosmetic industry

Papain is valued for its exfoliating properties. It helps in the removal of dead skin cells, promoting a smoother and more radiant complexion. Papain is also used in antiaging products to reduce the appearance of fine lines and wrinkles and in acne treatments due to its ability to reduce inflammation and prevent pore blockages (Khan, Akhtar, & Ali, 2014; Squirrels, 2023).

2.1.1.4 Detergent industry

Papain is an important component in some laundry detergents and cleaning products. It helps break down protein-based stains such as blood, sweat, and food, enhancing the overall cleaning efficacy of detergents. Its biodegradable nature also makes it an environmentally friendly choice for cleaning products (Khaparde & Singhal, 2001; Sangeetha & Abraham, 2006; Shouket et al., 2020).

2.1.1.5 Textile and leather industry

Papain is used in the bating process to soften and remove hair from hides and skins, improving the texture and quality of the leather (Shouket et al., 2020). This enzymatic treatment is a more environmentally friendly alternative to traditional chemical methods.

2.1.1.6 Agriculture

Papain is used as a feed additive to improve the digestibility of animal feed (Corporation, 2024; Fernández-Lucas et al., 2017), enhancing the nutritional uptake for livestock. It also finds applications in the production of plant protein hydrolysates used in fertilizers.

2.1.1.7 Additional industrial applications (Shouket et al., 2020):

Clotting of Milk as Rennet: Papain is used as a milk-clotting agent in cheese production, serving as an alternative to traditional rennet.

Obtaining Oil from Liver of Tuna: It aids in the extraction of oil from the liver of tuna, improving yield and quality.

Conditioners in Shampoos: Papain is used in hair conditioners and shampoos to improve hair texture and manageability.

Rubber Manufacturing: The enzyme is utilized in the rubber industry to modify the properties of latex, improving its quality.

Removing Dust from Soft Lenses (Optics): Papain is employed in cleaning solutions for soft contact lenses, effectively removing protein deposits and other residues.

Photography: It is used in the photographic industry for various processes, including the preparation of certain photographic films and papers.

2.1.2 Research of encapsulation of papain

The researches for studying papain encapsulation with different coatings materials and encapsulation methods which is to protect papain from unsuitable environment on the human body or during storage/process as shown in Table 2.1.

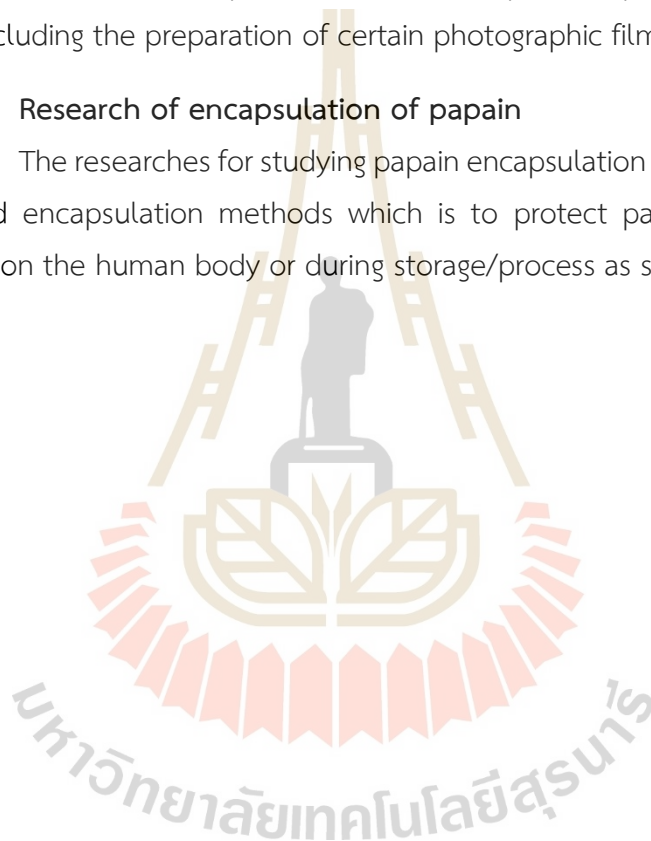


Table 2.1 Research of encapsulation of papain.

Coating material	Encapsulation method	Application	Encapsulation efficiency (%)	Particle size	Reference
Chitosan reinforced Alginate	Emulsification/internal gelation techniques	Oral drug delivery	95.79	315-560 μm (Spherical)	(Arisanti et al., 2012)
Poly (lactic-co-glycolic acid) (PLGA)	The emulsion solvent diffusion in water (ESD) and the w/o/w emulsion solvent evaporation (ESE) methods	Human skin (cytotoxicity)	ESE > ESD (43.03 > 19.42)	200-300 nm	(Chankhampan et al., 2012)
Poly (vinyl alcohol) (PVA) nanofibers	Electrospinning method	-	13	80-170 nm (nanofibers)	(Moreno-Cortez et al., 2015)
Biosilica Matrix	Biomimetic silicification process	-	82.60	200-500 nm (nearly spherical)	(Zhou, Wang, Jiang, & Gao, 2013)
Poly (vinyl alcohol) (PVA) nanofibers	Electrospinning method	Wound dressing	>50	200-400 nm (nanofiber)	(Shoba, Lakra, Kiran, & Korrapati, 2014)
Poly(ϵ -caprolactone) (PCL)	Double-emission precipitation method	Controlled drug delivery systems	80.4	242.9 nm (spherical)	(Budama-Kilinc et al., 2018)

Table 2.1 Research of encapsulation of papain (continued).

Coating material	Encapsulation method	Application	Encapsulation efficiency (%)	Particle size	Reference
Solid lipid nanoparticles	the melt dispersion-ultrasonication technique	Colorectal Cancer Therapy	76	157 nm	(Chandran et al., 2018)
hydroxypropyl methylcellulose phthalate (HPMCP), Eudragit L 100, and Eudragit S 100	w/o/w emulsion solvent evaporation	To protect papain from gastric inactivation	74.49-79.76	52.4-60.2 μm (spherical)	(Manu Sharma, Vinay Sharma, Amulya K Panda, & Dipak K Majumdar, 2011)

2.2 Starch

Starch is a natural, renewable, biodegradable, biocompatible, and cost-effective polysaccharide (Jin, Li, & Malaki Nik, 2018; Mahmoudi Najafi et al., 2016). It is a carbohydrate that accumulates in many plants, such as corn, potato, cassava, rice, wheat, sorghum, and barley (Morán et al., 2021) which commonly consumed as a major carbohydrate source for humans (Jin et al., 2018). In the starch industry, starch extracted directly from the plant is called "native starch" and starch that has been chemically and physically modified at least once to achieve specific properties is known as "modified starch" (Morán et al., 2021).

Over the years, both native and modified starches have found extensive applications across various industries including food, beverage, cosmetic and pharmaceutical industries. Starch is commonly utilized to impart texture and stability as a film-forming property for food production. Additionally, starch is integral in the manufacturing of paper, paperboard, pharmaceutical products, renewable packaging and more (Jin et al., 2018). Its versatility and biocompatibility make it a preferred choice in diverse industrial applications.

Starch granules vary in size, shape and crystals depending on the type of crop, as shown in Table 2.2. The structure and processing response of the granules are of great importance for the modification and application of starch. For the modified cold water insoluble starch recovered from the slurries more easily than water-soluble hydrocolloids. In most applications of starch, it undergoes gelatinization, in which the transformation of starch from crystals/granules to dissociated forms of molecules generally occurs at high temperatures. In most applications of starch, it undergoes gelatinization, in which the transformation of starch from crystals/granules to dissociated forms of molecules generally takes place at high temperatures. This temperature is called the gelatinization temperature, which depends on the grain morphology, crystallinity, molecular structure and chemical modification (Jin et al., 2018).

Starch is a polysaccharide composed of glucose molecules linked by glycosidic bonds, forming both linear and branched structures. It consists of two types of glucose polymers: amylose and amylopectin, as shown in Figure 2.1. Amylose is generally a linear molecular structure formed by α -(1,4) linkages (Table 2.3), which is found in starch approximately 20–30% by weight (Table 2.2), and amylopectin has a branched

molecular structure consisting of linear segments connected through α -(1,4) linkages and branched segments connected through α -(1,6) (Table 2.3), which found in starch about 70 – 80% by weight (Table 2.2). In addition, the size of the native starch granules highly depends on the source of the starch. Since Amylose and amylopectin have different molecular structures, they have different functional behaviors according to the data in Table 2.3 (Jin et al., 2018; Klein, 2009). In the starch granule, the amylopectin is formed in concentric circles with the amylose dispersed between and held together by hydrogen bonds. Starch is an abundance of hydroxyl, thus giving it hydrophilic properties, giving it affinity of moisture and dispersibility in water. However, the starch granules are insoluble in cold water (Garcia, Garcia, & Faraco, 2020).

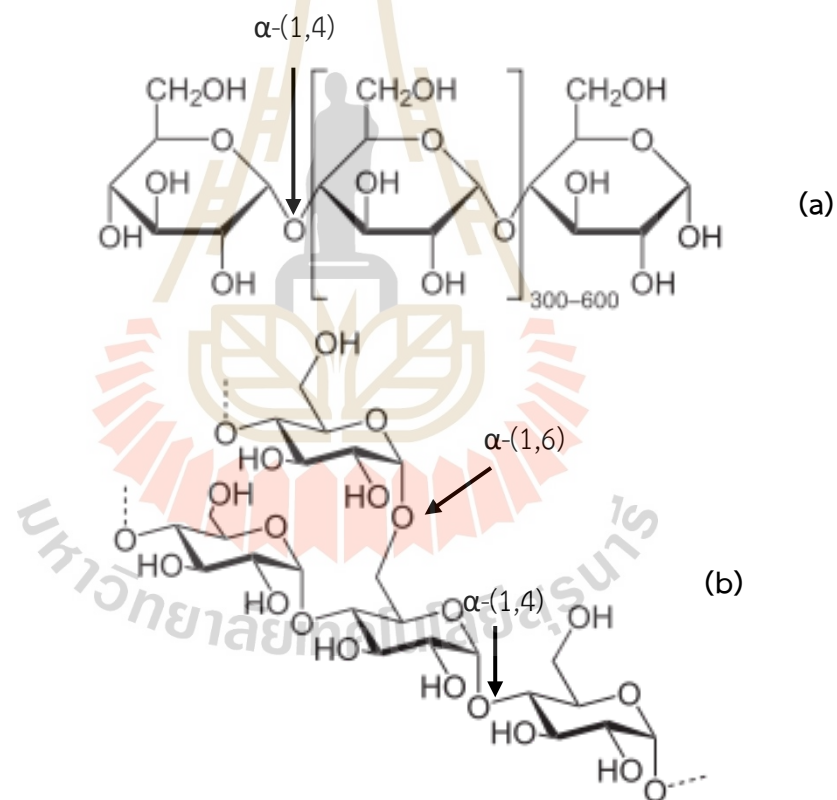


Figure 2.1 Molecular structures of (a) amylose and (b) amylopectin (Jin et al., 2018).

Table 2.2 A list of different starch sources (Jin et al., 2018).

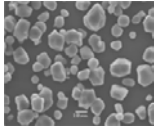
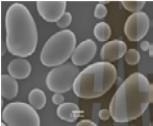
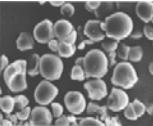
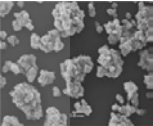
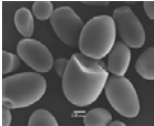
Source of Starch	Corn	Potato	Tapioca (Cassava)	Rice	Sago
Granule size (μm)	14	41	17	3	33
Amylose content	25%	20%	17%	19%	28%
Amylopectin content	65%	80%	83%	81%	72%
Morphology (SEM)					

Table 2.3 Comparison of Amylose and Amylopectin (Jin et al., 2018).

Types	Linkage	Structure	Mw	Properties	Application
Amylose	α -(1,4)	Linear	10^{5-6}	Retrogradation	Film forming
				Moisture resistance	Gelling
				High gelatinization temperature	Controlled digestion
Amylopectin	α -(1,4) & α -(1,6)	Branched	10^{7-8}	Solution stability	Lipid complexation
				High viscosity	Texturizing
					Stabilization
					Encapsulation
					Emulsification

2.2.1 Modified starch

Modified starch is obtained by taking native starch through a structural alteration process that changes its properties as needed, such as reduced viscosity, increased stability to heat, acidity, and shear strength. The modification process can be done either by chemical, physical, enzymatic or by microorganisms. The physicochemical properties of modified starch depend on the degree of substitution (DS) and the type of functional group used, with the maximum possible DS value of 3 since each glucose unit along the starch chain contains a hydroxyl group of only three

groups. for methods related to microencapsulation will be highlighted below (Garcia et al., 2020; Jin et al., 2018; Pimpen & Nithiya, 2010).

2.2.1.1 Starch hydrolysis

Starch hydrolysis involves breaking down starch molecules into shorter polymers through various methods. It typically includes three main steps: gelatinization, liquefaction, and saccharification.

Waxy starch, composed mostly of amylopectin, exhibits high viscosity due to its large molecular weight polymer. Hydrolysis reduces this molecular weight, leading to decreased viscosity and enhanced functionality. Starch hydrolysis occurs naturally in human digestion, facilitated by acids and enzymes. Alternatively, it can be induced chemically through oxidation with peroxides or mechanically through processes like extrusion.

Enzymatic hydrolysis is widely utilized to produce hydrolyzates with low molecular weight or degree of polymerization (DP), such as maltodextrins (DE 5-12), oligosaccharides (DE 10-50), syrups (DE 20-45), and sugars (DE 50-100). The degree of hydrolysis is often quantified by dextrose equivalent (DE), reflecting the number of reducing ends in the hydrolyzate.

Dry thermal treatment, another method, involves high-temperature hydrolysis of native starch under acidic conditions, known as dextrinization. This process leads to the formation of dextrins, where the hydrolyzed sugary fractions re-polymerize with additional branching. Dextrins are highly water-soluble and stable even at low temperatures due to their low molecular weight and branched structure. (Jin et al., 2018).

2.2.1.2 Chemical modification

Chemically modified starch undergoes structural changes through chemical processes, which are primarily used at the industrial level. In the food industry, various factors such as high shear loads, high temperatures, extreme pH, and salinity can impact product stability and safety. Therefore, to manage starch use under these conditions, chemical modification is a way to improve the viscosifying power, process tolerance, and product stability of starches, which can be modified in various ways depending on the type of chemical used and the degree of substitution (DS) (Jin et al., 2018; Pimpen & Nithiya, 2010) for example:

1) Etherification

Carboxymethyl Starch (CMS, Sodium starch glycolate): It is extensively utilized in the pharmaceutical field as an excipient to prolong drug release. The carboxymethylation process occurs in two stages: first, the formation of alkoxide groups in a basic medium, followed by the generation of CMS from the reaction between alkoxides and monochloroacetic acid or its sodium salt. Typically, CMS derived from corn starch possesses a degree of substitution (DS) value of less than 0.3. CMS exhibits several favorable characteristics that make it suitable for pharmaceutical applications. It possesses high swelling properties, facilitating rapid hydration upon contact with water. Furthermore, it demonstrates good solubility at ambient temperatures, low gelatinization temperatures, low intrinsic viscosity, and a reduced tendency to retrograde. These properties are primarily attributed to the substitution of hydroxyl groups by carboxymethyl groups. Notably, the extent of substitution dictates the solubility characteristics of CMS; a higher degree of substitution results in enhanced solubility, enabling starch to dissolve readily in cold water. These attributes contribute to the effectiveness of CMS as an excipient in pharmaceutical formulations designed to control drug release. (Garcia et al., 2020).

Hydroxy propylated Starch: It is synthesized through the reaction between native starch and propylene oxide, where propylene oxide substitutes primarily at the HO-2-hydroxyl in the starch anhydroglucose unit. This substitution weakens the bond structure within the starch granules, leading to a reduction in gelatinization temperature. The extent of hydroxypropyl substitution correlates with a lower gelatinization temperature, making the starch more thermally responsive. Moreover, the hydroxypropyl group imparts several advantageous properties to the starch paste. It inhibits retrogradation and prevents water from separating through syneresis during freeze-thaw cycles. Consequently, this modification enhances the shelf-life, freeze-thaw stability, cold-storage stability, clarity, and texture of starch paste. These improved characteristics render hydroxypropylated starch suitable for controlling drug release in pharmaceutical formulations. (Garcia et al., 2020).

2) Esterification

Acetylated starch: Acetylated starch is synthesized through the esterification of native starch with acetic anhydride and acetic acid, or vinyl acetate. This chemical reaction replaces hydroxyl groups on the anhydroglucose units of starch with acetyl groups, resulting in the formation of starch acetates or esters. The degree of acetylation can be controlled by adjusting factors such as reactant concentration, pH, reaction time, and the presence of catalysts. One of the primary benefits of acetylated starch is its ability to prevent retrogradation by disrupting the linear structure of amylose and amylopectin branches. This modification reduces the tendency of starch solutions to undergo changes in clarity, texture, and syneresis when stored at low temperatures.

Acetylated starch exhibits reduced susceptibility to swelling and enzymatic degradation compared to native starch due to the hydrophobic nature and steric bulkiness of the acetyl groups. This impedes water absorption and enzyme access to the starch molecules, resulting in improved stability in aqueous environments and enhanced resistance to enzymatic breakdown. These properties make acetylated starch suitable for various applications in the food, pharmaceutical, and industrial sectors.

The properties of acetylated starch can be tailored by adjusting the degree of substitution (DS) of acetyl groups. Starches with higher DS values are more hydrophobic and exhibit greater solubility in organic solvents such as chloroform. This increased hydrophobicity not only enhances resistance to swelling and enzymatic degradation but also enables dissolution in non-aqueous solvents, thereby expanding the range of potential applications for acetylated starch. A lower DS acetylated starch finds utility in various domains, including film forming, binding, adhesion, thickening, stabilizing, and texturing. This versatility stems from its ability to imbue desirable properties, such as improved stability and resistance to retrogradation, in a wide range of formulations across industries. (Ackar et al., 2015; Garcia et al., 2020; Mahmoudi Najafi et al., 2016; Xiao et al., 2019).

Succinate starch: It is a modified starch that is produced by reacting native starch with succinic anhydride, resulting in the formation of a half-ester. This modification process can be achieved by treating native starch with various alkenyl succinic anhydrides, with octenyl succinic anhydride being a commonly used example.

Starch derivatives containing succinate groups exhibit unique properties that make them highly versatile in various applications. One notable characteristic is their low gelatinization temperature, which allows for easier processing compared to unmodified starch. Additionally, succinate starch has a tendency to swell in cold water, leading to significant viscosity improvement. This property makes it particularly suitable for applications requiring thickening or gelling, such as in food and pharmaceutical formulations. Moreover, succinate starch demonstrates excellent filming properties, enabling the production of bioplastics, films, and coatings. These films can be utilized in a wide range of applications, including packaging materials, agricultural films, and diagnostic testing supports. Furthermore, succinate starch serves as an effective matrix material for drug delivery systems. For instance, octenyl succinic anhydride (OSA-starch) is widely employed as an encapsulation material due to its ability to form stable complexes and enhance the solubility and bioavailability of encapsulated active compounds. (Garcia et al., 2020)

3) Cross-linked starch

Cross-linked starch refers to starch molecules that have been chemically modified to form a network structure through the creation of intra- and inter-molecular bonds. This process enhances the structural integrity of starch, making it more stable and resistant to various environmental conditions such as high temperature, low pH, and high shear forces. Several crosslinking agents can be used for this purpose, including monosodium phosphate (SOP), sodium trimetaphosphate (STMP), sodium tripolyphosphate, epichlorohydrin, phosphoryl chloride (POQ), as well as various anhydrides such as adipic and acetic anhydrides, and succinic anhydride combined with vinyl acetate.

The cross-linking of starch molecules results in the formation of a network that improves the performance of starch in controlled release formulations. This network provides mechanical strength and stability, allowing the starch to withstand harsh conditions without losing its structural integrity. As a result, cross-linked starch is particularly useful as a matrix in formulations requiring controlled release of active ingredients.

However, there are some drawbacks associated with cross-linked starch. Cross-linking agents may impart opacity to the resulting gels, which can affect the visual appearance of formulations. Additionally, cross-linked starches may

exhibit reduced water retention capacity during storage, which can impact their performance over time.

Overall, cross-linked starch offers significant advantages in terms of stability and controlled release properties, making it a valuable ingredient in various pharmaceutical and industrial applications. However, careful consideration of formulation requirements and potential limitations is necessary when utilizing cross-linked starch in product development (Garcia et al., 2020).

4) Oxidized starch

Oxidized starch plays a crucial role in the development of novel drug delivery systems due to its altered chemical structure, which enhances its reactivity and suitability for various applications. The oxidation process involves the opening of the pyranosidic ring within the starch structure, resulting in the formation of two new aldehyde groups, typically positioned between the C-2 and C-3 carbons of the pyranosidic ring. These aldehyde groups are highly reactive, facilitating further chemical modifications of the starch molecule.

Various methods can be employed to oxidize starch, including the use of hydrogen peroxide, oxygen, ozone, bromine, chromic acid, permanganate, and nitrogen dioxide. Among these, hypochlorite oxidation is the most used method in industrial production due to its efficiency and effectiveness. During oxidation, glycosyl residues within the starch molecule are replaced by carboxyl and carbonyl groups to different extents, depending on the type of starch and reaction conditions employed.

The degree of oxidation can be quantified based on the number of carboxyl and carbonyl groups present in the oxidized starch, with modifications typically occurring at the C-2, C-3, and C-6 positions of hydroxyl groups. Following modification, the viscosity of the starch tends to increase, while the gelatinization temperature decreases. Despite these structural alterations, oxidized starch retains its biocompatibility and biodegradability, making it a desirable polymer for various biomedical applications, including drug delivery systems.

Overall, oxidized starch serves as a versatile excipient in drug delivery formulations, offering enhanced reactivity and functionality compared to native starch, thereby facilitating the development of innovative therapeutic strategies (Garcia et al., 2020).

2.2.1.3 Physical modification

Physically modified starch is the process of altering the molecular structure within the starch granules using heat, pressure, moisture, and shear forces to provide better functionality, which, as the molecular structure changes, also changes the properties of the starch (Jin et al., 2018; Pimpfen & Nithiya, 2010). For example:

- 1) Pregelatinized starch
- 2) Granular cold water-soluble starch
- 3) Annealing starch
- 4) Heat treatment starch
- 5) Mechanical milling starch

2.2.2 Research of starch as coat material

The researches for studying the active ingredient encapsulation in different types of starch are shown in Table 2.4.



Table 2.4 Research of starch as coat material.

Active Ingredient	Types of starch	Encapsulation method	Encapsulation efficiency (%)	Particle size	Release studies	Reference
Curcumin	native sago starch	in situ nanoprecipitation and a water-in-oil microemulsion	78	87 nm (spherical)	curcumin was released from the starch nanoparticles in a physiological environment over a period of 10 days.	(Chin, Mohd Yazid, & Pang,
Curcumin	native green banana starch and acetylated banana starch (DS = 0.33)	Nanoprecipitation method	80-92	168-210 nm	Curcumin release from the composite films in various food simulants is enhanced in lipophilic substances and can be controlled by acetylating the starch nanovehicle to reduce its polarity.	(Nieto-Suaza, Acevedo-Guevara, Sánchez, Pinzón, & Villa,
Quercetin	pea, corn and potato starch	Nanoprecipitation method	49 (Potato) 44 (Pea) 20 (Corn)	90-260 nm	For all samples, the maximum quercetin release was reached after 3 hours, with all types of starch exhibiting similar release profiles.	(Farrag et al., 2018)

Table 2.4 Research of starch as coat material (continued).

Active Ingredient	Types of starch	Encapsulation method	Encapsulation efficiency (%)	Particle size	Release studies	Reference
Luteolin	oxidized lotus root starch (OLRS)	Nanoprecipitation method	87.2	305 nm	OLRS NPs effectively stabilized luteolin in simulated gastric juice and sustained its release in	(Y. Y. Chen et al., 2021)
Ciprofloxacin (CFX)	acetylated corn starch (ACS) (DS = 0.33, 2.00, and 2.66)	Nanoprecipitation method	48.5-89.1	312 nm (spherical)	-	(Mahmoudi Najafi et al., 2016)
Curcumin	native and acetylated starch (DS = 0.33)	Nanoprecipitation method	>80	<250 nm	acetylated banana starch nanoparticles facilitated a more controlled release, likely due to their enhanced hydrogen bond interactions with curcumin.	(Acevedo-Guevara et al., 2018)
Diclofenac sodium (DS)	cross-linked starch	Nanoprecipitation method	95.01	21.04 nm	The DS release was sustained up to 6 hours in phosphate buffer of pH 5.5. and cross-linked starch is a good carrier for controlled release and successful permeation.	(El-Naggar, El-Rafie, El-sheikh, El-Feky, & Hebeish, 2015)

Table 2.4 Research of starch as coat material (continued).

Active Ingredient	Types of starch	Encapsulation method	Encapsulation efficiency (%)	Particle size	Release studies	Reference
Nisin	zein- octenyl succinic anhydride (OSA)	microfluidic chip	10-50	117.8-317.6 nm	-	(Liu, Ibarra-Sanchez, Miller, & Lee, 2022)
Zeaxanthin	Corn starch	the anti-solvent precipitation method	74	(Composites)	Rapid zeaxanthin release in intestinal simulations from the composites, indicating the potential for intestines-targeted controlled-release delivery and Corn starch/Zeaxanthin composites offer enhanced storage stability.	(Li et al., 2023)

2.3 Encapsulation

Encapsulation is the process by which a solid, liquid, or gaseous substance is coated or encapsulated by another substance. The encapsulated substance, which contains an active ingredient such as vitamins, active pharmaceutical ingredients, proteins, peptides, volatile oils, food materials, pigments, dyes, monomers, catalysts, or pesticides, is referred to as the core material or internal phase (Figure 2.2 and 2.3). The encapsulation material, which protects the core material, is known as the wall material, membrane, shell, or coating material. This encapsulation material is typically made from polymers or substances that can form walls or shells, such as ethyl cellulose, hydroxyl propyl methyl cellulose, sodium carboxy methyl cellulose, sodium alginate, PLGA, gelatin, polyesters, or chitosan (Figure 2.2 and 2.3) (Abdelkader et al., 2018; Benjar, 2007).

Microcapsules typically range in size from 1 to 1000 μm (Schrooyen, van der Meer, & De Kruif, 2001), and Nano capsules range in size from 1 to 1000 nm (Kothamasu et al., 2012).

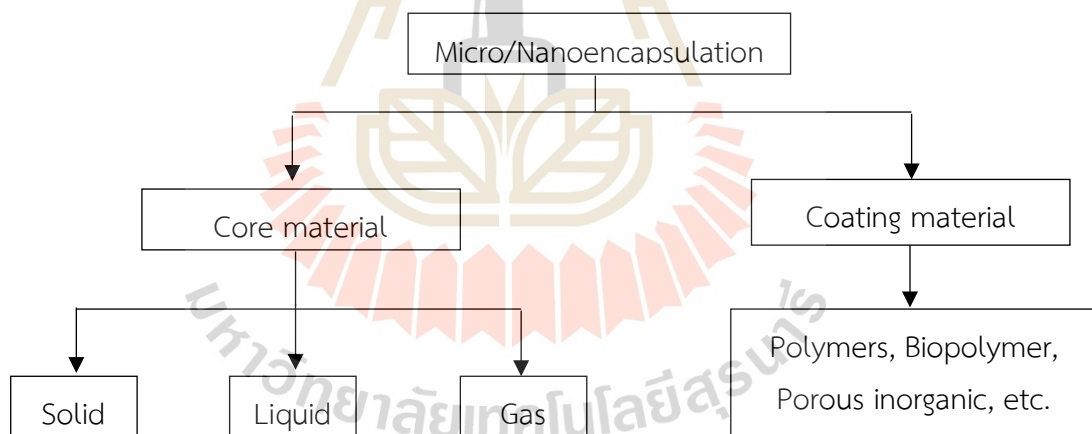


Figure 2.2 Fundamental consideration of encapsulation.
(Abdelkader, Hussain, Abdullah, & Kmaruddin, 2018)

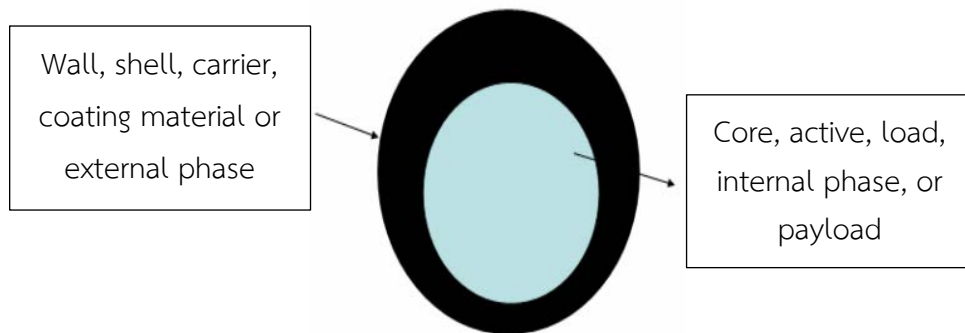


Figure 2.3 Structure of the Capsule (Benjar, 2007).

2.3.1 Benefit of encapsulation

Encapsulation improves the stability of substances and protects sensitive substances to light, temperature and pH or volatile substances, etc. which will allow the substance to be preserved for a longer time. It can also control the release of the substance to the desired area in a timely manner (Bundit, Jureerut, Tueanjit, Pranithi, & Patcharee, 2014), so it is very useful in medical practice.

2.3.2 Classification of micro/nano capsules

The classification of micro/nano capsules is based on several criteria, including the nature of the core substance, the coating material, and the capsule manufacturing method. Generally, they can be classified into two main types based on the nature of the core and two main types based on the nature of the wall: (Bundit et al., 2014; Corrêa-Filho, Moldão-Martins, & Alves, 2019).

2.3.2.1 Multi-wall with single:

These capsules feature multiple layers of coating materials surrounding either a single core (Figure 2.4 (a)), offering superior protection and the ability to control the release of the core substance over time. This type of capsule is beneficial in environments where the core needs to be shielded from external factors such as moisture, pH, or temperature changes.

2.3.2.2 Single wall with single or multi-cores:

These capsules have a single layer of coating material encapsulating either a single core or multiple cores (Figure 2.4(b) and (c)). They are easier and cheaper to produce compared to multi-wall capsules. However, they offer less protection and release control, making them more suitable for applications where these factors are less critical.

The shape of the capsules can be either spherical or irregular.

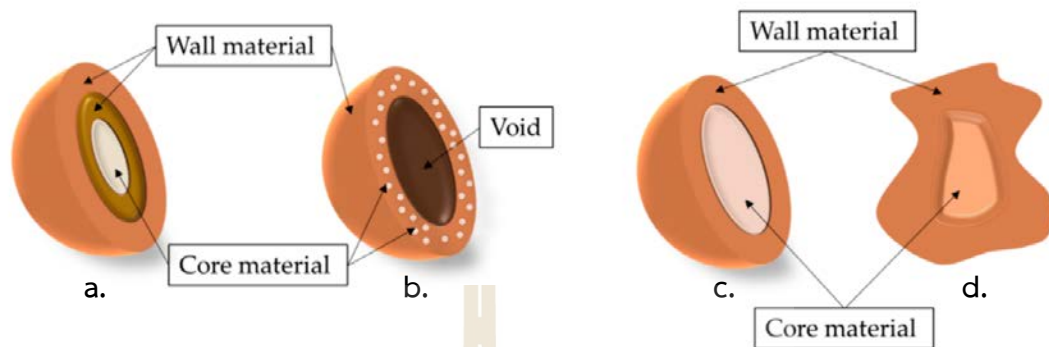


Figure 2.4 Main morphologies of loaded microcapsules. (a) multi-wall with single core, (b) single-wall with multi-core, (c) single-wall with single core, and (d) irregular shape with single core and wall (Corrêa-Filho et al., 2019).

2.3.3 Encapsulation technique.

2.3.3.1 Chemical methods

- 1) Interfacial polymerization
- 2) Poly condensation
- 3) Polyelectrolyte complexation
- 4) Cryogenic solvent extraction
- 5) Phase separation (Coacervation)
- 6) Solvent evaporation and extraction
- 7) Interfacial polymerization
- 8) Suspension polymerization
- 9) Complex coacervation
- 10) In situ polymerization
- 11) Emulsion Polymerization
- 12) Matrix polymerization
- 13) Liposome technology

2.3.3.2 Physical methods

- 1) Spray drying
- 2) Spray chilling
- 3) Spray desolvation
- 4) Air-suspension coating

- 5) Vibration nozzle
- 6) Pan coating
- 7) Centrifugal extrusion

2.3.3.3 Physico-chemical methods

- 1) Polymer incompatibility
- 2) Ionotropic gelation
- 3) Sol-gel encapsulation
- 4) Supercritical fluid assisted microencapsulation

2.4 Anti-solvent precipitation

Anti-solvent precipitation, which also known as nanoprecipitation, liquid-liquid dispersion, liquid desolvation, drawing-out precipitation, or solvent displacement, is achieved by reducing the solubility of the active ingredient in the solution. In addition, the term coacervation can also be used to describe this process, but in the food industry it is often used to refer to hydrophilic colloids (Joye & McClements, 2013; Nelemans, Buzgo, & Simate, 2020).

Anti-solvent precipitation can be achieved by adding a non-solvent agent, also known as anti-solvent, to reduce the solubility of the solute until the solution is saturated, which in turn drives the solute precipitate. However, the anti-solvent used must be mixed well with the solvent used. Therefore, it is necessary to select the anti-solvent carefully and appropriately, taking into account the coating material and active ingredient used to produce the required particles. There are generally a number of substances that are both solvent and anti-solvent, such as water and organic solvents. The main driving force for particle formation during anti-solvent precipitation is the intermolecular reaction imbalance of the solute, solvent, and anti-solvent, and importantly after the particle formation, the intermolecular repulsion must be sufficient to prevent particles from merging. The different production steps can be distinguished in the anti-solvent precipitation step as shown in Figure.2.5 (Joye & McClements, 2013)

In this method was first described and patented by Fessi et al. in 1989 (Fessi, Puisieux, Devissaguet, Ammouy, & Benita, 1989), two miscible solvents are required in which coating material and active ingredient are dissolved in the first solvent but not in the second solvent (Anti-solvent) which the method is shown in Figure 2.6, the first step is to prepare the organic phase solution, which consists of the active ingredient,

coating material and the first solvent and then mixed into the second solvent. (Anti-solvent), then precipitation will occur immediately because the second solvent will reduce the solubility of the first solvent causing the precipitation of the active substance and coating material. The resulting particles have a particle size of 20–300 nm, depending on the specific material and conditions used for the synthesis (de Boer et al., 2019).

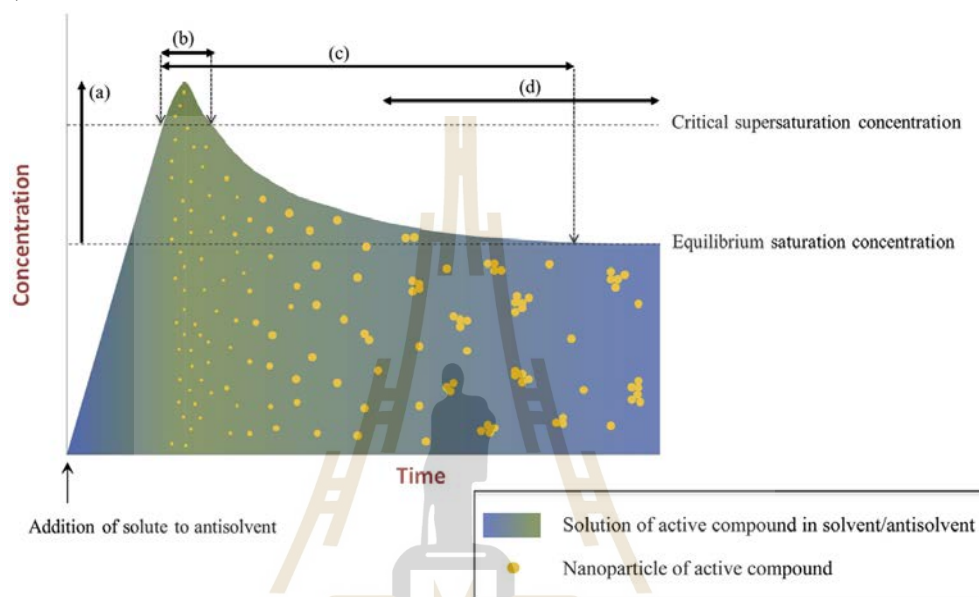


Figure 2.5 Schematic representation of the anti-solvent process. The different stages, i.e. supersaturation (a), nucleation (b), particle growth by condensation (c) and by coagulation (d) are indicated on the scheme (Joye & McClements, 2013).

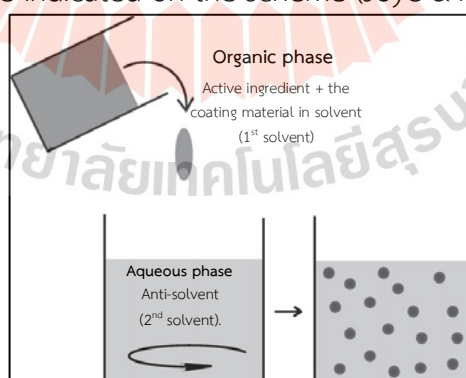


Figure 2.6 Schematic overview of an anti-solvent precipitation process. (de Boer et al., 2019)

The encapsulation of the active ingredient by this method can be divided into three types.

2.4.1 One-step liquid anti-solvent precipitation.

This method is the traditional one to be carried out in a single way until the end of the process. This will have a total of 3 steps (Figure 2.7). (Swati Tyagi et.al, 2016, Levi et.al, 2020)

Step 1: Add active ingredient and coat material to an organic solvent which is a solvent that both active ingredient and coat material can dissolve.

Step 2: The solution in step 1 is added to the anti-solvent. An anti-solvent is a solvent that will dissolve well with organic solvents but will not dissolve with active ingredients and coating material.

Step 3: Stirring at a certain speed using a magnetic stirrer for about 5-10 minutes, nanoparticle formation will occur.

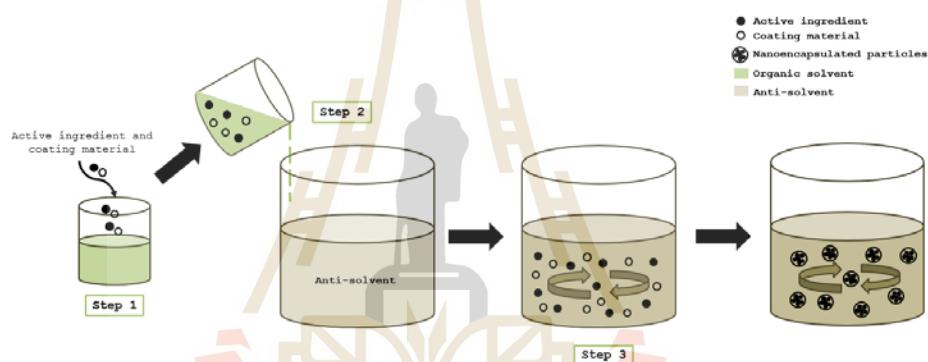


Figure 2.7 Schematic representation of a one-step anti-solvent precipitation process.

2.4.2 Two-step liquid anti-solvent precipitation.

This method is developed from the one-step anti-solvent precipitation process because the one-step anti-solvent precipitation process is not suitable for protein encapsulation because most proteins are not directly soluble or lose their activity in these organic solvents. This approach has a total of two steps (Figure 2.8) (X. Chen, Moonshi, Nguyen, & Ta, 2023; Morales-Cruz et al., 2012; Nelemans et al., 2020; Wang & Tan, 2016).

Step 1: Precipitate the active ingredient by injecting non-solvent into the active ingredient solution, stirring, and leaving for 5-10 minutes at room temperature.

Step 2: Slowly add coat material/non-solvent solution into the precipitated protein mixture in step 1 under proper velocity stirring and the sample is immediately precipitated. Following that, the samples were added drop by drop to

the surfactant under appropriate stirring, resulting in instantaneous encapsulation but also the formation of empty nanoparticles devoid of active components.

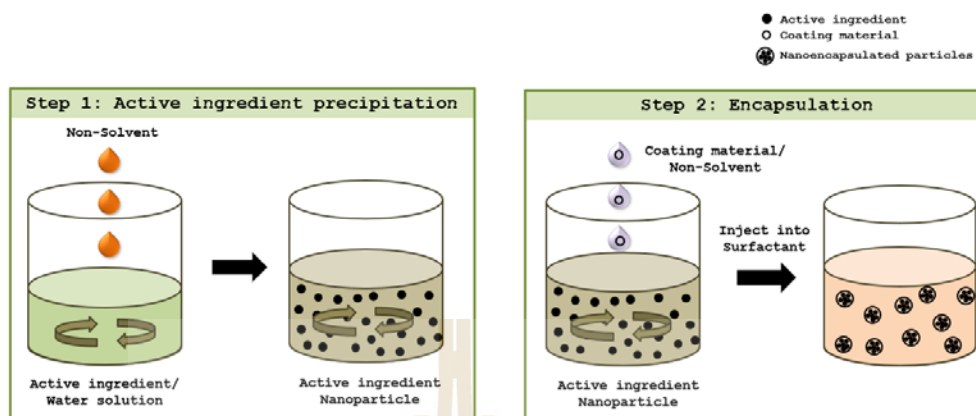


Figure 2.8 Schematic representation of a two-step anti-solvent precipitation process.

2.4.3 Stepwise liquid anti-solvent precipitation.

The stepwise liquid anti-solvent precipitation method shares similarities with the two-step anti-solvent precipitation method but differs in its application to polymers that are insoluble in non-solvents. In contrast, the two-step method is used with polymers that are soluble in non-solvents. The stepwise method can be categorized into two types based on the sequence of precipitation and encapsulation processes (Yang, Dai, Sun, & Gao, 2018).

Type 1 (Figure 2.9(a))

1. **Simultaneous Precipitation:** In this type, the APIs and coating material are precipitated simultaneously by adding the solution containing both components to the anti-solvent (non-solvent) or adding the anti-solvent to the solution containing both components.

2. **Surfactant Addition:** Following precipitation, surfactant is introduced to disperse the encapsulated particles, ensuring uniform distribution.

Type 2 (Figure 2.9(b))

1. **API and Surfactant Precipitation:** Initially, the APIs and surfactant are precipitated together by the addition of anti-solvent to their solution or the addition of their solution to anti-solvent.

2. **Coating Material Addition:** Subsequently, the coating material is added to encapsulate the precipitated particles, forming the final encapsulated product.

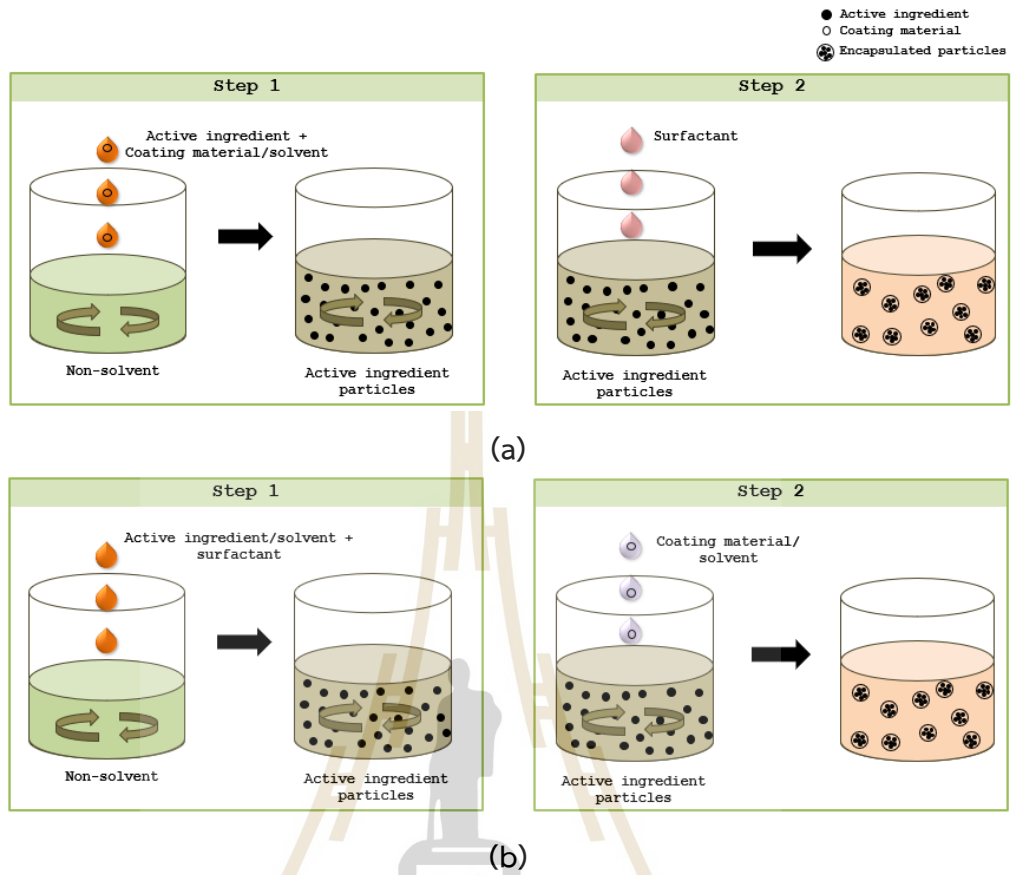


Figure 2.9 Schematic representation of a stepwise anti-solvent precipitation process (a) type 1 and (b) type 2.

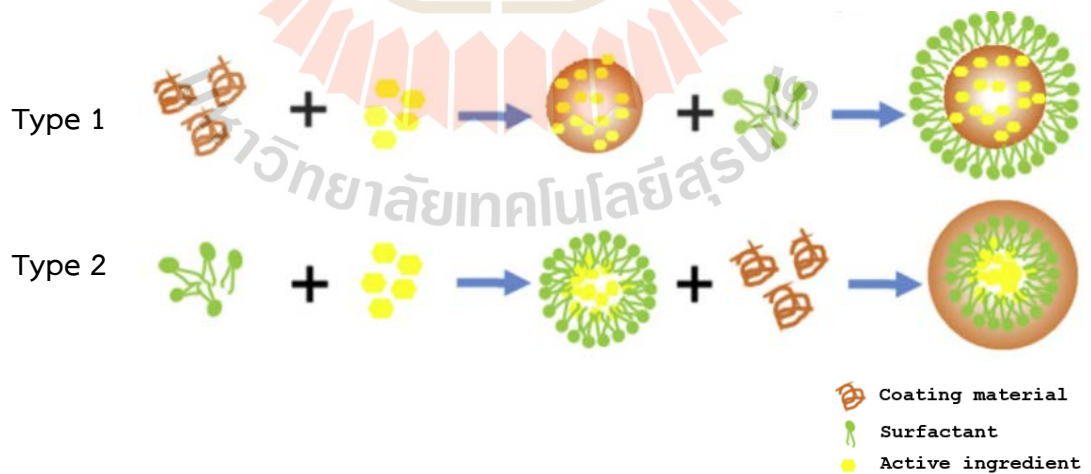


Figure 2.10 An illustration of formation mechanisms and possible structures by stepwise anti-solvent precipitation (Yang et al., 2018).

2.4.4 Anti-solvent precipitation mechanism

Anti-solvent precipitation (Nanoprecipitation) consists of four steps: generation of supersaturation, nucleation, growth, and coagulation (see Figure 2.5).

2.4.4.1 Supersaturation and nucleation

Adding an anti-solvent to the solute solution (or vice versa) reduces the solubility of the solute in the solvent, leading to supersaturation. Supersaturation occurs when the solute concentration (c) exceeds the equilibrium saturation concentration (c_{eq}). When solute concentration (c) surpasses the critical supersaturation concentration, nucleation is triggered. The time interval between the onset of supersaturation and the appearance of nuclei is known as the induction time.

The range of solvent/anti-solvent compositions where nucleation does not occur within a specific time frame is termed the metastable zone. For precise control and rapid nucleation, it is advantageous to narrow the metastable zone. This adjustment ensures a high and uniform nucleation rate, which is crucial for producing nanoparticles with consistent properties (Joye & McClements, 2013; Martínez Rivas et al., 2017).

The degree of supersaturation S can be described as the ratio of the solute concentration (c) over the equilibrium saturation concentration (c_{eq}) under specific conditions (Joye & McClements, 2013):

$$S = \frac{c}{c_{eq}} \quad (2.1)$$

Nucleation can be divided into two types: the presence or absence of foreign particles or surfaces that promote nucleation, which is referred to as heterogeneous or homogeneous nucleation, respectively. In what follows, homogeneous nucleation is considered (Joye & McClements, 2013; Martínez Rivas et al., 2017).

The nucleation rate is according to the classical theory of homogeneous nucleation given by (Joye & McClements, 2013):

$$J = A \text{Exp} \left(- \frac{B}{\ln S^2} \right) \quad (2.2)$$

$$A = N_0 v \quad (2.3)$$

$$B = \frac{16\pi\sigma^3 V_s^2}{3k^3 T^3} \quad (2.4)$$

$$v \approx \frac{kT}{3\pi a_0^3 \eta} \quad (2.5)$$

where N_0 is the number of molecules of solute per unit volume,
 v is the frequency of molecular transport to the solid-liquid interface,
 σ is the interfacial tension at the solid-liquid interface,
 V_s is the volume of a solute molecule,
 k is the Boltzmann constant,
 T is the temperature,
 v is the frequency of molecular transport,
 η is the viscosity of the surrounding solution,
 a_0 is the mean effective diameter of the diffusing species

According to classical nucleation theory, the rate of nucleation in a homogeneous system is influenced by the surface tension at the interface between particles and the solution. This rate is inversely related to temperature, meaning lower temperatures generally favor higher nucleation rates.

Equation (2.2) from classical nucleation theory indicates that rapid and significant supersaturation increases the nucleation rate. Supersaturation is crucial as it determines key properties of nanoparticles such as their size, crystallinity, morphology, and purity. When the solute concentration surpasses the critical solute concentration, leading to supersaturation, smaller particle sizes are typically observed.

However, when the solute concentration becomes very high, there is a tendency for particle sizes to increase due to enhanced collision frequencies among particles. This phenomenon can result in particle agglomeration.

In summary, while high supersaturation is a primary driving force for precipitation, leading to smaller nanoparticles, excessively high solute concentrations can lead to larger particles and particle agglomeration, affecting the desired properties of the nanoparticles. (Joye & McClements, 2013; Martínez Rivas et al., 2017)

Furthermore, the initiation of the nucleus depends on the energy barrier (ΔG), which is the energy that must be overcome to form nuclei. (Joye & McClements, 2013):

$$\Delta G = \frac{16\pi\sigma^3 V_s^3}{3k^2 T^2 (\ln S)^2} \quad (2.6)$$

High supersaturation and low surface tension reduce the energy barrier to more easily overcome this energy, thereby enabling faster nucleation. Consequently, the product yields more and smaller particle sizes. In addition, the system viscosity plays an important role in the number and size of particles formed. (Joye & McClements, 2013; Martínez Rivas et al., 2017)

Nucleation stops when the solute concentration falls below the critical supersaturation concentration and the number of nuclei does not change anymore, while the nuclei grow by coagulation and condensation. (Joye & McClements, 2013; Martínez Rivas et al., 2017)

2.4.4.2 Nuclei growth through condensation

Condensation in the context of particle growth involves the addition of solute molecules to the surface of existing particles. This process typically occurs in two distinct steps: (Joye & McClements, 2013; Martínez Rivas et al., 2017).

1) Diffusion step: Initially, solute molecules diffuse from the bulk fluid towards the surface of nuclei or existing particles. This movement through the solution boundary layer adjacent to the particle surface is driven by concentration gradients.

2) Deposition step: In this step, the solute molecules that have diffused to the particle surface are deposited onto the nuclei or particle matrix. This deposition involves the integration of the absorbed solute molecules into the existing particle structure.

The growth of particles through condensation continues until the concentration of free (non-adsorbed) solute in the solution decreases below the equilibrium saturation concentration. At this point, further condensation ceases as the driving force for particle growth diminishes.

2.4.4.3 Particle growth through coagulation

Particle coagulation is a significant factor influencing particle growth when the solute concentration is below the equilibrium saturation concentration (Figure 2.5). Coagulation refers to the aggregation of particles due to attractive interactions (such as Van der Waals forces and hydrophobic interactions) overcoming repulsive interactions (like steric or electrostatic repulsion) between particles (Joye & McClements, 2013; Martínez Rivas et al., 2017).

The rate of coagulation is primarily controlled by the collision frequency, which depends on factors such as particle concentration, size, and motion (e.g., Brownian, gravitational, or mechanical motion). The efficiency of collisions leading to coagulation is termed collision efficiency and is influenced by the balance between attractive and repulsive interactions among particles.

To mitigate coagulation and stabilize particles during preparation, stabilizing agents can be employed. These agents typically adsorb onto the surface of nanoparticles (NPs) and introduce repulsive interactions that counteract attractive forces, thereby preventing aggregation (Joye & McClements, 2013; Martinez Rivas et al., 2017). This approach helps maintain the integrity and desired properties of nanoparticles throughout processing and application.

2.4.4.4 From hydrosol to powder

Hydrosols, which are aqueous suspensions of microparticles formed after the anti-solvent precipitation stage, often require removal of both solvent and anti-solvent in industrial applications. This can be achieved through methods like filtration, centrifugation, washing, and drying (e.g., air drying). However, the removal of liquid phases can impact the integrity and release properties of the particles.

To mitigate these challenges, small molecule excipients are commonly employed to enhance the stability of the particles produced by this method. These excipients play crucial roles in maintaining the physical and chemical stability of the particles throughout processing and storage. They can stabilize particle surfaces, prevent aggregation, and preserve desired release characteristics.

Therefore, careful selection and utilization of appropriate small molecule excipients are essential steps to ensure the quality and functionality of particles during and after the removal of solvents and anti-solvents in industrial applications.

2.4.5 Important parameters

Important for commercial applications is the ability to control the particle size distribution and the stability of ultrafine particles caused by anti-solvent precipitation. Typically, the production of fine particles with a low polydispersity index that have good growth stability and separation from gravity is required by manufacturers. These properties can be achieved by changing the process conditions, those conditions are shown below (Joye & McClements, 2013).

2.4.5.1 Mixing technologies

1) Mechanical stirring

Mechanical stirring applied to a solution plays a crucial role in achieving uniform supersaturation throughout the system. When solvent and anti-solvent phases are mixed, three distinct scales of turbulent mixing are observed: macro-mixing, meso-mixing, and micro-mixing.

Macro-mixing: This scale involves mixing on a large scale, influencing the overall flow pattern and distribution of solvent and anti-solvent within the vessel.

Meso-mixing: At this intermediate scale, local turbulence and eddies are generated, enhancing the mixing of solvent and anti-solvent at a more localized level within the bulk solution.

Micro-mixing: This scale refers to the smallest turbulent fluctuations and eddies that occur at very fine scales. Micro-mixing is critical as it promotes thorough interdiffusion of solvent and anti-solvent molecules, ensuring uniform supersaturation and promoting nucleation and particle formation.

Each scale of mixing contributes differently to the process: macro-mixing sets the overall flow patterns, meso-mixing enhances local mixing gradients, and micro-mixing ensures molecular-level homogeneity, thus affecting the nucleation kinetics and final particle characteristics.

2) Ultrasound

The propagation of high-intensity ultrasound through a liquid induces cavitation, forming gas bubbles during the negative-pressure phase of the pressure wave. When these bubbles collapse, they generate intense temperature and pressure gradients, capable of breaking up particles. Ultrasound applied during nucleation offers several benefits: it reduces induction time, accelerates nucleation rates by influencing solubility and mixing, and widens the metastable zone.

However, ultrasound also doubles particle aggregation by increasing collision frequency while reducing contact time between crystals, thus contributing to particle size reduction through frictional effects. The frequency, intensity, and duration of ultrasound waves all impact its effectiveness. Factors such as horn tip diameter, immersion depth, solution volume, and sonication duration also

play crucial roles. For instance, larger horn diameters lead to faster precipitation rates and smaller particle sizes.

2.4.5.2 Addition of solute to anti-solvent

The speed and order of adding solvent to anti-solvent or vice versa are crucial for determining particle properties, as these parameters influence the rate and degree of supersaturation. This, in turn, significantly affects the nucleation rate and particle growth kinetics. Increasing the speed at which the active compound solution is added to the anti-solvent enhances mixing efficiency, resulting in smaller nanoparticles due to the increased extent of mixing per unit time. Similarly, injecting the anti-solvent into the active compound solution achieves the same effect, leading to a reduction in particle size.

2.4.5.3 Anti-solvent to solvent ratio

The volume of both the anti-solvent and the solvent used in nanoparticle preparation significantly influences the properties of the resulting particles. Research indicates that increasing the volume of the anti-solvent tends to reduce particle size.

Additionally, the increased anti-solvent volume leads to a more rapid reduction in solvent concentration, resulting in higher instantaneous supersaturation. This higher supersaturation enhances nucleation and promotes the formation of smaller particles. Moreover, at lower solute concentrations, crystal growth is reduced. However, as particle growth proceeds, it becomes partially hindered at higher anti-solvent volumes due to the increased diffusion distance for the growing species, leading to a diffusion-limited process.

2.4.5.4 Compound concentration

The concentration of active compounds in the substrate significantly influences the particle formation process through several mechanisms.

First, a higher solute concentration increases the degree of supersaturation, which can lead to the formation of a greater number of smaller nuclei. However, simultaneously, the growth of these nuclei is also enhanced due to increased collision frequency, albeit with a shorter diffusion length.

Second, increase in the solute concentration results in an increase in viscosity, which impedes diffusion between the solvent and the anti-solvent phases. This uneven diffusion limits the uniformity of supersaturation, thereby slowing

down nucleation rates and potentially increasing particle aggregation. The elevated viscosity reduces both collision frequencies and mass transfer rates via diffusion, further affecting particle growth and stability.

In composite particles, the ratio of polymer to active compound also plays a crucial role. This parameter influences particle formation dynamics, stability, and loading capacity. When higher amounts of solute are used, it tends to impact particle size, potentially leading to variations in size distribution and overall particle characteristics.

Therefore, careful control and optimization of active compound concentration and polymer ratios are essential for achieving desired particle properties, including size, stability, and loading capacity, in particle engineering processes.

2.4.5.5 Temperature

Temperature exerts significant influence on particle formation processes due to its impact on various key factors such as equilibrium saturation, supersaturation concentration, diffusion rates, and system viscosity. These factors collectively affect particle size by influencing nucleation rates, crystal growth, coagulation, and agglomeration.

Higher temperatures generally result in larger particles with a broader size distribution. This is because elevated temperatures increase compound solubility, thereby reducing the degree of supersaturation upon mixing. As a result, nucleation rates slow down, leading to crystal growth and the formation of larger particles that typically exhibit lower crystallinity. Additionally, higher temperatures promote faster diffusion, which can further contribute to particle growth.

Conversely, lower temperatures of the anti-solvent phase increase viscosity depending on the anti-solvent used, which slows molecular transport and reduces the frequency of particle collisions. This reduction in collision frequency decreases particle growth through coagulation and agglomeration. Furthermore, temperature can also impact excipients or surfactants by altering their structure or stability, potentially affecting particle formation processes and stability.

In summary, temperature control is critical in particle engineering processes as it directly influences particle size, distribution, and stability through its effects on solubility, nucleation, growth kinetics, and the behavior of additives.

2.4.5.6 Selection of an appropriate (anti-)solvent

The anti-solvent and solvent used is very important in controlling the settling process. A prerequisite for selecting an anti-solvent is the solubility of the anti-solvent in the solvent phase. The solubility parameters of the solvent and anti-solvent have a strong effect on supersaturation change, viscosity, surface tension, particle size and morphology. And the nature of the anti-solvent affects the crystal structure. Additionally, if the anti-solvent is water and the compound and/or the drug additive is a protein-based material, the pH and ionic strength will have a significant effect on the particle size and polydisperse index. This effect depends on the nature of the protein used, for example, when the buffer pH is close to the isoelectric point, the particles are smaller.

2.4.5.7 Effect of stabilizers

Surfactants reduce surface tension and promote nucleation, thereby contributing to smaller particle size. Certain polymers can further stabilize particles through steric and electrostatic mechanisms. Properties such as rigidity, polarity, and hydrophobicity of these polymers are crucial in controlling particle growth inhibition.

Protein-based composite particles tend to aggregate near their isoelectric points. Polymers or surfactants can be added to the solution to adjust and mitigate this settling process.

These additives play a significant role in manipulating the physical and chemical properties of the particles, ensuring stability and functionality in various applications.

2.4.6 Nanoparticle structure

In the pharmaceutical field, nanoparticles produced by anti-solvent precipitation are generally divided into two types: compound particle and composite particle. The resulting particles may have different morphology according to their chemical and physical characteristics of active compounds and excipients, as well as the conditions used to prepare the particles (Joye & McClements, 2013).

1) Compound particles (Figure 2.11 A): These are particles that are fully formed by active compounds themselves. Typically, the result is a crystal or an amorphous solid that will show many different morphologies such as cubic, spherical, and elliptical. As the physical state of the active ingredient affects the dissolution rate

of the drug, it needs to be closely controlled during its formation. Amorphous forms tend to dissolve faster than crystalline forms due to their higher internal energy and better molecular motion. Likewise, different polymorphic forms tend to have different solubility rates. Therefore, control of preparation conditions is essential to obtain the desired polymorphism of crystals.

2) Composite particle (Figure 2.11 B-D): It is a particle formed by one or more active compounds and excipients, usually polymers or surfactants. The production of composite nanoparticles by anti-solvent method usually has a spherical form, but differs in internal structure, which can be divided into three types:

Molecular composites: It is a structure consisting of the distribution of the active compound molecules across the polymer matrix. (Figure 2.11C)

Dispersion composites: It is the colloidal distribution structure of the active compound across the polymer matrix. (Figure 2.11B)

Core-Shell: It is a structure in which the active core is surrounded by a polymer shell (Figure 2.11E) or a polymer core surrounded by an active shell (Figure 2.11D).

Composite particles are often formed by precipitation of cores (e.g. active ingredients) and coatings (e.g. biopolymers, polymers). The polymer not only stabilizes the particles and active ingredients during processing, but also controls the release of the compound. In this particle, bioactive compounds should interact physically and chemically binding together with excipients.

In dispersion composites and core-shell structure, the active ingredient may be either liquid, amorphous or crystalline depending on its properties. Surfactants are used to as excipients to facilitate particle formation.

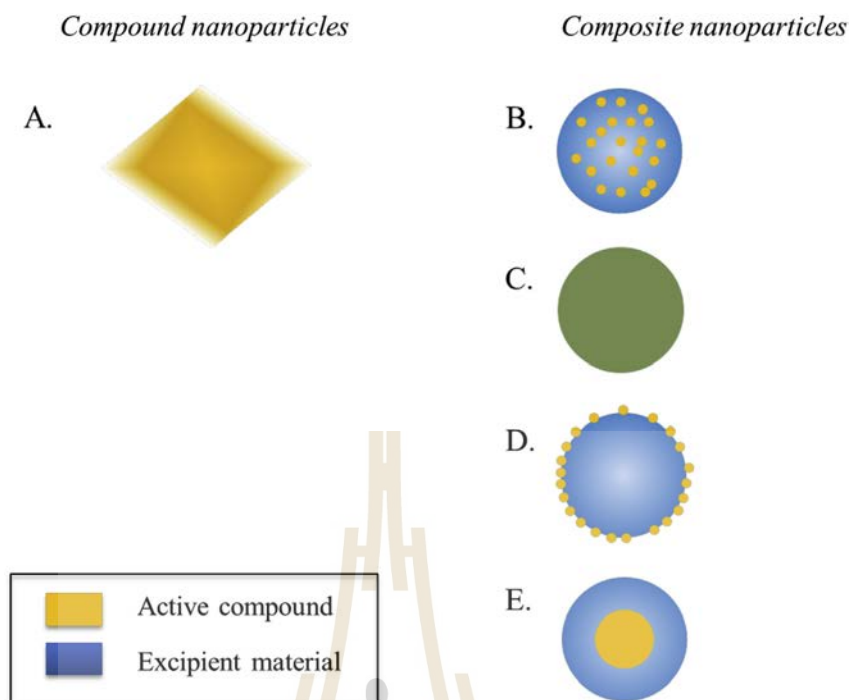


Figure 2.11 Cross sections of different nanoparticle structure.

The nanoparticle can be composed of pure compound of interest (A: Compound particle) or contain an excipient matrix material, in which the active compound is enclosed as a colloidal (B: Dispersion composite), or molecular dispersion (C: Molecular composite), or at which surface it is adsorbed (D) and structure is core which consists of the compound of interest, which is protected by a surface layer composed of the excipient material (E). (The structure B-E are typical examples of composite particles) (Joye & McClements, 2013).

2.5 Oral administration

Oral administration is the most used method of administration due to its convenience and injury-free. Generally, most of the medication is absorbed in the small intestine. For oral absorption of the drug, there are prerequisites: The drug must be dissolved before it reaches the point of action because only the dissolved drug can be absorbed through the gastrointestinal (GI) membrane and then into the blood flow and to the point of action. as shown in Figure 2.12.

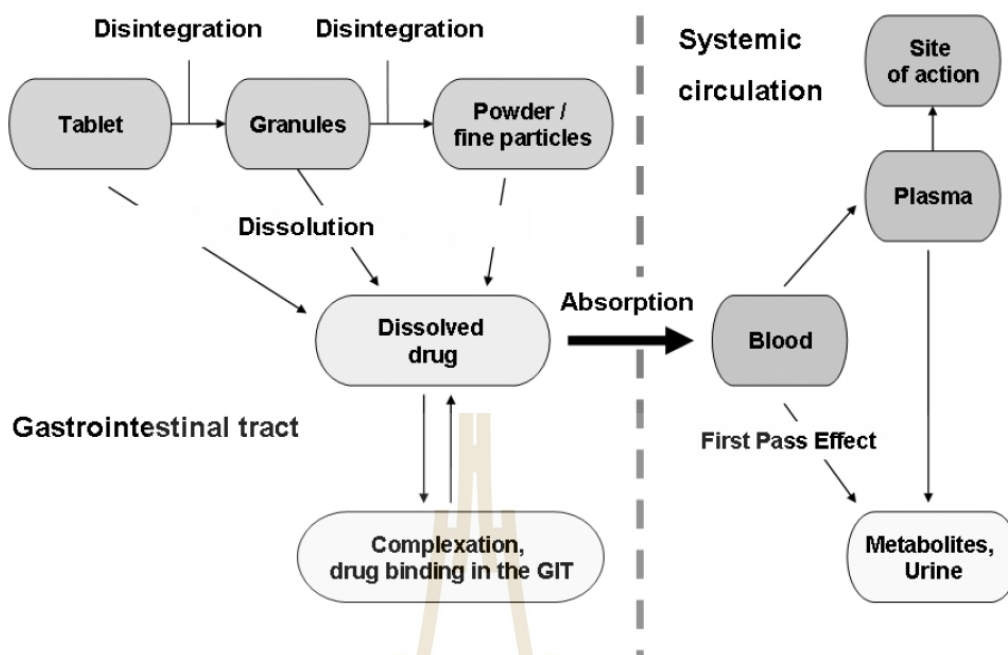


Figure 2.12 Schematic representation of the processes involved in the dissolution and absorption process of a drug after oral administration (Klein, 2009).

2.5.1 Factors Affecting Gastrointestinal Absorption

Gastrointestinal motility: The function of the gastrointestinal tract affects the speed of absorption because the faster the drug travels to the small intestine, the faster the drug is absorbed.

Splanchnic blood flow: Some drug needs to be taken after meals because eating increases blood flow, which, if the blood flow is good, the absorption of the drug is good.

Particle size and formulation: Particle size and formulation are important for drug absorption because if the drug is the same drug but the dose is different, the absorption of the drug will also differ.

Physicochemical factor: The intake of certain foods and medications can affect the absorption of other drugs.

Due to the factors affecting drug absorption, it must take into account the design of the dosage form and the size of the drug to be appropriate for the purpose of the drug and must take into account the GI parameter as shown in Figure 2.13. Table 2.5 summarizes the processes and important parameters in different parts of the human digestive tract. However, in addition to the factors affecting absorption,

it is important to choose a protective material as some drugs are also sensitive to the environment in the human body. (Klein, 2009; Sasima & Rattanaporn, 2011).

Table 2.5 Segments of the GI tract and their corresponding functions (Klein, 2009)

Organ	Main process	Secretion/ Enzymes	pH
Mouth	Mechanical digestion of food (chewing, grinding)	Amylase (is saliva)	-
Esophagus	Passage of food from mouth through stomach	-	-
Stomach	Storage and mechanical digestion of food Start of chemical digestion (Pepsinogen secretion and activation) Reduction of the number of bacteria	Pepsinogen ↓ HCl Pepsin	1.3 Fasted 4.7 fed
Small intestine	Continuation and completion of chemical digestion of carbohydrates, protein & lipids adsorption of small soluble nutrients	Pancreatic juice Intestinal juice Bile	pH-gradient along the SI ≈ 5 - 7.5
Large intestine (Colon)	Water absorption from indigestible feces (proximal) (distal)		Proximal 5-7 Distal ≈7

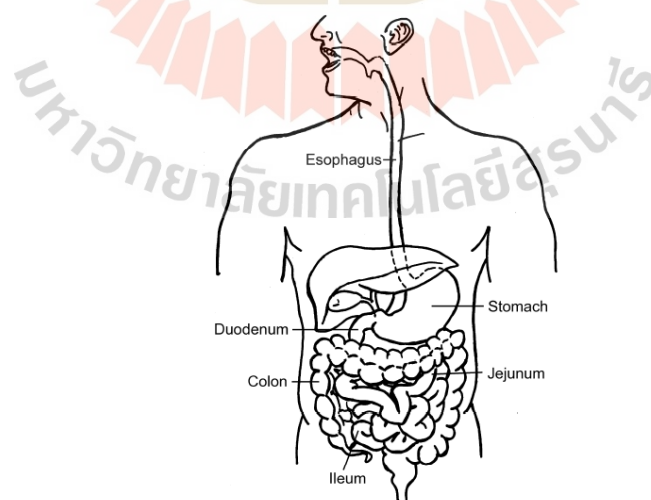


Figure 2.13 Anatomy of the human GI-tract relevant for oral drug absorption (Klein, 2009)

2.6 Conclusion

From the literature review, it was found that papain is an enzyme that has a wide range of benefits across various industries. However, papain also presents certain limitations for practical applications, particularly for oral drug delivery and during storage or processing. One way to eliminate these limitations is through encapsulation. Encapsulation can be done using a variety of methods, but this research chose the anti-solvent precipitation method because it is simple, fast, and can be performed without the need for many tools or chemicals. Importantly, it is convenient for scaling up to industrial levels. Regarding the materials used for encapsulation, there are various materials available. One particularly interesting material is cassava starch, which is abundantly produced in Thailand and cassava production is mostly located in Northeastern Thailand. The aim is to increase its value and benefits beyond just its traditional use in cooking. From the literature review, it was found that acetylated starch has been used to encapsulate various substances, including pigments, plant extracts, and drugs. This type of starch was chosen for this research due to its reduced susceptibility to swelling and enzymatic degradation, as well as its ability to prevent retrogradation at low temperatures. However, these properties depend on the degree of substitution (DS) value of the starch. Most research uses this type of starch with a very high DS value, which is not commonly produced in Thailand. Therefore, this study aims to take on the challenge of using acetylated starch with a low DS value, which is commonly produced in Thailand, for encapsulating papain. The goal is to determine whether it can successfully encapsulate papain using the anti-solvent precipitation method. In addition, important parameters for the creation of particles are studied, such as types of anti-solvent, solvent to anti-solvent ratios, papain concentrations, starch concentrations, starch solution volumes and surfactant.

CHAPTER III

RESEARCH METHODOLOGY

This research focuses on the encapsulation of papain using modified cassava starch obtained from industrial plants in Thailand, employing the stepwise anti-solvent precipitation method. The process involves first precipitating papain and then encapsulating the precipitated papain with the modified starch. This chapter outlines the research methodology, covering the research topics, which can be divided into the following steps:

3.1 Research Methodology.

- 1) Design the experimental and research equipment.
- 2) Study the effect of anti-solvent on papain precipitation.
- 3) Study the solubility of papain in water and water/anti-solvent mixture.
- 4) Study and determine the optimum conditions for papain precipitation by investigating the following parameters.
 - Papain concentrations
 - Solvent to anti-solvent volume ratios
 - Type and concentration of surfactants
- 5) Study and determine the optimum condition for papain encapsulation by investigating the following parameters.
 - Starch concentrations
 - Starch solution volumes
 - Type and concentration of surfactants
- 6) Characterize the obtained particles.

3.2 Location of Research

- 1) Equipment Building 1 (F1) at Suranaree University of Technology, Nakhon Ratchasima for experiments.
- 2) Equipment Building 5 (F5) at Suranaree University of Technology, Nakhon Ratchasima for analysis.

3.3 Chemicals and Instruments.

3.3.1 Materials

- 1) Papain was purchased from HIMEDIA, Indian (GRM058, Mw = 23 kDa).
- 2) Acetylated casava starch with DS = 0.037 was supported from Sanguan Wongse Industries Co., Ltd. (SWI).

3.3.2 Chemicals

- 1) Ethanol (GR Grade) 99.9% was purchased from Duksan pure chemical.
- 2) Acetone (Analysis) 99.8% was purchased from Carlo Erba.
- 3) Acetonitrile (Analysis) 99.5% was purchased from Carlo Erba.
- 4) Tween 20 (Extra pure) was purchased from Loba Chemie™
- 5) Tween 80 (Extra pure) was purchased from Loba Chemie™
- 6) L-cysteine hydrochloride monohydrate (GRM046) was purchased from HIMEDIA.
- 7) α -N-benzoyl-L-arginine ethyl ester hydrochloride (BAEE) was purchased from Alfa Aesar
- 8) N α -benzoyl-DL-arginine 4-nitroanilide (BAPNA) was purchased from Sigma-Aldrich
- 9) Ethylenediaminetetraacetic acid (EDTA) was purchased from RCI Labscan
- 10) Deionized water

3.3.3 Equipment

- 1) Magnetic stirrer + Magnetic bar
- 2) Burette 25 ml
- 3) Pipette (1, 5, 10 ml) and micro pipette (1000 μ l).
- 4) Jacketed Reactor (25 and 100 ml)
- 5) Beaker (10, 25, 50, 100 and 250 ml)
- 6) Volumetric flask (10, 50, 100, and 250 ml)
- 7) Cylinder (10, 25, and 50 ml)
- 8) Water bath
- 9) Shaking water bath
- 10) pH meter

- 11) Desiccator
- 12) Oven
- 13) Ultrasonic processor
- 14) Freeze dryer
- 15) Centrifugation
- 16) Vacuum pump
- 17) Buchner funnel and flask set
- 18) Membrane filter 0.2 μm
- 19) Test tube
- 20) Quartz and glass cuvette (3.5 ml)

3.3.4 Measuring and analytical instruments

- 1) Particle characterization.
 - Scanning Electron Microscope (SEM)
 - Field Emission Scanning Electron Microscope (FESEM)
 - Focus Beam Reflectance Measurement (FBRM)
 - Malvern Zetasizer
- 2) Confirmation of present of encapsulation.
 - Fluorescent Spectroscopy
 - Fourier Transform Infrared Spectrometer (FTIR)
- 3) Determining the precipitation yield, encapsulation efficiency, loading capacity and activity.
 - UV-Vis Spectroscopy
 - pH meter

3.4 Solubility Measurement

Papain solubility in water/anti-solvent mixtures at mass fractions of anti-solvent 0, 0.2, 0.4, 0.5, 0.6, and 0.8 was measured using the gravimetric method according to (Kongsamai, Phoumixay, & Wantha, 2020) and (Qureshi, Vyas, & Upadhyay, 2022). The procedure involved adding an excess amount of solid papain into 10 g of the binary solvent mixture (water:anti-solvent) in a jacketed crystallizer maintained at 25 °C. The suspension was stirred at 700 rpm and allowed to equilibrate for at least 24 hours. After equilibration, the suspension was centrifuged at 8000 rpm for 10 minutes to separate the solid papain. The supernatant containing dissolved papain was sampled

and weighed at room temperature. The solvent and anti-solvent were evaporated at 105 °C in a hot air oven, leaving behind the solid residue of papain. The residue was weighed repeatedly until a constant weight was achieved, indicating the complete removal of solvent and anti-solvent. This investigation was used to consider the parameters like optimal anti-solvent and various mass fractions for selecting suitable solvent-to-anti-solvent volume ratio ranges in the effect study.

The solubility of papain was calculated in terms of mass fraction of papain in the solution by Eq. 3.1:

$$X = \frac{\text{mass of papain}}{\text{mass of papain} + \text{mass of water} + \text{mass of ethanol}} \quad (3.1)$$

3.5 Preparation of Standard Curve of Papain

Creating a standard curve for determining the papain concentration involved utilizing various concentrations of papain, and subsequently recording the corresponding absorbance values at 278 nm. This approach allows for the establishment of a reliable relationship between the concentration of papain and its absorbance, providing a basis for accurate quantification in subsequent analyses. This calibration curve was shown in Figure 3.1.

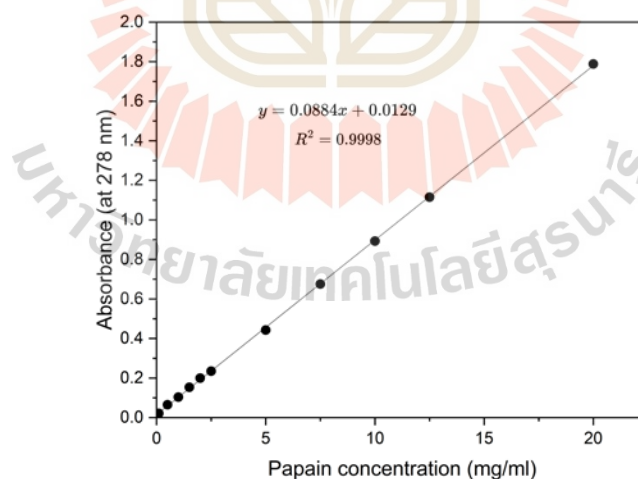


Figure 3.1 Calibration curve of papain.

3.6 Preparation of ACS Solution

The ACS solution was meticulously prepared through two-step preparation involving heating/gelatinization and subsequent ultrasonication, following a well-

established method (Chang et al., 2017; Dong, Chen, Zhang, Gao, & Vasanthan, 2021; Dong, Zhang, Gao, Chen, & Vasanthan, 2022). The procedure for preparation of starch solution is as follows:

- 1) 5 g of dry ACS was dispersed in DI water to get 100 mg/ml.
- 2) The dispersion underwent gelatinization in a shaking water bath at 90 °C for 30 minutes, with the shaking set at 180 rpm.
- 3) The gelatinized starch paste was cooled to approximately 60 °C.
- 4) The cooled starch paste was then subjected to ultrasonication for 10 minutes using a kHz ultrasonic processor (Branson SFX250 Digital Sonifier, Branson Ultrasonics, USA) equipped with a probe transducer with a flat tip of 1/2" (13 mm) at 60% amplitude with a pulse function (5/2s on/off) to minimize heat generation.
- 5) The homogeneous starch solution was further diluted to concentrations of 10, 15, 30, and 60 mg/ml in preparation for the subsequent encapsulation process.

3.7 Papain Precipitation

The precipitation of papain is a crucial step in the encapsulation process using the stepwise anti-solvent precipitation method, which has been adapted from two-step anti-solvent precipitation (Morales-Cruz et al., 2012; Nelemans et al., 2020) and step wise anti-solvent precipitation (Yang et al., 2018) The steps for the precipitation of papain are as follows:

- 1) Preparation of papain solution by dissolving papain in DI water to obtain a solution at different concentration (10, 15, 20, 25, 30, 35 mg/ml).
- 2) Anti-solvent (acetone, ethanol, and acetonitrile) was added to the papain solution in various solvent-to-anti-solvent volution ratios (1:1, 1:4, 1:6 and 1:8).
- 3) Leave it for 5 minutes to allow papain to precipitate. Then papain suspension was obtained.
- 4) The resulting suspension underwent analysis to determine particle size, size distribution, polydispersity index, and zeta potential by zetazizer.
- 5) The papain particles were separated from the remaining solution by centrifugation and then freeze dried at -45 °C for 15-20 hr.
- 6) The papain particles were then characterized to determine the enzyme activity by amidase method or titration of hydrolysis of α -N-benzoyl-L-arginine ethyl ester hydrochloride (BAEE) method and morphology by Field Emission Scanning

Electron Microscope (FE-SEM), while the supernatant was utilized to determine the precipitation yield.

3.8 Papain Encapsulation

After determining the optimal conditions for papain precipitation, the encapsulation of the precipitated papain with ACS proceeds as follows:

- 1) Add surfactants (Tween 20 and Tween 80) to the anti-solvent used for papain precipitation at varying surfactant concentrations (1%, 2%, and 3% v/v) to prevent starch aggregation.
- 2) Add acetylated cassava starch (ACS) solutions at different concentrations (10, 15, 30, and 60 mg/ml) and volumes (1, 3, and 7 ml) to the papain suspension obtained from step 1).
- 3) Stir the mixture for 30 minutes at 500 rpm to achieve a homogenous dispersion.
- 4) Homogenize the mixture using a homogenizer at 8000 rpm for 1 minute to facilitate the settling of fine particles. At this step, obtain ACS/Papain composites dispersions for analysis using fluorescent spectroscopy.
- 5) Collect the resulting sediments by centrifugation (BKC-TH16RII, BIOBASE) for 10 minutes at 3000 rpm.
- 6) Wash the ACS/Papain composites with ethanol to dehydrate them. After that, filter the mixture using a 0.25 μm membrane with a vacuum pump and dry the resulting composites in a desiccator to remove any remaining moisture.
- 7) Analyze the dry composites using Fourier-transform infrared spectroscopy (FTIR) and scanning electron microscopy (SEM) to confirm encapsulation and determine morphology.

3.9 Papain Precipitate Characteristics

3.9.1 Precipitation Yield (%)

The papain suspension was centrifuged at 8000 rpm for 10 minutes (BKC-TH16RD, BIOBASE), and the supernatant was collected and measured its absorbance at 278 nm using UV-visible spectroscopy (DR6000, Hach) to determine the remaining papain concentration, quantified using a prepared calibration curve (Figure 3.1). The yield of nanoparticle formation was then calculated using the following equation:

$$\text{Precipitation Yield (\%)} = \frac{W_1 - W_2}{W_1} \times 100\% \quad (3.2)$$

Where W_1 is the total amount of papain used and W_2 is the amount of dissolved papain remaining in supernatant.

3.9.2 Dynamic light scattering

Dynamic light scattering is a technique used to measure the size in the nano-scale range (1-1000 nm), polydispersity index (PDI), and zeta potential of papain particles in the suspension obtained from precipitation, utilizing laser light scattering dispersion analysis. The procedure involves:

- 1) Dilute the papain suspension obtained from section 3.8 by a factor of 50 with a water-ethanol mixture used for precipitation.
- 2) Transfer 1 ml of the diluted suspension into a 3.5 ml plastic cuvette, as shown in Figure 3.2a, for particle size and polydispersity index (PDI) measurements. For zeta potential measurements, use a U-shaped cuvette as depicted in Figure 3.2b.
- 3) Place the cuvette into the Zetasizer instrument (Nano ZS, Malvern Instruments, Worcestershire, U.K.), as illustrated in Figure 3.3.
- 4) Before initiating the measurements, adjust the refractive index (RI) of papain, viscosity, and dielectric constant of the solvent each time when changing the experimental conditions. The analysis should be conducted at a scattering angle of 173° in a temperature-regulated cell at 298.15 K.

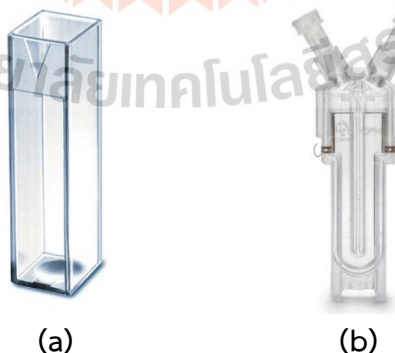


Figure 3.2 Cuvette for Zetasizer (Nano ZS, Malvern Instruments, Worcestershire, U.K.)
(a) plastic cuvette and (b) U-shaped cuvette.

(Ref: a. <https://www.atascientific.com.au/products/zetasizer-ultra/> and b. <https://www.spectralinstrument.com/15487693/cuvettes-cells>)



Figure 3.3 Zetasizer (Nano ZS, Malvern Instruments, Worcestershire, U.K.)

(Ref: <https://www.americanpharmaceuticalreview.com/25604-Pharmaceutical-Particle-Size-Analyzers/12040043-Zetasizer-Nano-ZS-Size-Analyzer/>)

3.9.3 Morphology

For the morphology analysis of papain nanoparticles, field emission scanning electron microscopy (FE-SEM) was utilized. This technique employs a focused beam of electrons to interact with the surface of the sample, generating various signals that are then converted into images. The analysis procedure involves sample preparation and analysis steps as follows:

- 1) Cut the carbon tape (Figure 3.4a) into small pieces and affix them onto stubs (Figure 3.4b). Ensure that the sample numbers are clearly labeled.
- 2) Sprinkle papain nanoparticles onto the carbon tape affixed to the stub. Remove excess powder with a rubber dust blower (Figure 3.4c) from the sides to ensure that the nanoparticles remain firmly attached to the carbon tape during analysis.
- 3) Coat the prepared samples with carbon to prevent charging and ensure good electrical conductivity, which is necessary for obtaining clear images. This step helps prevent image distortion due to sample charging during analysis.
- 4) Insert the coated sample into the analysis chamber of the FE-SEM JEOL JSM-7800F model, as shown in Figure 3.5, and begin imaging using an accelerating voltage of 3 kV.

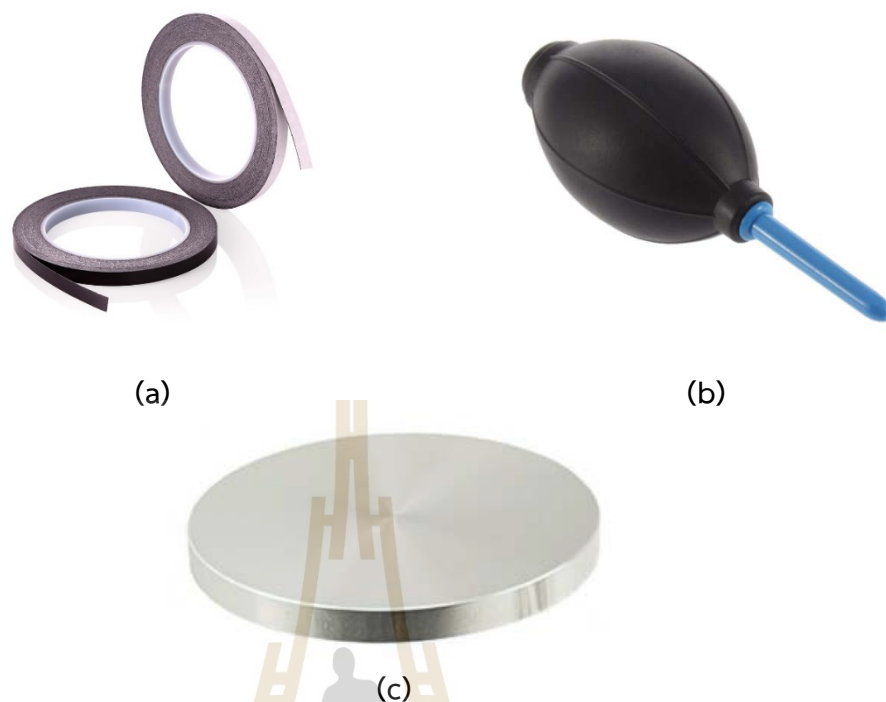


Figure 3.4 Equipment for sample preparation before SEM analysis. (a) Carbon Tape, (b) Rubber Dust Blower and (c) Stub.

(Ref: (a) <https://www.techinstro.com/shop/carbon-tape/carbon-tape/> (b) <https://www.amazon.com/YUOCU-Cleaner-Compatible-Keyboard-Computer/dp/B07FL8ZG86> and (c) <https://www.labtech.com/em/hitachi-m4-sem-specimen-stubs-and-mounts>)



Figure 3.5 JSM-7800F Schottky Field Emission Scanning Electron Microscope.

(Ref: <https://www.jeol.com/products/scientific/sem/JSM-7800F.php>)

3.10 ACS/Papain Composites Characteristics

3.10.1 Encapsulation efficiency (EE) and loading capacity (LC)

The encapsulation efficiency (EE) and loading capacity (LC) of the ACS/papain composites were evaluated by measuring the absorbance of free papain in the collected solution at 278 nm using a spectrophotometer (DR6000, Hach, USA). Simultaneously, a blank sample, consisting of composites devoid of papain but possessing an identical composition to the test sample, was prepared, and subjected to the same procedure as the test sample. This step aimed to mitigate potential contributions from other components to the absorbance readings. Subsequently, the papain content was quantified against the standard calibration curve of papain in DI water (Figure 3.1). EE and LC of papain were calculated using the following equations:

$$EE (\%) = \frac{\text{Total papain added} - \text{Free papain}}{\text{Total papain added}} \times 100\% \quad (3.3)$$

$$LC (\%) = \frac{\text{Total papain added} - \text{Free papain}}{\text{Weight of composites}} \times 100\% \quad (3.4)$$

The method for quantifying the amount of free papain (unencapsulated papain) varied based on the volume of starch solution used in the encapsulation process. For starch solution volumes of 1 and 3 ml, the free papain was quantified by combining the free papain in the supernatant with the free papain obtained by twice washing the dried precipitate with an ethanol solution (1:1 water: ethanol with surfactant). Conversely, for a starch solution volume of 7 ml, only the supernatant obtained after centrifugation was utilized to determine the amount of free papain.

3.10.2 Fluorescence analysis

To assess the encapsulation of papain within starch, both papain and papain-loaded starch particles were subjected to analysis using a fluorescence spectrometer (FP-8300, JASCO Corp., Japan), as illustrated in Figure 3.6. Fluorescence spectrometry is a technique employed to quantify the intensity of fluorescent light emitted from a sample upon excitation with a specific wavelength of light. During the process, when a molecule absorbs light at a particular wavelength (excitation), it becomes excited and subsequently emits light at a longer wavelength (emission). The disparity in wavelength between the absorbed and emitted light is termed the Stokes shift. Fluorescence spectra of pure papain (1 mg papain dissolved in 1 ml of DI water

and then mixed with 8 mL ethanol), and ACS/Papain composite dispersions were recorded. Excitation was initiated at 280 nm, and the emission spectra were collected within the range of 290 nm to 450 nm employing a quartz cell with a 10 mm path length. Both the excitation and emission bandwidths were set at 5 nm. All data were gathered at room temperature.

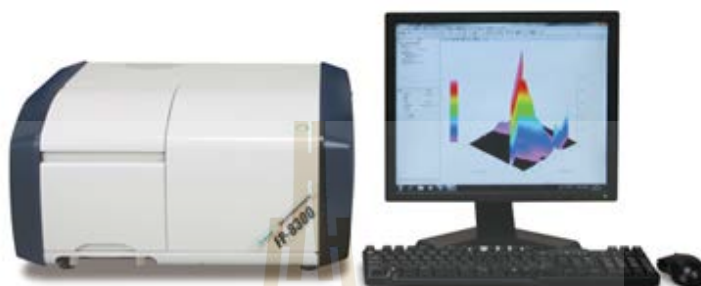


Figure 3.6 FP-8300 Spectrofluorometer.

(Ref: <https://www.jascoint.co.jp/asia/products/spectroscopy/fluorescence/fp8300.html>)

3.10.3 Fourier transform infrared (FTIR) analysis.

Fourier-transform infrared spectroscopy (FTIR) was employed to analyze the functional groups on the surface by observing the energy absorbed and transmitted by the sample using infrared radiation. The characteristic peaks appearing at different wave numbers (cm^{-1}) correspond to the functional groups of the substance. The analysis was conducted using a Bruker Tensor 27 with an Attenuated Total Reflectance (ATR) accessory, featuring a KBr sample holder as shown in Figure 3.7. The sample powder was placed on the KBr sample holder, and the analysis was carried out in the wave number range of $4000\text{--}400\text{ cm}^{-1}$ with a resolution of 2 cm^{-1} .



Figure 3.7 Bruker Tensor 27 with an Attenuated Total Reflectance (ATR) accessory.

(Ref: <https://de.wikipedia.org/wiki/Datei:Bruker-Tensor-27.jpg>)

3.10.4 Morphology

For the morphology analysis of ACS/Papain composites, scanning electron microscopy (SEM) was utilized. The experimental procedure is similar to that described in section 3.9.3, but with the following modifications: the samples were coated with gold instead of carbon and began imaging using SEM JEOL JSM-6010LV model (Figure 3.8) at an accelerating voltage of 10 kV.



Figure 3.8 JEOL JSM-6010LV Scanning Electron Microscope.

(Ref: https://th.jeol.com/products/scientific/sem/JSM-6010PLUS_LA.php)

3.11 Residual Activity (%)

The evaluation of enzyme activity, based on Arnon Ruth's methodology (1970) (Arnon, 1970; Moreno-Cortez et al., 2015), involved the utilization of two distinct substrates: α -N-benzoyl-L-arginine ethyl ester hydrochloride (BAEE) and $N\alpha$ -benzoyl-DL-arginine 4-nitroanilide (BAPNA).

3.11.1 α -N-benzoyl-L-arginine ethyl ester hydrochloride (BAEE) method

Principle:



Reagents:

A. 80 mM $N\alpha$ -Benzoyl-L-Arginine Ethyl Ester (BAEE) in deionized water.

- B. 20 mM Ethylenediaminetetraacetic acid (EDTA) in deionized water.
- C. 50 mM L-Cysteine, pH 6.2 at 25 °C in reagent B adjust pH to 6.2 by 1 M NaOH.
- D. 3 M Sodium Chloride solution (NaCl) in deionized water.
- E. 20 mM Sodium Hydroxide Titrant, Standardized in deionized water.
- F. Papain solution 5 mg/ml in cold deionized water.

Procedure:

The pH-stat method was employed at 25°C. The reaction mixture contained 7 ml of substrate solution (Reagent A), 1 ml of activators (Reagent C), and 1 ml of NaCl (Reagent D) adjusted to pH 6.3. Subsequently, either 1 ml of free-papain solution (Reagent F) or papain sample solution was added, and the pH was monitored until it reached 6.2. To maintain pH 6.2, 20 mM NaOH was added, and the time taken to consume 50 µl of 20 mM NaOH was recorded.

Units: One unit of enzyme activity is defined as the amount that hydrolyzes 1 µmole of BAEE per minute at 25°C.

Specific Activity: Specific activity is expressed as the number of enzyme units per milligram of protein.

Calculation:

$$\text{Activity (Units/ml enzyme)} = \frac{(0.05)(\text{Normality of NaOH})(1000)(df)}{(T)(1)} \quad (3.5)$$

$$\text{Specific activity (Units/mg enzyme)} = \frac{\text{Activity (Units/ml enzyme)}}{\text{Concentration (mg enzyme/ml enzyme)}} \quad (3.6)$$

Where 0.05 = Volume of Reagent E used to maintain the pH at 6.2 (ml)

1000 = Conversion from mmole to µmole

df = dilution factor

T = Time required to maintain the pH at 6.2 per 50 µl aliquot (min)

3.11.2 $N\alpha$ -benzoyl-DL-arginine 4-nitroanilide (BAPNA) method (Amidase method)

Reagents:

Substrate: 43.5 mg of benzoyl-DL-arginine-p-nitroanilide hydrochloride were dissolved in 1 ml of dimethyl sulfoxide (DMSO) and the volume was adjusted to 100 ml with 0.05 M Tris buffer pH 7.5 containing 0.005 M Cysteine and 0.002 M EDTA. The solution should be kept at above 25 °C.

Acid: 30%wt Acetic acid

Enzyme: Papain solution was prepared by dissolving papain precipitate in deionized water at 5 mg/ml.

Procedure:

1 ml of free-papain solution (5 mg/ml) or papain samples solution were placed into test tubes, followed by the addition of 5 ml of substrate solution. The mixtures were incubated for 25 minutes at 25°C, after which the enzymatic reaction was halted by adding 1 ml of 30% acetic acid. The liberated p-nitroaniline was quantified using spectrophotometric analysis at 410 nm (SP-UV 200, Spectrum Instruments). Control tubes without enzymes confirmed the absence of self-hydrolysis.

Units: The amount of substrate hydrolyzed by the enzyme is calculated based on the molar extinction of p-nitroaniline at 410 nm ($E = 8800$). One unit of BAPNA activity is defined as the amount of enzyme that hydrolyzes 1 micromole of substrate per minute under the specified conditions.

Specific Activity: Specific activity is expressed as the number of units per milligram of protein.

Calculation:

$$\text{BAPNA units} = \frac{A_{410\text{nm}}}{t} \times \frac{3 \times 1000}{8800} \quad (3.7)$$

$$\text{Specific activity (Units/mg enzyme)} = \frac{\text{BAPNA units}}{\text{Concentration (mg enzyme/ml enzyme)}} \quad (3.8)$$

where $A_{410\text{nm}}$ is absorbance at 410 nm, t is the time in minutes, which is the duration of the enzymatic reaction and $8800 \text{ M}^{-1}\text{cm}^{-1}$ is the p-nitroanilide molar extinction coefficient at 410 nm. Specific activity is expressed as units per milligram of protein.

CHAPTER IV

RESULTS AND DISCUSSION

This chapter discusses the results of the study on two main processes. The first process is the precipitation of papain using an anti-solvent. This process examines the effect of anti-solvent type, solvent-to-anti-solvent volume ratios, and papain concentration on precipitation yield, particle size, polydispersity index (PDI), zeta potential, residual activity, and morphology of papain particles. The second process involves encapsulating the precipitated papain obtained from the first process with a modified starch called acetylated starch, derived from cassava starch. This study investigates the effects of surfactant type and concentration, starch concentration, and volume of starch solution on encapsulation efficiency, loading capacity, residual activity, and morphology. Additionally, Fourier Transform Infrared Spectroscopy (FTIR) and fluorescence spectrometry were used to study the encapsulation of papain with starch, to confirm whether the encapsulation process was successful.

4.1 Papain Precipitation

4.1.1 The effect of anti-solvent types

The selection of an appropriate anti-solvent in the precipitation process of papain holds paramount importance due to its profound impact on the resultant particles' characteristics and the activity of the enzyme. Ensuring optimal control over particle size and morphology, maintaining the purity of the obtained papain, and influencing the overall efficiency and safety of the manufacturing process are all critical aspects directly influenced by the choice of anti-solvent. Thus, the initial consideration in the precipitation process revolves around selecting the most suitable type of anti-solvent. Papain's solubility in water at 25 °C is notably high, causing the solution to become highly viscous as papain dissolves. This high solubility made water the solvent of choice for papain precipitation. In conducting experiments to determine the most effective anti-solvent, three organic solvents—namely acetone, acetonitrile, and ethanol—were carefully selected. These solvents are widely acknowledged for their capability to induce protein precipitation, thus providing a promising avenue for

effectively separating papain from the solution. In the experiment, the anti-solvent was added to the papain solution at a concentration of 25 mg/ml, maintaining a solvent-to-anti-solvent volume ratio of 1:4. This addition process was facilitated using a burette with free-flow capabilities, ensuring precision with a flow rate of 1.22 ± 0.052 ml/s. Subsequently, the mixture was subjected to stirring for 5 minutes to ensure thorough mixing and interaction between the components. The results of the experiments revealed that acetonitrile exhibited the highest yield in precipitating papain from the aqueous solution, followed by acetone and ethanol, as illustrated in Table 4.1. However, upon closer examination of the precipitated papain, it was observed that acetonitrile induced a noticeable discoloration in the resultant product (Figure 4.1(b)). Furthermore, the particles produced using acetonitrile displayed a sticky consistency and tendency to adhere to the container walls, thereby complicating the determination of the enzyme's activity. This makes acetonitrile unsuitable for effective papain precipitation.

Acetone, while resulting in a higher precipitation yield than ethanol, also produced sticky particles with lower residual activity (Table 4.1). This stickiness compromised the practical handling and quality of the precipitated enzyme. On the other hand, ethanol, despite having a slightly lower precipitation yield compared to acetone, preserved the enzymatic activity more effectively and produced more manageable particles. Considering both the precipitation yield and the preservation of enzymatic activity, ethanol emerged as the most suitable anti-solvent among the tested options. Additionally, from an environmental perspective, ethanol is preferable as it is a less hazardous organic solvent compared to acetone and acetonitrile. Ethanol's lower toxicity and environmental impact further justify its selection for this process (Capello, Fischer, & Hungerbühler, 2007). In conclusion, while acetonitrile and acetone have their advantages in terms of precipitation yield, ethanol stands out as the optimal anti-solvent for papain precipitation due to its ability to maintain the enzyme's activity, produce manageable particles, and offer a safer and more environmentally friendly option.

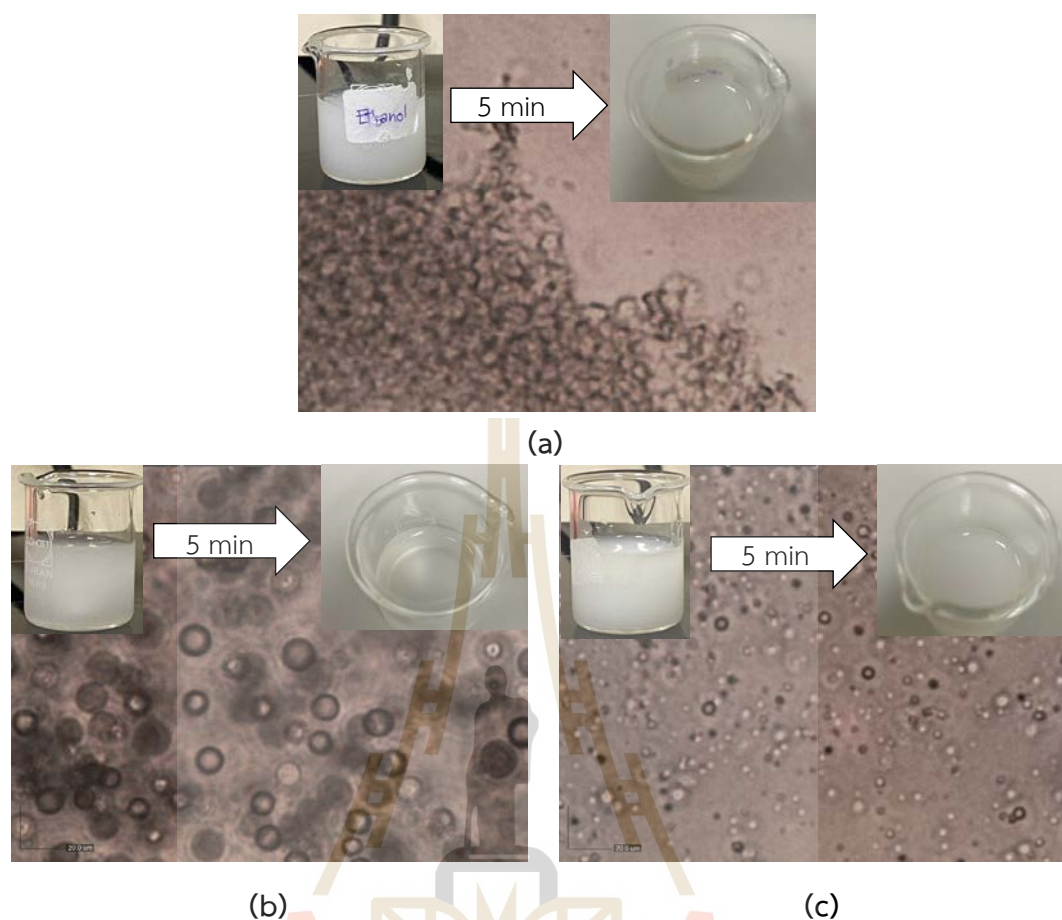


Figure 4.1 Photomicrographs of papain crystals obtained using different anti-solvent types: (a) ethanol, (b) acetonitrile, and (c) acetone.

Table 4.1 Residual activity of papain precipitate¹ and crystallization yield (%) at different anti-solvent types. *

Anti-solvent	Crystallization yield (%)	Residual activity (%)
Acetonitrile	98.67 ± 1.15	N/A**
Acetone	89.33 ± 2.31	25.16 ± 5.47
Ethanol	80.10 ± 9.33	82.47 ± 7.00

*Papain concentration: 25 mg/ml, volume ratio of solvent to anti-solvent: 1:4

**Can't find the value

¹Using amidase method (N α -benzoyl-DL-arginine 4-nitroanilide (BAPNA) as substrate)

4.1.2 The effect of solvent-to-anti-solvent volume ratios

The experiment explores papain's solubility in a water-ethanol mixture (Figure 4.2). It reveals that increasing ethanol content decreases papain solubility. This confirms ethanol's effectiveness as an anti-solvent, as it reduces papain solubility and

promotes precipitation. However, at mass fractions of 0 and 0.2, determining solubility is challenging as papain continued to dissolve, resulting in a viscous, sticky solution. Hence, anti-solvent addition at these ratios is deemed unsuitable for papain precipitation. Solubility determination becomes feasible from a mass fraction of 0.4 onwards, prompting the study to focus on mass fractions from 0.4 and above, corresponding to an approximate 1:1 volume ratio of water to ethanol.

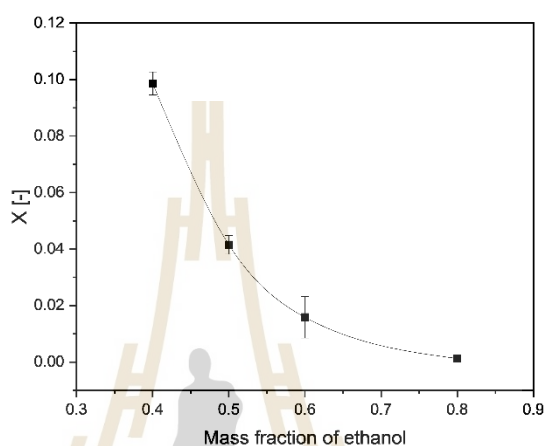


Figure 4.2 Solubility of papain in water/ethanol mixture at 25 °C.

The study explored different solvent-to-anti-solvent volume ratios—1:1, 1:2, 1:4, 1:6, and 1:8—to assess the impact of varying ethanol amounts on papain precipitation. Papain particles were generated by introducing different volumes of ethanol (as the anti-solvent) to a papain solution (concentration: 25 mg/ml) using a burette with free flow. Following anti-solvent addition, continuous stirring was sustained for 5 minutes.

Visual analysis of Figure 4.3(b) clearly indicates that varying solvent-to-anti-solvent ratios result in distinct differences in the suspended solutions' turbidity. This change is likely due to variations in particle number, particle size, and size distribution. Figures 4.3(a) and 4.3(b) illustrate that at ratios ranging from 1:1 to 1:4, particles present a uniform dispersion in the suspended solution without apparent agglomeration or larger particles. However, at ratios of 1:6 and 1:8, noticeable particle aggregation or the formation of larger particles occurred, confirmed by the multiple peaks in Figure 4.3(a). A smaller peak indicates the presence of aggregated or larger particles. This phenomenon is likely due to rapid supersaturation induced by molecular dehydration under high solvent-to-anti-solvent volume ratios.

Figure 4.3(d) shows that the solvent-to-anti-solvent volume ratios influence the zeta potential. As the solvent-to-anti-solvent volume ratios increases from 1:1 to 1:8, the zeta potential also increases from 10.8 to 40.1 mV. Zeta potential values greater than or equal to ± 30 mV indicate good colloidal stability (Jahanshahi & Babaei, 2008; Mahajan & Ramana, 2014). The zeta potential values for ratios of 1:1 and 1:2 are lower than the range associated with stable suspensions. From a ratio of 1:4 onwards, the suspension exhibited higher stability, as indicated by zeta potential values within the stable range.

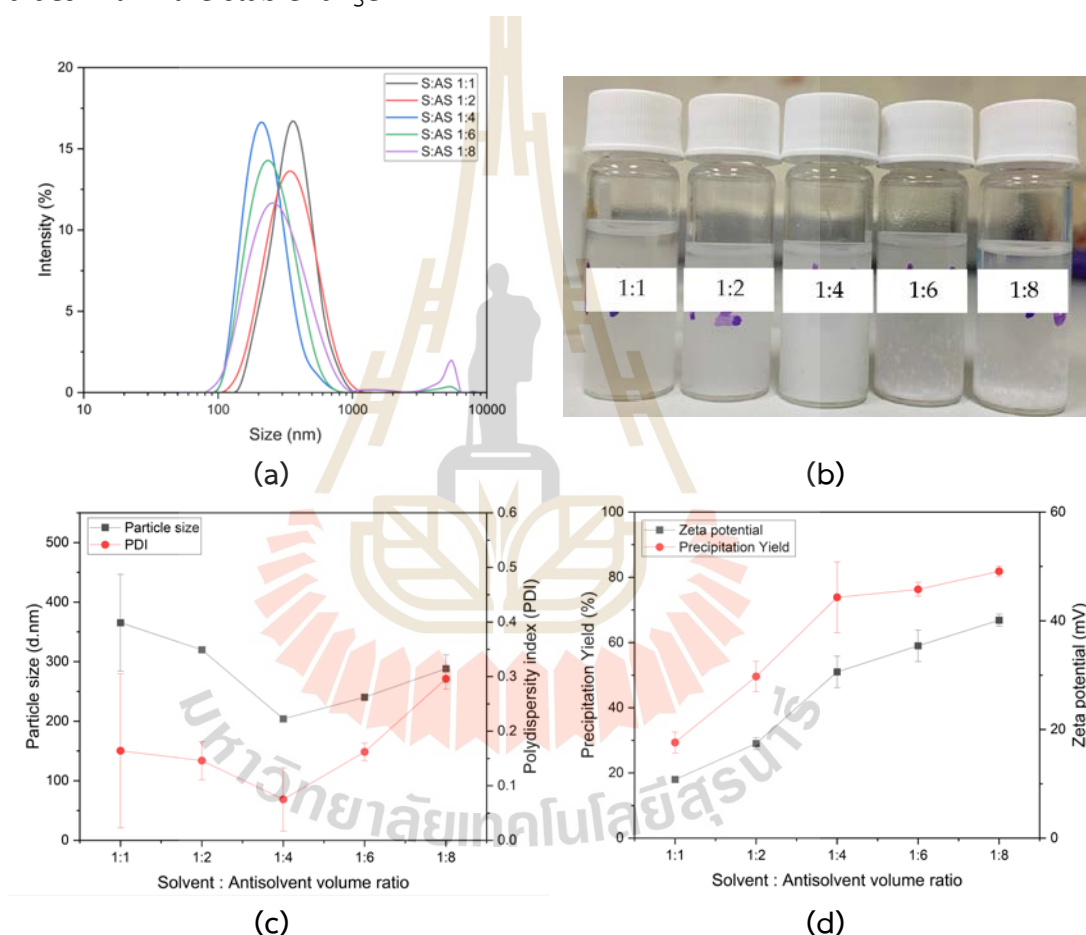


Figure 4.3 The effect of S:AS volume ratios: (a) particle size distribution, (b) photograph of the suspensions formed after mixing ethanol with papain solution, (c) z-average mean particle size (back line) and polydispersity index (PDI) (red line), (d) precipitation yield (red line) and zeta potential (back line) of particles with papain concentration of 25 mg/ml at different S:AS ratios.

The relationship between the volume of ethanol used and the precipitation yield is evident. With an increase in ethanol volume (from 1:1 to 1:8), the

precipitation yield also rises, ranging from 29.33% to 81.83%. Within the stable suspension range of 1:4 to 1:8, the precipitation yield remains consistently high, around 70-80%. Particle sizes obtained at ratios of 1:1, 1:2, 1:4, 1:6, and 1:8 were in the nanoparticle range, with average sizes of 365.4 nm, 320 nm, 204 nm, 240.3 nm, and 288.3 nm, respectively. The polydispersity index (PDI), reflecting particle size distribution, was lowest (PDI = 0.075) at a ratio of 1:4 as shown in Figure 4.3(a). This indicates that at a 1:4 ratio, particle size distribution is narrower, and more uniform compared to other ratios.

In conclusion, the experiment demonstrates that papain nanoparticles can be effectively produced using a solvent-to-anti-solvent ratio of 1:4, which provides the most suitable conditions for achieving the desired particle characteristics. This ratio ensures a high precipitation yield, stable suspension, and a narrow, uniform particle size distribution. Importantly, this favorable outcome was achieved without the need for excessive amounts of anti-solvent. Ethanol, as an anti-solvent, proves to be effective in facilitating papain precipitation under these optimal conditions, offering a practical and efficient approach for producing high-quality papain nanoparticles.

4.1.3 The effect of papain concentrations

The concentration of papain plays a critical role in the solution precipitation process. To explore its effects on particle size, distribution, zeta potential, and precipitation yield, six different papain concentrations were investigated: 10, 15, 20, 25, 30, and 35 mg/ml. Ethanol served as the anti-solvent at a volume ratio of 1:4 (solvent-to-anti-solvent) and was added to the papain solution using a burette with free flow.

Figure 4.4(a) reveals a noteworthy trend: as the concentration of papain increases, there is a significant rise in the average particle size, ranging from 170.3 nm at 10 mg/ml to 211.4 nm at 35 mg/ml. This observes correlation between papain concentration and particle size aligns with the previously discussed explanation: heightened viscosity due to increased papain concentration hampers effective diffusion between the solvent and anti-solvent. This disruption in diffusion causes non-uniform supersaturation, subsequently slowing down the nucleation rate and fostering particle aggregation, ultimately leading to larger particle sizes (Joye & McClements, 2013).

Regarding particle size distribution, both Figures 4.4(a) and 4.4(c) demonstrate a consistent pattern: at every concentration, there exists a narrow size

distribution, indicate by low polydispersity index (PDI) values, with sizes falling within a closely aligned range. This indicates that variations in papain concentration do not significantly impact the particle size distribution. The particles maintain a relatively uniform size across different concentrations, suggesting that the precipitation process is consistent in terms of size distribution regardless of papain concentration.

In terms of precipitation yield (Figure 4.4(b)), in the initial concentration range of 10-15 mg/ml, an increase in concentration resulted in a corresponding increase in yield, from 63.81% to 79.29%. However, beyond 15 mg/ml, the yield values remained relatively constant, hovering around 80%. This plateau suggests that there is a limit to how much increasing the concentration can affect the yield, likely due to reaching an optimal supersaturation point for efficient precipitation.

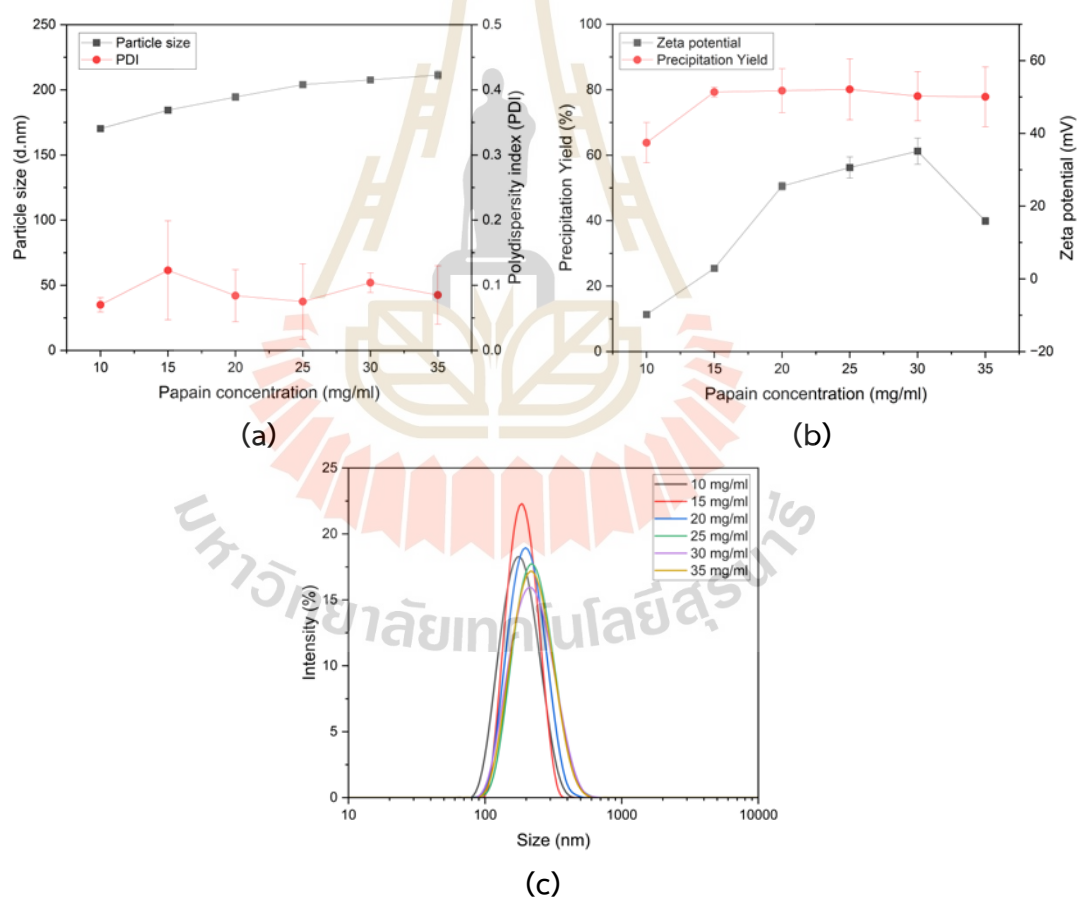


Figure 4.4 The effect of papain concentrations: (a) z-average mean particle size (back line) and polydispersity index (PDI) (red line), (b) precipitation yield (red line) and zeta potential (back line), and (c) particle size distribution of particles with papain concentration of 25 mg/ml at different AS:S ratios.

Regarding zeta potential, Figure 4.4(b) illustrates that the concentration of papain influences an increase in zeta potential from 10 mg/ml (-9.8 mV) to 30 mg/ml (35.1 mV), followed by a decrease at 35 mg/ml (15.9 mV). These values signify the stability of the formed colloids, with higher zeta potential values indicating better colloidal stability by reducing particle attraction and lowering aggregation (Jahanshahi & Babaei, 2008; Mahajan & Ramana, 2014). Consequently, at a concentration of 30 mg/ml, the suspension displays the highest stability, as indicated by the highest zeta potential value (35.1 mV). Furthermore, this concentration corresponds to the point where residual activity is highest (Table 4.2), suggesting that this concentration is optimal for maintaining both stability and enzymatic activity.

Table 4.2 Residual activity of papain precipitate at different papain concentration (25-35 mg/ml).¹

Concentration (mg/ml)	Residual activity (%)
25	89.68 ± 0.57
30	100.00 ± 6.55
35	90.87 ± 2.66

¹Using titration of the rate of hydrolysis of α -N-benzoyl-L-arginine ethyl ester hydrochloride (BAEE) method.

4.1.4 Scanning electron microscopy (SEM) analysis

Figure 4.5 showcases the morphology of papain particles using Field Emission Scanning Electron Microscopy (FE-SEM). The FE-SEM images depict papain particles with a spherical shape, while aggregated papain does not exhibit distinct shapes. In contrast, commercially papain particles (unprocessed) form crystals with irregular shapes. These images offer further confirmation that anti-solvent precipitation yields nanoparticles. Additionally, compare to commercially papain particles (unprocessed), anti-solvent precipitation in this study exhibits improved crystal quality, with obtained crystals displaying perfect spherical shapes and retaining enzymatic activity.

4.2 Papain Encapsulation

From the experimental study on the production of papain nanoparticles by anti-solvent precipitation, ethanol was identified as the most effective anti-solvent for this process. The optimal conditions for producing stable papain nanoparticles were found to be a papain concentration of 30 mg/ml and a solvent-to-anti-solvent volume

ratio of 1:4. These conditions ensured the stability of the papain. However, morphological studies (Figure 4.5) indicated that for further encapsulation applications, the papain precipitated at a 1:4 ratio showed a tendency to aggregate. Increasing the ratio to 1:8 resulted in smaller (179.1 ± 1.4 nm), more uniform papain precipitates with reduced aggregation and a relatively high zeta potential (43.9 ± 1.9 mV), suggesting that the precipitates were stable and suitable for encapsulation with starch. Despite this, the higher ratio (1:8) at 30 mg/ml of papain also led to the formation of larger particles (more than 1000 nm). Consequently, for the encapsulation experiments, a papain solution concentration of 30 mg/ml and a solvent-to-anti-solvent volume ratio of 1:8 was selected for the initial precipitation step.

After identifying the optimal conditions for papain precipitation, papain encapsulation was proceeded to form the ACS/Papain composites. In previous studies, (Morales-Cruz et al., 2012) encapsulated two proteins, lysozyme, and α -Chymotrypsin within PLGA nanoparticles using the two-step anti-solvent precipitation method. This is a method that first precipitates the protein to ensure that it remains stable after encapsulation. Similarly, (Nelemans et al., 2020) utilized the same method but used a different protein, specifically BSA (Bovine Serum Albumin). After protein precipitation with acetonitrile (ACN), PLGA solution was added into the protein suspension and precipitated PLGA using water with surfactant for dispersion. Therefore, this approach to maintain papain stability during encapsulation was adopted in this study. However, ethanol was used instead of ACN as the anti-solvent, as it is more compatible with papain. The polymer used was acetylated cassava starch with a DS value of 0.037, which cannot dissolve in ethanol. The stepwise anti-solvent precipitation was used for encapsulation. This technique is slightly modified from the method of (Yang et al., 2018), curcumin was encapsulated using gliadin-lecithin. This study the effects of starch concentration and starch volume on the process were investigated. Moreover, two surfactants, Tween 20 and Tween 80, at different concentrations were tested.

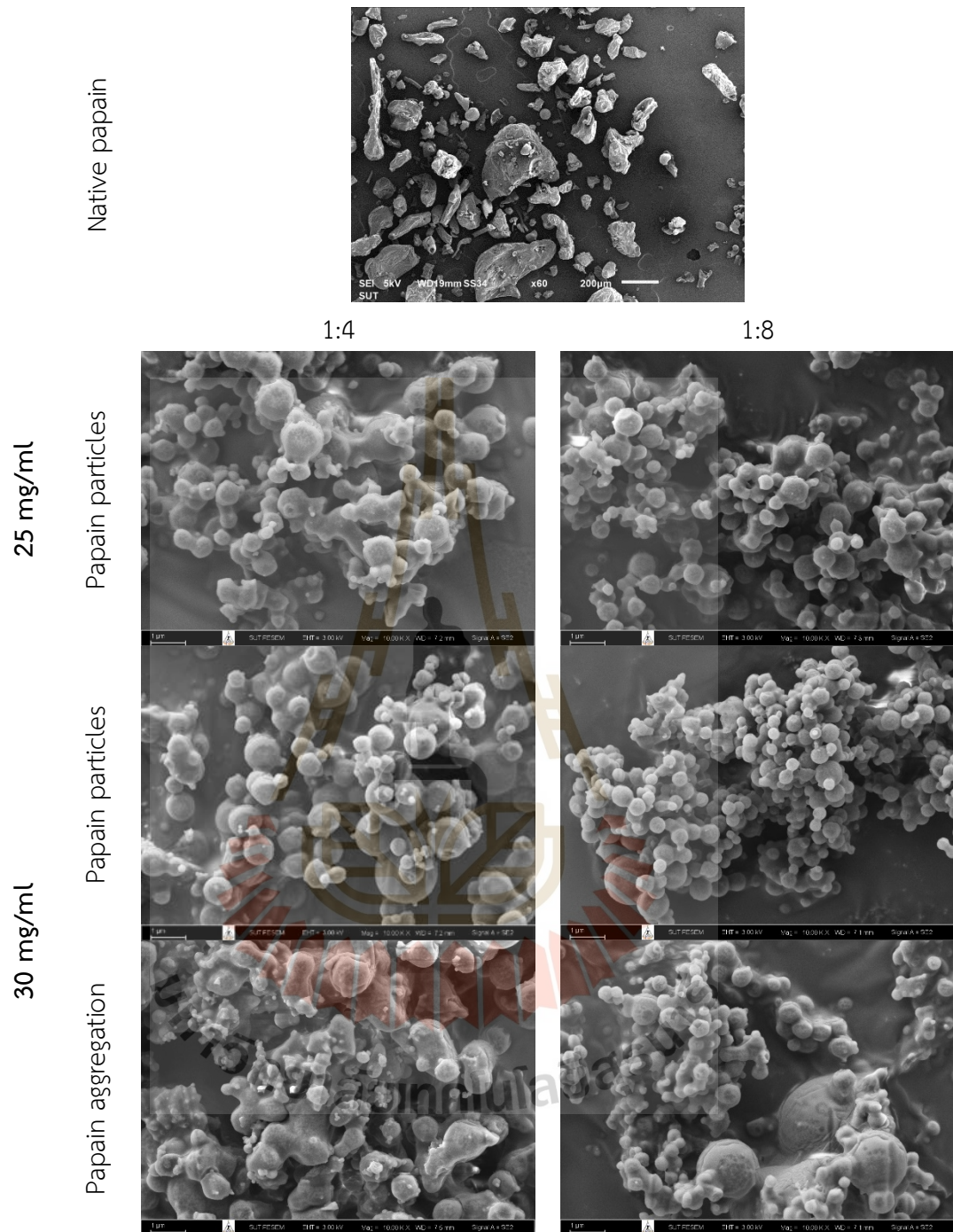


Figure 4.5 SEM photomicrographs of native papain and papain particles prepared by anti-solvent precipitation process under different operation parameters.

4.2.1 The effect of starch concentrations

The study of starch concentration's effects is crucial in encapsulation processes. In this investigation, various starch concentrations ranging from 10 mg/ml to 60 mg/ml were tested, with Tween 20 used as the surfactant at a concentration of 3%

v/v and a starch solution volume of 1 ml. Concentrations beyond the above range resulted in rapid agglomeration of starch particles, making effective papain encapsulation difficult. The results, depicted in Figure 4.6(a), illustrate the encapsulation efficiency and loading capacity of ACS/papain composites as functions of starch concentration. Within the concentration range of 10 to 30 mg/ml, the encapsulation efficiency rises significantly from 24.33 ± 1.56 to $52.70 \pm 1.38\%$. However, at a starch concentration of 60 mg/ml, encapsulation efficiency decreases to $45.99 \pm 1.97\%$. This trend aligns with similar observations in the encapsulation of *Lactobacillus acidophilus* into porous starch (Xing et al., 2014). The decline in encapsulation efficiency at higher starch concentrations is attributed to the increased viscosity of the starch solution at 60 mg/ml, which causes rapid precipitation and aggregation of starch particles. This higher viscosity inhibits diffusion between the starch solution and ethanol, resulting in non-uniform molecular supersaturation and slower nucleation rates. Consequently, larger and more aggregated particles are formed (Dong et al., 2021; Joye & McClements, 2013), reducing the encapsulation efficiency. Even with the addition of surfactant to aid in dispersion, these challenges persist due to the rapid self-aggregation of starch before effective encapsulation of papain can occur. Meanwhile, the loading capacity continuously decreases from $42.89 \pm 1.58\%$ at 10 mg/ml to $19.15 \pm 0.67\%$ at 60 mg/ml. The LC values at 15 mg/ml and 30 mg/ml are quite similar, at $37.02 \pm 0.60\%$ and $35.18 \pm 0.60\%$, respectively. This continuous reduction is likely due to the increase in the amount of starch as the starch concentration increases, which lowers the amount of papain encapsulated per unit of starch. At higher concentrations, the starch particles tend to aggregate, leading to less effective encapsulation. This aggregation reduces the available surface area for encapsulating papain, as a result, LC greatly decreased from $35.18 \pm 0.60\%$ at 30 mg/ml to $19.15 \pm 0.67\%$ at 60 mg/ml.

Therefore, the optimal starch concentration for encapsulation was determined to be 30 mg/ml, as it provided the highest encapsulation efficiency and a relatively high loading capacity without significant aggregation issues. Consequently, this concentration was utilized for subsequent experiments. While the methods proved effective in encapsulating papain particles, the efficiency decreased at higher starch concentrations due to particle aggregation.

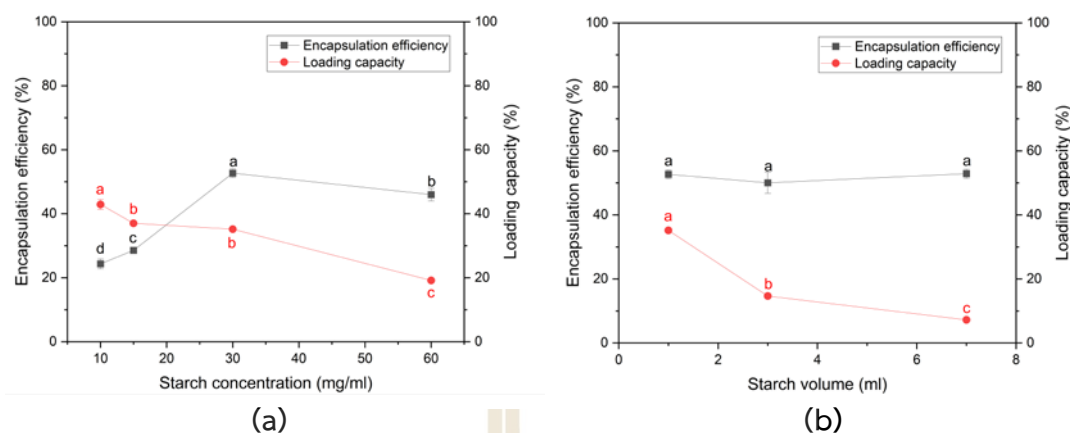


Figure 4.6 Encapsulation efficiency and loading capacity of ACS/papain composites as functions of (a) starch concentration with fixed volume of starch solution of 1 ml and Tween 20 concentration of 3%v/v, and (b) starch volume with fixed starch concentration of 30 mg/ml and Tween 20 concentration of 3%v/v.

4.2.2 The effect of starch solution volumes

In the study of the impact of starch volume on the encapsulation process to increase encapsulation efficiency without raising the starch concentration beyond 30 mg/ml, the volume of starch used was optimized. Volumes of 1, 3, and 7 ml were tested at a starch concentration of 30 mg/ml, with Tween 20 used as the surfactant at a concentration of 3% v/v. The results, illustrated in Figure 4.6(b), demonstrate the encapsulation efficiency and loading capacity of ACS/papain composites as functions of starch volume. Encapsulation efficiency at volumes of 1, 3, and 7 ml are $52.70 \pm 1.38\%$, $50.02 \pm 3.28\%$, and $52.89 \pm 1.47\%$, respectively. These values do not significantly differ from each other. However, the loading capacity gradually decreases as the volume of starch increases. This reduction occurred because although more starch was used for encapsulation, the amount of papain encapsulated remained the same.

Despite the similar encapsulation efficiencies, a starch volume of 7 ml was selected as the optimal choice. This decision was based on practical considerations related to the separation and purification of the final product. At a volume of 7 ml, any free papain that is not encapsulated dissolves back into the solution, making it easier to separate from the final product. In contrast, at volumes of 1 and 3 ml, unencapsulated residual papain remains in solid form, which necessitates additional steps for its removal. These additional steps would not only increase the complexity of the process but also generate more waste. Moreover, these extra

washing steps increase the risk of papain degradation, further complicating the purification of the final product.

Therefore, a starch solution volume of 7 ml seemed the most suitable for subsequent experiments. This volume ensures easier separation of the unencapsulated papain, maintains process efficiency, and reduces the risk of enzymatic degradation during purification. By choosing 7 ml, the encapsulation process is streamlined, minimizing potential losses, and improving the overall quality of the final product.

4.2.3 The effect of surfactant types and concentrations

In the process of encapsulating papain with starch, surfactants such as Tween 20 and Tween 80 play a crucial role in effectively dispersing starch particles, thereby preventing aggregation and clumping (Figure 4.7). Besides facilitating particle dispersion, Tween surfactants are widely studied in pharmaceutical applications to ensure protein stability. For instance, (Duskey et al., 2021) investigated the influence of different types of Tween—20, 60, and 80—on enzyme activity and stability during the encapsulation process of β -glucosidase (β -Glu) in PLGA nanoparticles. Furthermore, other studies have shown that Tween surfactants can enhance enzyme activity (Kamande, Baah, Cheng, McAllister, & Shelford, 2000) and protect protein surfaces from denaturation (Arsiccio, McCarty, Pisano, & Shea, 2018). However, the effect of Tween surfactants on enzyme activity can vary; while they may enhance activity for some enzymes, they can also decrease activity for others. For example, (Battestin & Macedo, 2007) and (Kar, Banerjee, & Bhattacharyya, 2003) observed that Tween surfactants reduced tannase activity when using Tween 20, 40, 60, and 80 at concentrations ranging from 0.025-1% v/v.

In this study, the effects of Tween 20 and Tween 80 on papain activity during the precipitation process were examined. The results indicated that increasing the concentration of both surfactants led to a decrease in papain activity (Figure 4.8(c)). This decline is attributed to the predominance of oleic acid in Tween 80 and lauric acid in Tween 20, which similarly affected tannase activity. Despite this, the system utilizing Tween 20 retained slightly higher papain activity compared to Tween 80. This difference could be attributed to the varying lengths and saturation levels of the fatty acid tails. Specifically, lauric acid in Tween 20 is shorter and more saturated compared to oleic acid in Tween 80 (Kerwin, 2008). This structural difference may influence their

interactions with the papain molecule, potentially causing less disruption (Figure 4.8(c)).

Regarding the impact of Tween 20 and Tween 80 on encapsulation efficiency and loading capacity (Figure 4.8(a), (b)), the results showed that both parameters were influenced by the concentration and type of the surfactants. With Tween 20, encapsulation efficiency and loading capacity initially decreased within the range of 1 to 2% v/v but then remained relatively constant from 2 to 3% v/v. This decrease is attributed to Tween 20 molecules' interaction with both papain and starch particles. This interaction hinders papain encapsulation, thereby reducing encapsulation efficiency and loading capacity. This effect of Tween 20 mirrors findings from (Duskey et al., 2021), who observed a similar trend: an initially decreased both encapsulation efficiency and loading capacity and was then relatively constant.

Conversely, for Tween 80, both parameters increased as the concentration increased from 1 to 3% v/v. This trend aligns with findings reported by (Ali Attia Shafie, 2013). The longer oleic acid tail in Tween 80 may facilitate enhanced interactions with both starch and papain, contributing to improved encapsulation efficiency and loading capacity.

For residual activity after the encapsulation process, give an example of the result at 3% v/v Tween 80, the post-encapsulation papain activity remained at $55.70 \pm 7.18\%$. Remarkably, no additional loss in activity was observed after encapsulation compared to the initial precipitation step, where the activity was $53.21 \pm 0.94\%$, indicating no additional activity loss during the final step.

At the highest encapsulation efficiency and loading capacity, Tween 20 achieved $69.87 \pm 2.36\%$ and $8.96 \pm 0.30\%$, respectively, at 1% v/v. In comparison, Tween 80 reached $96.23 \pm 2.06\%$ and $12.40 \pm 0.23\%$, respectively, at 3% v/v.

Interestingly, Tween 20's highest residual activity occurred at the same point as its peak EE and LC, yielding approximately 87%. In contrast, Tween 80's highest residual activity occurred at a concentration of 1% v/v, where it reached approximately 80%, alongside EE and LC values of $75.14 \pm 6.10\%$ and $9.95 \pm 0.73\%$, respectively.

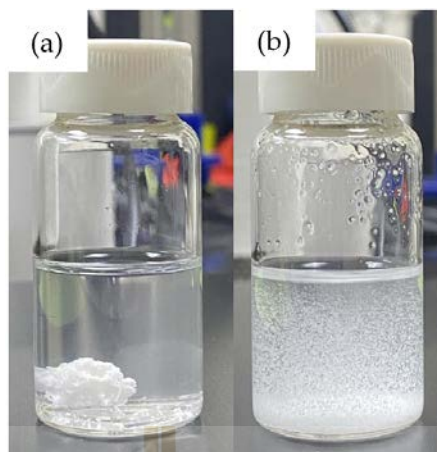


Figure 4.7 Effect of surfactants on starch particle dispersion: (a) Without surfactant and (b) With surfactant.

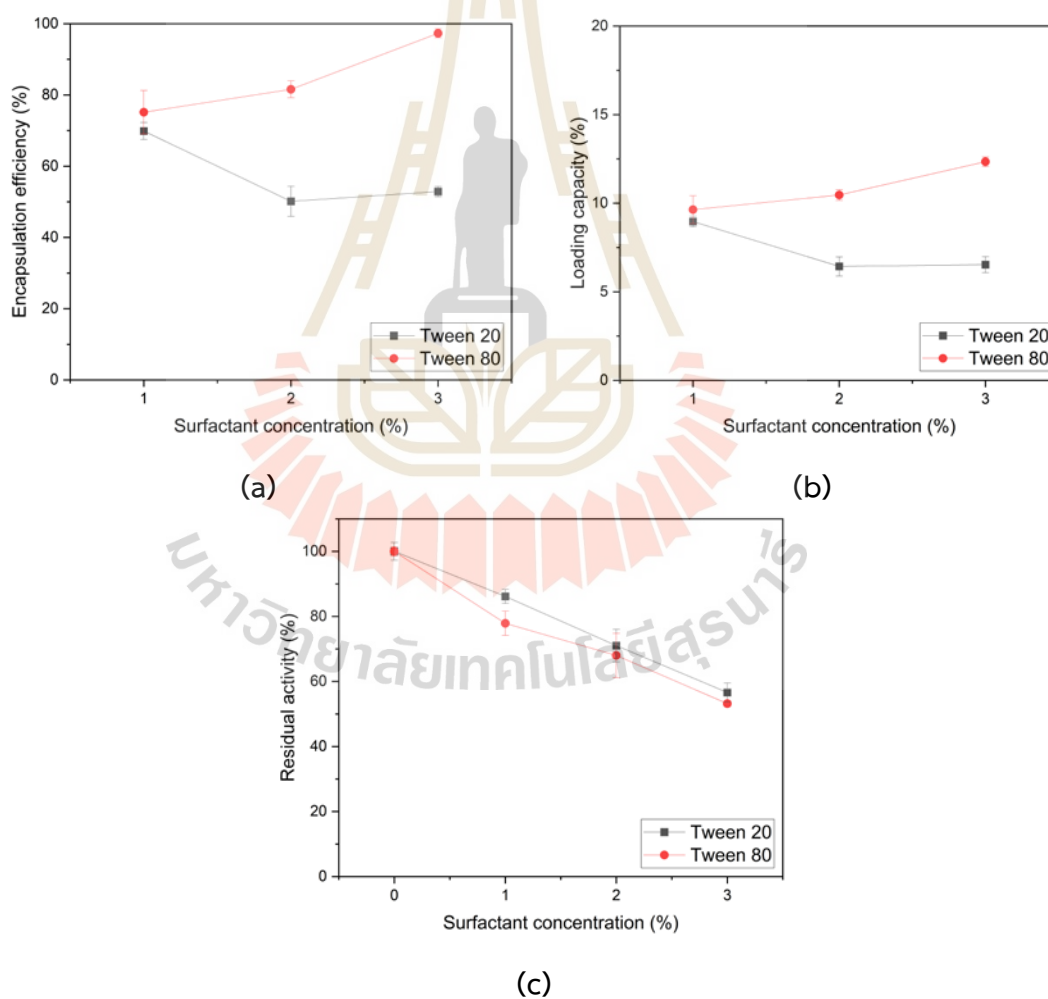


Figure 4.8 Encapsulation efficiency (a) and loading capacity (b) with fixed starch concentration of 30 mg/ml and starch solution volume of 7 ml, (c) residual activity after papain precipitation as functions of surfactant concentration (%v/v) and surfactant types.

4.2.4 Fluorescent spectrum

Fluorescence spectroscopy analysis was employed to confirm the encapsulation process of papain within ACS composites. Figure 4.9 presents the emission spectra of pure papain and ACS/papain composite dispersions upon excitation at 280 nm. As shown in Figure 4.9(d), the maximum emission wavelength of pure papain is observed at 322 nm (black spectrum), which aligns closely with a previously reported value of 332 nm (Budama-Kilinc et al., 2018).

The fluorescence intensities of ACS/papain composites, at varying starch concentrations (1 ml), exhibit distinct values that correlate with the encapsulation efficiency (%EE) (Figure 4.9(a)). Specifically, as the %EE increases, indicating a higher degree of successful encapsulation of papain within the carrier material, the intensity tends to decrease. This decrease is attributed to the reduction in the presence of free papain molecules, unencapsulated papain molecules, which typically contribute to the overall intensity observed in the solution or solid form. This relationship suggests that the ACS encapsulation effectively shields papain, reducing the availability of papain to emit fluorescence in response to excitation. Conversely, when the %EE is lower, indicating a lesser extent of encapsulation, the intensity tends to be higher, reflecting a higher concentration of free papain molecules in the solution or solid state.

In Figure 4.9(b), the fluorescence intensities at the peak wavelength remain similar for different starch volumes. This matches the %EE values, indicating that changing the starch volume doesn't significantly affect the fluorescence emission. This may be because the encapsulation efficiency stays consistent across varying starch volumes.

In the surfactant results (Fig. 4.9(c)), the fluorescence intensities at various Tween 80 concentrations correspond well with the %EE values obtained. However, for Tween 20, the sample at 1% v/v (with the highest %EE) shows a higher fluorescence intensity than the sample at 3% v/v (with a lower %EE). This increased intensity at 1% v/v suggests a greater amount of papain present on the composite surface.

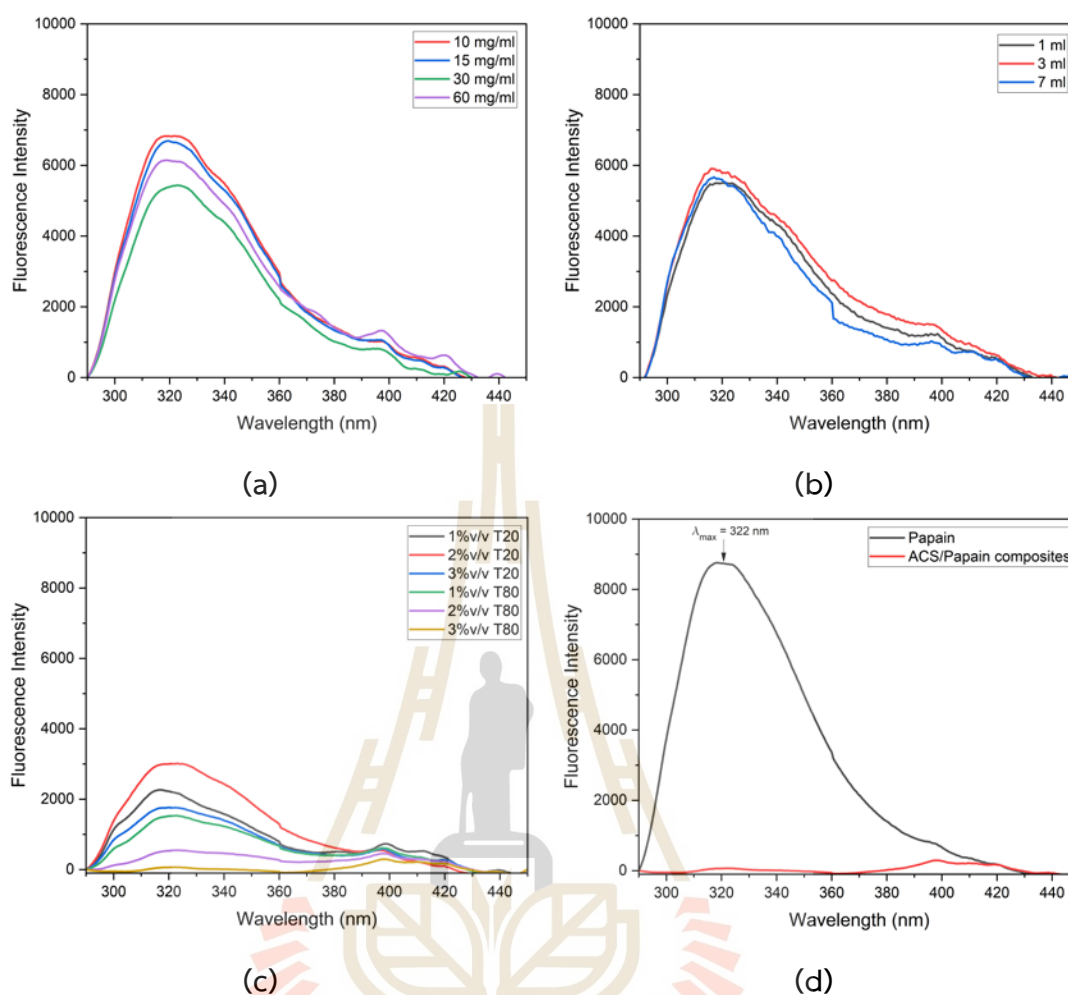


Figure 4.9 Fluorescence spectra of ACS/papain composites: (a) at different starch concentrations, (b) at different starch volume, (c) at different surfactant type and concentrations, and (d) at optimum condition (30 mg/ml, 7 ml, and 3%v/v Tween 80) and pure papain.

In Figure 4.9(d), the sample with the highest %EE ($96.23 \pm 2.06\%$) shows no emission maximum (red spectrum). This lack of emission is due to the effective encapsulation of papain by ACS, leaving minimal unencapsulated papain. This result indicates successful encapsulation, as the surrounding ACS effectively isolates the papain molecules, reducing their detectable fluorescence. This comprehensive analysis confirms the efficiency of the encapsulation process and highlights the relationship between encapsulation efficiency and fluorescence intensity, providing a reliable method for assessing encapsulation success. This is similar to the findings obtained by (Budama-Kilinc et al., 2018).

4.2.5 FTIR analysis

The FTIR spectra of ACS, papain, ACS composites, and ACS/papain composites are detailed in Table 4.3 and Tabel 4.4. Figure 4.10 displays these spectra, highlighting the molecular structures and interactions within the samples.

In the FTIR spectra of ACS and ACS composites, several absorption bands characteristic of starch are observed (Figure 6a). Notably, bands at 1150, 1076, and 1012 cm^{-1} are attributed to C-O bond stretching, while additional characteristic absorption bands appear at 995, 923, 860, 765, and 572 cm^{-1} are attributed to the stretching vibrations of the anhydroglucose ring, reflecting the basic structural components of the starch. The peaks at 1641 cm^{-1} correspond to water adsorption, indicating the presence of bound water within the starch. The band around 2931 cm^{-1} is attributed to C-H stretching vibrations, and an extremely broad band around 3300 cm^{-1} is assigned to the vibration stretches associated with free, inter-, and intramolecular bound hydroxyl groups comprising the starch structure. Furthermore, as the starch used is acetylated starch, additional peaks are observed at 1720, 1419, and 1363 cm^{-1} , assigned to carbonyl C=O, CH_3 anti-symmetry bending vibration, and CH_3 symmetry bending vibration, respectively. These additional peaks confirm the introduction of acetyl groups into the starch granules.

The FTIR spectra of papain shows a broad absorption band at 3300 cm^{-1} due to N-H stretching of secondary amide bonds, representing the protein backbone. The band at 2931 cm^{-1} is associated with $-\text{CH}_2-$ asymmetric stretching. Bands at 1645 and 1539 cm^{-1} correspond to amide-I and amide-II, respectively, while peaks between 1150, 1078, 846 cm^{-1} and 705-574 cm^{-1} can be attributed to sulphide and disulphide –CS stretching. Additionally, the peak observed at 846 cm^{-1} is also attributed to the aromatic residues of tryptophan or tyrosine.

For ACS composites processed without papain but with Tween 80, the FTIR spectra closely resemble those of raw ACS. However, noticeable changes in peak intensity and position occur. Specifically, the carbonyl C=O peak sharpens and shifts from 1720 to 1731 cm^{-1} , and the C-O bond stretching peak becomes more pronounced, shifting from 1012 to 1022 cm^{-1} and becomes more pronounced. These changes are likely due to the addition of Tween 80 and the reprecipitation process, which can alter the structure and properties of ACS. The O-H stretching vibration shifts from 3300 to

3340 cm^{-1} , indicating stronger hydrogen bonding within the matrix, possibly due to interactions with the surfactant and cross-linking.

Comparing the spectra of papain, ACS composites, and ACS/papain composites reveals that many papain peaks overlap with those of ACS composites. However, distinguishing peaks include the amide-II peak at 1537 cm^{-1} for papain and the carbonyl C=O peak at 1731 cm^{-1} for ACS composites. In the ACS/papain composite spectra, the amide-II peak is absent, while the carbonyl C=O peak is present. This indicates that papain has been encapsulated within ACS, with no free papain remaining outside the composite. Previous studies have reported similar results (Acevedo-Guevara et al., 2018; Ahmad et al., 2019; Budama-Kilinc et al., 2018; Y. Y. Chen et al., 2021), where the peak representing the core material disappears or shows lower intensity, confirming the successful encapsulation. Additionally, the increased intensity of the amide-I peak (1645 cm^{-1}) and the O-H stretching (3340 cm^{-1}) compared to ACS composites indicates interactions between the papain and ACS, likely through hydrogen bonding between the hydroxyl (-OH) and carboxyl groups (-COOH) of ACS and the amide groups of papain. This further confirms the enhanced hydrogen bonding in ACS/papain composites, supporting the successful encapsulation of the enzyme.

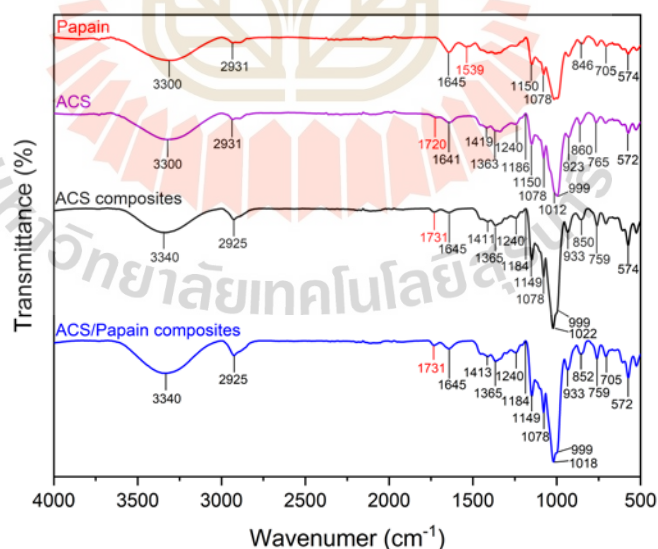


Figure 4.10 The FTIR spectra of papain, ACS, ACS composites and ACS/papain composites.

Other studies utilizing starch as a coating material have demonstrated similar encapsulation behavior for active ingredients, highlighting interactions through

hydrogen bonding with hydroxyl and carboxyl groups (Acevedo-Guevara et al., 2018; Buljeta, Pichler, Ivic, Simunovic, & Kopjar, 2021; Mahmoudi Najafi et al., 2016). In this study, the encapsulation of papain with acetylated cassava starch (ACS) is achieved through similar interactions. The hydroxyl groups (-OH) and carboxyl groups (-COOH) on acetylated starch form hydrogen bonds with functional groups on papain, such as the amide groups found in proteins. This interaction facilitates the entrapment of papain within the ACS matrix, stabilizing the enzyme within the composite. These hydrogen bonds not only aid in the encapsulation process but also contribute to maintaining the structural integrity and activity of papain, enhancing the overall efficacy of the encapsulation.

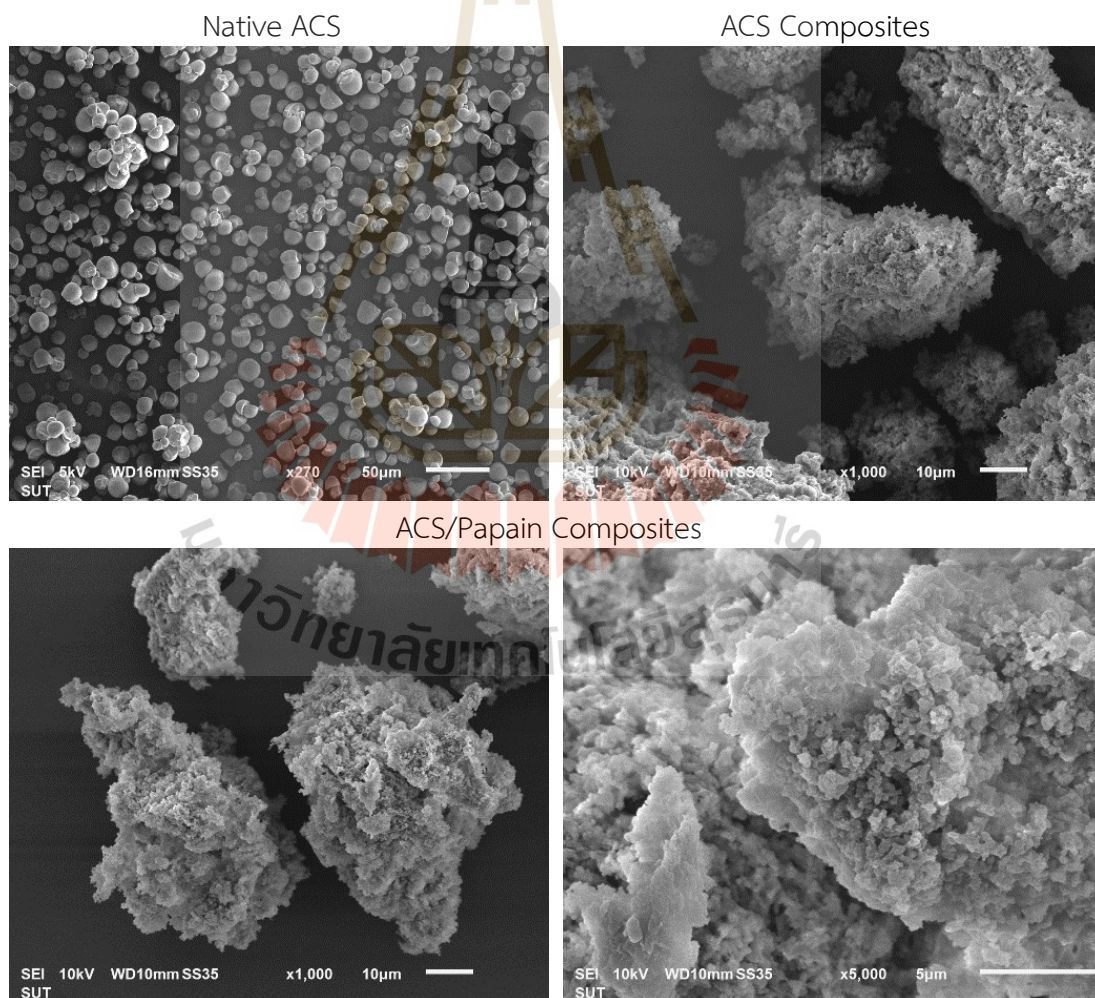


Figure 4.11 SEM photomicrographs of (a) native ACS particles, (b) ACS composites, and (c), and (d) ACS/papain composites.

Table 4.3 The FTIR spectrum of Papain and ACS/Papain composite.

Assignment of Papain	References	This study
N-H stretching of secondary amide bond	3300 cm ⁻¹ 3289 cm ⁻¹ 3450-3225 cm ⁻¹ (Peres, Armelin, Moreno-Martinez, Alemán, & Ferreira, 2015) (Budama-Kilinc et al., 2018)	Papain 3300 cm ⁻¹ 3340 cm ⁻¹
-CH ₂ -asymmetric stretching	2924 cm ⁻¹ 2931 cm ⁻¹ (M. Sharma, V. Sharma, A. K. Panda, & D. K. Majumdar, Peres et al., 2015)	2927 cm ⁻¹ 2925 cm ⁻¹
-CONH amide I	1637 cm ⁻¹ 1652 cm ⁻¹ 1645.2 cm ⁻¹ (Budama-Kilinc et al., 2018) (Peres et al., 2015) (M. Sharma et al., 2011)	1645 cm ⁻¹ 1645 cm ⁻¹
-CONH amide II	1551 cm ⁻¹ 1557 cm ⁻¹ (Peres et al., 2015) (Budama-Kilinc et al., 2018)	1537 cm ⁻¹ -
Aromatic residue of tryptophan or tyrosine	868, 850 cm ⁻¹ (Manu Sharma et al., 2011; Shoba et al., 2014)	846 cm ⁻¹ 852 cm ⁻¹
-CS stretching (disulphide)	852 cm ⁻¹ 705-570 cm ⁻¹ (Peres et al., 2015) (Shoba et al., 2014)	846 cm ⁻¹ 703-574 cm ⁻¹ 705-572 cm ⁻¹

Table 4.3 The FTIR spectrum of Papain and ACS/Papain composite (continued).

Assignment of Papain	References	
	Papain	ACS/Pap.co
-CS stretching	1150 cm ⁻¹	1149 cm ⁻¹
(sulphide)	1173 cm ⁻¹	1078 cm ⁻¹
	1150-1050 cm ⁻¹	
	1076 cm ⁻¹	
	1080 cm ⁻¹	

Table 4.4 The FTIR spectrum of ACS, ACS composites and ACS/Papain composite.

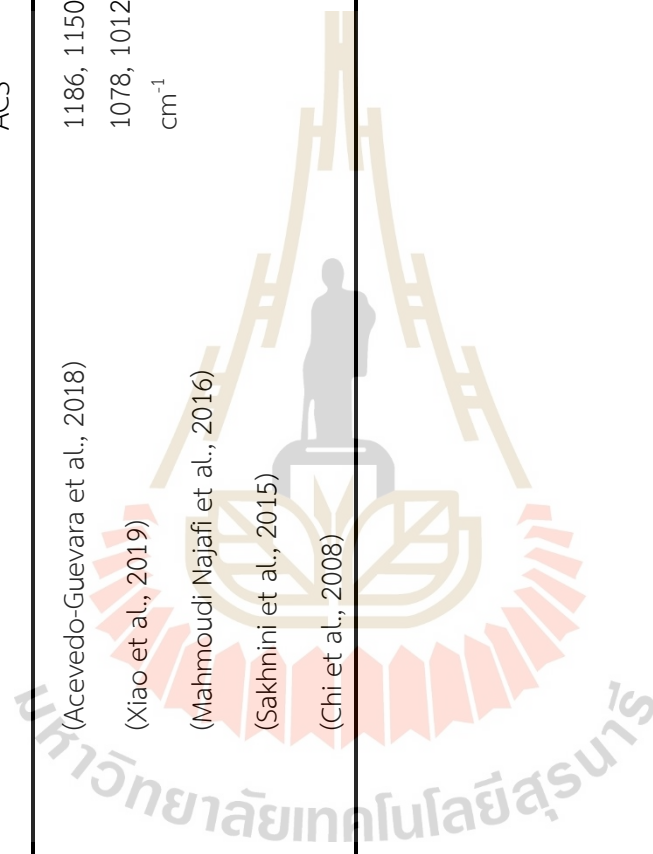
Assignment of ACS	References	This study		
		ACS	ACS com.	ACS/Pap.com
O-H stretching	3405 cm ⁻¹ 3388 cm ⁻¹ 3421 cm ⁻¹ 3404 cm ⁻¹ 3000-3700 cm ⁻¹	(Acevedo-Guevara et al., 2018) (Xiao et al., 2019) Chi et al., 2008; Mahmoudi Najafi et al., 2016) (Li et al., 2023) (Sakhnini, Al-Zoubi, Al-Obaidi, & Ardakani, 2015)	3300 cm ⁻¹ 3340 cm ⁻¹	3340 cm ⁻¹ 3340 cm ⁻¹
C-H stretching	2930 cm ⁻¹ 2935 cm ⁻¹	(Acevedo-Guevara et al., 2018; Mahmoudi Najafi et al., 2016) (Sakhnini et al., 2015)	2931 cm ⁻¹ 2925 cm ⁻¹	2925 cm ⁻¹ 2925 cm ⁻¹
Water adsorption	1644 cm ⁻¹ 1655 cm ⁻¹	(Li et al., 2023) (Sakhnini et al., 2015)	1641 cm ⁻¹ 1645 cm ⁻¹	1645 cm ⁻¹ 1645 cm ⁻¹
carbonyl C=O stretching	1731 cm ⁻¹ 1754 cm ⁻¹ 1750 cm ⁻¹	(Acevedo-Guevara et al., 2018) (Chi et al., 2008; Xiao et al., 2019) (Mahmoudi Najafi et al., 2016)	1720 cm ⁻¹ 1731 cm ⁻¹	1731 cm ⁻¹ 1731 cm ⁻¹
vibration	1760 cm ⁻¹	(Sakhnini et al., 2015)		

Table 4.4 The FTIR spectrum of ACS, ACS composites and ACS/Papain composite (continued).

Assignment of ACS	References	This study		
		ACS	ACS com.	ACS/Pap.com
Carbonyl	1240 cm ⁻¹	1240 cm ⁻¹	1240 cm ⁻¹	1240 cm ⁻¹
C-O stretching vibration	1193 cm ⁻¹	(Chi et al., 2008; Sakhnini et al., 2015) (Xiao et al., 2019)		
CH ₃ antisymmetry bending vibration	1435 cm ⁻¹ 1373 cm ⁻¹	1419 cm ⁻¹	1411 cm ⁻¹	1413 cm ⁻¹
CH ₃ symmetrical deformation vibration	1245 cm ⁻¹ 1375 cm ⁻¹ 1380 cm ⁻¹	1365 cm ⁻¹	1365 cm ⁻¹	1365 cm ⁻¹
Anhydro glucose ring stretching vibration	992, 930, 862, 763, 574 cm ⁻¹ 935, 855, 767, 577 cm ⁻¹ 992, 929, 861, 765, 575 cm ⁻¹	999, 923, 860, 765, 572 cm ⁻¹	999, 933, 850, 759, 574 cm ⁻¹	999, 933, 852, 759, 572 cm ⁻¹

Table 4.4 The FTIR spectrum of ACS, ACS composites and ACS/Papain composite (continued).

Assignment of ACS	References	This study		
		ACS	ACS com.	ACS/Pap.com
C-O bond stretch	1160, 1082, 1017 cm ⁻¹	1186, 1150,	1184, 1149,	1184, 1149,
	1193 cm ⁻¹	1078, 1012	1078, 1022	1078, 1018
stretching	1024 cm ⁻¹	cm ⁻¹	cm ⁻¹	cm ⁻¹
	1155, 1086, 1022 cm ⁻¹			
1159, 1082, 1014 cm ⁻¹				



4.2.6 Scanning electron microscopy (SEM) analysis

The morphological characteristics of native ACS particles, ACS composites, and ACS/papain composites under optimal conditions were thoroughly examined using scanning electron microscopy (SEM), as depicted in Figure 4.10. The optimal conditions were identified as a starch concentration of 30 mg/ml, a starch volume of 7 ml, and a Tween 80 concentration of 3% v/v. The SEM images of native ACS particles reveal a variety of shapes, including elliptical, kettledrum, and spherical truncated forms (Figure 4.11(b)). However, some granules show signs of damage. These diverse shapes and occasional damaged granules indicate the intrinsic structural variability and potential fragility of the raw starch particles. In contrast, the ACS/papain composites (Figure 4.11(c) and (d)) and ACS composites (Figure 4.11(b)) display a markedly different morphology from native ACS. These composites appear as rough, indistinct clusters, with their surfaces densely packed with small starch nanoparticles. This clustered appearance suggests successful encapsulation, where papain molecules are embedded within the ACS matrix, forming rough aggregates. The observed morphology of ACS/papain composites aligns with findings from previous studies, such as the work of (Li et al., 2023), who encapsulated zeaxanthin with corn starch using a one-step anti-solvent precipitation method. Li et al. reported the formation of a rough appearance with thin lamellar structures, highlighting the efficacy of anti-solvent precipitation in creating encapsulated structure.

CHAPTER V

CONCLUSIONS AND RECOMMENDATIONS

5.1 Conclusions

The study successfully identified optimal conditions for the precipitation of papain nanoparticles using the anti-solvent precipitation method. Among the anti-solvents tested, ethanol proved to be the most suitable, as it had the least impact on papain activity and produced fewer sticky precipitates compared to acetone and acetonitrile.

The optimal solvent-to-anti-solvent volume ratio was determined to be 1:4, which balanced the need for effective precipitation without excessive use of the anti-solvent. The best concentration of papain for achieving stable nanoparticles with high activity was 30 mg/ml.

Under these conditions, the papain nanoparticles had an average size of 207.6 nm with a narrow size distribution and a precipitation yield of 80.89%. This combination of conditions ensured the production of stable papain nanoparticles that maintained their enzymatic activity.

For the encapsulation of papain nanoparticles within acetylated cassava starch (ACS) with a degree of substitution (DS) of 0.037, the study established that a solvent-to-anti-solvent volume ratio of 1:8 was optimal. This ratio produced smaller, more uniform precipitates with reduced aggregation, enhancing the stability of the particles.

Starch concentration generally improved encapsulation efficiency and loading capacity, but excessive concentrations led to decreased efficiency and capacity due to starch aggregation, while starch volume primarily influenced loading capacity.

In this encapsulation process, surfactant was used to aid in dispersing the particles that form. Without the addition of a surfactant, the particles would aggregate, forming clumps. Both the type and concentration of the starch affect the encapsulation efficiency, loading capacity, and papain activity. However, higher concentrations of surfactants, particularly Tween 80, improved encapsulation efficiency and loading capacity but resulted in decreased papain activity. The encapsulation experiments revealed that a starch concentration of 30 mg/ml, a starch

solution volume of 7 ml, and a surfactant concentration of 3% v/v (Tween 80) provided the best results.

Under these conditions, the encapsulation efficiency was $96.23 \pm 2.06\%$, and the loading capacity was $12.40 \pm 0.23\%$, with approximately 56% of papain activity retained. The successful encapsulation of papain within acetylated starch was confirmed through FTIR and fluorescence spectroscopy, which showed distinct differences in peak positions and intensities compared to pure papain and ACS.

This research demonstrates that through careful optimization of precipitation and encapsulation parameters, papain can be effectively stabilized and protected using acetylated starch. These findings open new possibilities for the application of papain in environments where it would otherwise be unstable, enhancing its utility in various industries such as food processing, pharmaceuticals, and cosmetics.

5.2 Recommendations

1. Further studies should explore a wider range of surfactants and their concentrations to find the optimal balance between encapsulation efficiency and retention of papain activity. This could help in fine-tuning the encapsulation process for different applications.
2. Conducting long-term stability studies of the encapsulated papain to assess its shelf life under various storage conditions. This will help in understanding how the encapsulated enzyme performs over time and under different environmental stresses.
3. Investigating the release kinetics and bioavailability of the encapsulated papain in different gastrointestinal conditions. This will provide valuable information for developing oral drug formulations and other therapeutic applications.
4. Investigating the method of collection of the final product because method of collection affects the morphology of the final product.

REFERENCES

- Abdelkader, H., Hussain, S., Abdullah, N., & Kmaruddin, S. (2018). Review on micro-encapsulation with Chitosan for pharmaceuticals applications. *MOJ Curr. Res. Rev*, 1(2), 77-84.
- Acevedo-Guevara, L., Nieto-Suaza, L., Sanchez, L. T., Pinzon, M. I., & Villa, C. C. (2018). Development of native and modified banana starch nanoparticles as vehicles for curcumin. *Int. J. Biol. Macromol*, 111, 498-504. doi:10.1016/j.ijbiomac.2018.01.063
- Ackar, D., Babic, J., Jozinovic, A., Milicevic, B., Jokic, S., Milicevic, R., . . . Subaric, D. (2015). Starch modification by organic acids and their derivatives: A review. *Molecules*, 20(10), 19554-19570. doi:10.3390/molecules201019554
- Ahmad, M., Mudgil, P., Gani, A., Hamed, F., Masoodi, F. A., & Maqsood, S. (2019). Nano-encapsulation of catechin in starch nanoparticles: Characterization, release behavior and bioactivity retention during simulated in-vitro digestion. *Food Chem.*, 270, 95-104. doi:10.1016/j.foodchem.2018.07.024
- Ali Attia Shafie, M. (2013). Formulation and evaluation of betamethasone sodium phosphate loaded nanoparticles for ophthalmic delivery. *J. Clin. Exp. Ophthalmol.*, 04(02). doi:10.4172/2155-9570.1000273
- Arisanti, C., Rachmawati, H., Pamudji, J., & Sumirtapura, Y. (2012). Chitosan reinforced alginate microcapsules retained the release of papain in simulated gastric fluid. *J. Pharm. Sci. Appl.*, 1(1).
- Arnon, R. (1970). Papain. In *Methods in enzymology* (Vol. 19, pp. 226-244): Elsevier.
- Arsiccio, A., McCarty, J., Pisano, R., & Shea, J. E. (2018). Effect of surfactants on surface-induced denaturation of proteins: evidence of an orientation-dependent mechanism. *J. Phys. Chem. B*, 122(49), 11390-11399. doi:10.1021/acs.jpcc.8b07368
- Battestin, V., & Macedo, G. A. (2007). Effects of temperature, pH and additives on the activity of tannase produced by *Paecilomyces variotii*. *Electron. J. Biotechnol.*, 10(2), 0-0. doi:10.2225/vol10-issue2-fulltext-9
- Benjar, C. (2007). Encapsulation and control release of food flavoring. In *Synthetic Food Ingredients Technology* (pp. 119-153).

- Budama-Kilinc, Y., Cakir-Koc, R., Kecel-Gunduz, S., Zorlu, T., Kokcu, Y., Bicak, B., . . . Ozel, A. E. (2018). Papain loaded poly(epsilon-caprolactone) nanoparticles: In-silico and In-vitro studies. *J. Fluoresc.*, *28*(5), 1127-1142. doi:10.1007/s10895-018-2276-6
- Buljeta, I., Pichler, A., Ivic, I., Simunovic, J., & Kopjar, M. (2021). Encapsulation of fruit flavor compounds through Interaction with polysaccharides. *Molecules*, *26*(14). doi:10.3390/molecules26144207
- Bundit, P., Jureerut, D., Tueanjit, K., Pranithi, H., & Patcharee, B. (2014). Microencapsulation Techniques and its Role in Medicine. *Srinagarind Med J.*, *29*(1).
- Capello, C., Fischer, U., & Hungerbühler, K. (2007). What is a green solvent? A comprehensive framework for the environmental assessment of solvents. *Green Chem.*, *9*(9). doi:10.1039/b617536h
- Chandran, S. P., Nachinmuthu, K. P., Natarajan, S. B., Inamdar, M. G., & Shahimi, M. S. B. M. (2018). Papain loaded solid lipid nanoparticles for colorectal cancer therapy. *Curr. Cancer Ther. Rev.*, *14*(1), 75-87. doi:10.2174/1573394713666170929160933
- Chang, Y., Yan, X., Wang, Q., Ren, L., Tong, J., & Zhou, J. (2017). High efficiency and low cost preparation of size controlled starch nanoparticles through ultrasonic treatment and precipitation. *Food Chem.*, *227*, 369-375. doi:10.1016/j.foodchem.2017.01.111
- Chankhampan, C., Manosroi, J., Yamamoto, H., Tahara, K., Manosroi, W., Kawashima, Y., & Manosroi, A. (2012). Chemical stability enhancement and cytotoxicity reduction of papain loaded in PLGA nanospheres. *J. Exp. Nanosci.*, *9*(2), 138-151. doi:10.1080/17458080.2011.636385
- Chen, X., Moonshi, S. S., Nguyen, N. T., & Ta, H. T. (2023). Preparation of protein-loaded nanoparticles based on poly(succinimide)-oleylamine for sustained protein release: a two-step nanoprecipitation method. *Nanotechnol.*, *35*(5). doi:10.1088/1361-6528/ad0592
- Chen, Y. Y., Liu, K., Zha, X. Q., Li, Q. M., Pan, L. H., & Luo, J. P. (2021). Encapsulation of luteolin using oxidized lotus root starch nanoparticles prepared by anti-solvent precipitation. *Carbohydr. Polym.*, *273*, 118552. doi:10.1016/j.carbpol.2021.118552
- Chi, H., Xu, K., Wu, X., Chen, Q., Xue, D., Song, C., . . . Wang, P. (2008). Effect of acetylation on the properties of corn starch. *Food Chem.*, *106*(3), 923-928. doi:10.1016/j.foodchem.2007.07.002

- Chin, S. F., Mohd Yazid, S. N. A., & Pang, S. C. (2014). Preparation and characterization of starch nanoparticles for controlled release of curcumin. *Int. J. Polym Sci., 2014*, 1-8. doi:10.1155/2014/340121
- Corporation, E. D. (2024). Papain Retrieved May 20, 2024 from <https://papain.com/applications/>
- Corrêa-Filho, L., Moldão-Martins, M., & Alves, V. (2019). Advances in the application of microcapsules as carriers of functional compounds for food products. *Appl. Sci., 9*(3). doi:10.3390/app9030571
- da Silva, C. R., Oliveira, M. B., Motta, E. S., de Almeida, G. S., Varanda, L. L., de Padula, M., . . . Caldeira-de-Araujo, A. (2010). Genotoxic and cytotoxic safety evaluation of papain (carica papaya L.) using in vitro assays. *J. Biomed. Biotechnol., 2010*, 197898. doi:10.1155/2010/197898
- de Boer, F. Y., Imhof, A., & Velikov, K. P. (2019). Encapsulation of colorants by natural polymers for food applications. *Color. Technol., 135*(3), 183-194. doi:10.1111/cote.12393
- Department of Industrial Promotion. (2008). Production of Papain enzyme for industrial application. Retrieved September 30, 2022, from <http://library.dip.go.th/multim6/ebook/2552/HAN%20%E0%B8%81%E0%B8%AA%E0%B8%AD56%20%E0%B8%8151-13.pdf>
- Deulgaonkar, S. U., & Thorat, B. N. (2008). The purification, formulation and drying of papain. *Int. J. Food Eng., 4*(8). doi:10.2202/1556-3758.1512
- Dong, H., Chen, L., Zhang, Q., Gao, J., & Vasanthan, T. (2021). Optimization of processing parameters to produce nanoparticles prepared by rapid nanoprecipitation of pea starch. *Food Hydrocoll., 121*. doi:10.1016/j.foodhyd.2021.106929
- Dong, H., Zhang, Q., Gao, J., Chen, L., & Vasanthan, T. (2022). Preparation and characterization of nanoparticles from cereal and pulse starches by ultrasonic-assisted dissolution and rapid nanoprecipitation. *Food Hydrocoll., 122*. doi:10.1016/j.foodhyd.2021.107081
- dos Anjos, M. M., da Silva, A. A., de Pascoli, I. C., Mikcha, J. M. G., Machinski, M., Peralta, R. M., & de Abreu Filho, B. A. (2016). Antibacterial activity of papain and bromelain on *Alicyclobacillus* spp. *Int. J. Food Microbiol., 216*, 121-126. doi:10.1016/j.jfoodmicro.2015.10.007
- Duskey, J. T., Ottonelli, I., Rinaldi, A., Parmeggiani, I., Zambelli, B., Wang, L. Z., . . . Ruozi, B. (2021). Tween((R)) preserves enzyme activity and stability in PLGA nanoparticles. *Nanomaterials., 11*(11). doi:10.3390/nano11112946

- El-Naggar, M. E., El-Rafie, M. H., El-sheikh, M. A., El-Feky, G. S., & Hebeish, A. (2015). Synthesis, characterization, release kinetics and toxicity profile of drug-loaded starch nanoparticles. *Int. J. Biol. Macromol.*, *81*, 718-729. doi:10.1016/j.jbiomac.2015.09.005
- Ezekiel, A., & Florence, M. (2012). Papain, a plant enzyme of biological importance: A review. *Am. J. Biochem. Biotechnol.*, *8*(2), 99-104. doi:10.3844/ajbbsp.2012.99.104
- Farrag, Y., Ide, W., Montero, B., Rico, M., Rodriguez-Llamazares, S., Barral, L., & Bouza, R. (2018). Preparation of starch nanoparticles loaded with quercetin using nanoprecipitation technique. *Int. J. Biol. Macromol.*, *114*, 426-433. doi:10.1016/j.jbiomac.2018.03.134
- Fernández-Lucas, J., Castañeda, D., & Hormigo, D. (2017). New trends for a classical enzyme: Papain, a biotechnological success story in the food industry. *Trends Food Sci.*, *68*, 91-101. doi:10.1016/j.tifs.2017.08.017
- Fessi, H., Puisieux, F., Devissaguet, J. P., Ammoury, N., & Benita, S. (1989). Nanocapsule formation by interfacial polymer deposition following solvent displacement. *Int. J. Pharm.*, *55*(1), R1-R4.
- García, M. A. V. T., García, C. F., & Faraco, A. A. G. (2020). Pharmaceutical and biomedical applications of native and modified starch: A review. *Starch - Stärke*, *72*(7-8). doi:10.1002/star.201900270
- Hassani, L. N., Hindre, F., Beuvier, T., Calvignac, B., Lautram, N., Gibaud, A., & Boury, F. (2013). Lysozyme encapsulation into nanostructured CaCO₃ microparticles using a supercritical CO₂ process and comparison with the normal route. *J. Mater. Chem. B*, *1*(32), 4011-4019. doi:10.1039/c3tb20467g
- Jahanshahi, M., & Babaei, Z. (2008). Protein nanoparticle: a unique system as drug delivery vehicles. *Afr. J. Biotechnol.*, *7*(25).
- Jin, Y., Li, J. Z., & Malaki Nik, A. (2018). Starch-based microencapsulation. In *Starch in Food* (pp. 661-690).
- Joye, I. J., & McClements, D. J. (2013). Production of nanoparticles by anti-solvent precipitation for use in food systems. *Trends Food Sci Technol*, *34*(2), 109-123. doi:10.1016/j.tifs.2013.10.002
- Kamande, G., Baah, J., Cheng, K.-J., McAllister, T., & Shelford, J. (2000). Effects of Tween 60 and Tween 80 on protease activity, thiol group reactivity, protein adsorption, and cellulose degradation by rumen microbial enzymes. *J. dairy sci.*, *83*(3), 536-542.

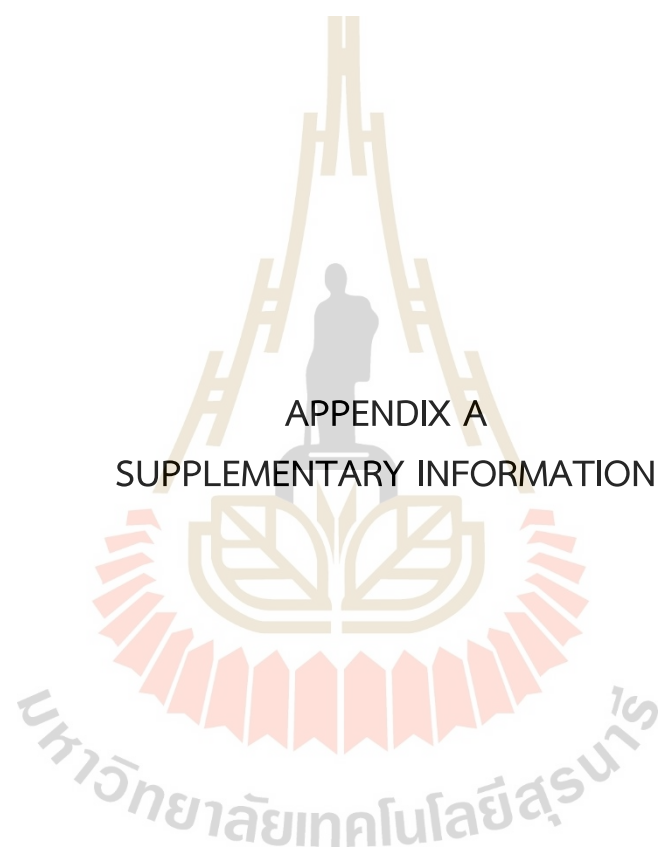
- Kar, B., Banerjee, R., & Bhattacharyya, B. C. (2003). Effect of additives on the behavioural properties of tannin acyl hydrolase. *Process Biochem.*, *38*(9), 1285-1293. doi:10.1016/s0032-9592(02)00329-1
- Kerwin, B. A. (2008). Polysorbates 20 and 80 used in the formulation of protein biotherapeutics: structure and degradation pathways. *J. Pharm. Sci.*, *97*(8), 2924-2935. doi:10.1002/jps.21190
- Khan, H., Akhtar, N., & Ali, A. (2014). Effects of cream containing ficus carica L. fruit extract on skin parameters: in vivo evaluation. *Indian J. Pharm. Sci.*, *76*(6), 560.
- Khaparde, S. S., & Singhal, R. S. (2001). Chemically modified papain for applications in detergent formulations. *Bioresour. Technol.*, *78*(1), 1-4.
- Klein, S. (2009). *Polysaccharides in oral drug delivery—recent applications and future perspectives*. ACS Symposium Series: Washington, DC, USA.
- Kongsamai, P., Phoumixay, C., & Wantha, L. (2020). Experiments and correlations of the solubility of γ -DL-Methionine in binary solvent mixtures. *Chem. Eng. Technol.*, *43*(6), 1079-1086. doi:10.1002/ceat.201900642
- Kothamasu, P., Kanumur, H., Ravur, N., Maddu, C., Parasuramrajam, R., & Thangavel, S. (2012). Nanocapsules: the weapons for novel drug delivery systems. *Bioimpacts*, *2*(2), 71-81. doi:10.5681/bi.2012.011
- Kwon, K. C., & Daniell, H. (2016). Oral delivery of protein drugs bioencapsulated in plant cells. *Mol. Ther.*, *24*(8), 1342-1350. doi:10.1038/mt.2016.115
- Li, S., Feng, D., Li, E., & Gilbert, R. G. (2023). Formation, structural characterization, and functional properties of corn starch/zeaxanthin composites. *Foods*, *12*(10). doi:10.3390/foods12102076
- Liu, X., Ibarra-Sanchez, L. A., Miller, M. J., & Lee, Y. (2022). Fabrication of zein-modified starch nanoparticle complexes via microfluidic chip and encapsulation of nisin. *Curr. Res. Food Sci.*, *5*, 1110-1117. doi:10.1016/j.crfs.2022.07.005
- Mahajan, A., & Ramana, E. (2014). Patents on magnetoelectric multiferroics and their processing by electrophoretic deposition. *Rec. Pat. on Mate. Sci.*, *7*(2), 109-130. doi:10.2174/1874464807666140701190424
- Mahmoudi Najafi, S. H., Baghaie, M., & Ashori, A. (2016). Preparation and characterization of acetylated starch nanoparticles as drug carrier: Ciprofloxacin as a model. *Int. J. Biol. Macromol.*, *87*, 48-54. doi:10.1016/j.ijbiomac.2016.02.030
- Martínez Rivas, C. J., Tarhini, M., Badri, W., Miladi, K., Greige-Gerges, H., Nazari, Q. A., . . . Elaissari, A. (2017). Nanoprecipitation process: From encapsulation to drug delivery. *Int. J. Pharm.*, *532*(1), 66-81. doi:10.1016/j.ijpharm.2017.08.064

- McClements, D. J. (2018). Encapsulation, protection, and delivery of bioactive proteins and peptides using nanoparticle and microparticle systems: A review. *Adv. Colloid Interface Sci.*, *253*, 1-22. doi:10.1016/j.cis.2018.02.002
- Mishra, B., Patel, B. B., & Tiwari, S. (2010). Colloidal nanocarriers: a review on formulation technology, types and applications toward targeted drug delivery. *Nanomed.: Nanotechnol. Biol. Med.*, *6*(1), 9-24. doi:10.1016/j.nano.2009.04.008
- Morales-Cruz, M., Flores-Fernandez, G. M., Morales-Cruz, M., Orellano, E. A., Rodriguez-Martinez, J. A., Ruiz, M., & Griebenow, K. (2012). Two-step nanoprecipitation for the production of protein-loaded PLGA nanospheres. *Results Pharma. Sci.*, *2*, 79-85. doi:10.1016/j.rinphs.2012.11.001
- Morán, D., Gutiérrez, G., Blanco-López, M. C., Marefati, A., Rayner, M., & Matos, M. (2021). Synthesis of starch nanoparticles and their applications for bioactive compound encapsulation. *Appl. Sci.*, *11*(10). doi:10.3390/app11104547
- Moreira Filho, R. N. F., Vasconcelos, N. F., Andrade, F. K., Rosa, M. F., & Vieira, R. S. (2020). Papain immobilized on alginate membrane for wound dressing application. *Colloids Surf. B Biointerfaces*, *194*, 111222. doi:10.1016/j.colsurfb.2020.111222
- Moreno-Cortez, I. E., Romero-García, J., Gonzalez-Gonzalez, V., Garcia-Gutierrez, D. I., Garza-Navarro, M. A., & Cruz-Silva, R. (2015). Encapsulation and immobilization of papain in electrospun nanofibrous membranes of PVA cross-linked with glutaraldehyde vapor. *Mater. Sci. Eng. C Mater. Biol. Appl.*, *52*, 306-314. doi:10.1016/j.msec.2015.03.049
- Muss, C., Mosgoeller, W., & Endler, T. (2013). Papaya preparation (Caricol®) in digestive disorders. *Neuro Endocrinol. Lett.*, *34*(1), 38-46.
- Nelemans, L. C., Buzgo, M., & Simaite, A. (2020). *Optimization of protein precipitation for high-loading drug delivery systems for immunotherapeutics*. Paper presented at the The 1st International Electronic Conference on Pharmaceutics.
- Nieto-Suaza, L., Acevedo-Guevara, L., Sánchez, L. T., Pinzón, M. I., & Villa, C. C. (2019). Characterization of Aloe vera-banana starch composite films reinforced with curcumin-loaded starch nanoparticles. *Food Structure*, *22*. doi:10.1016/j.foostr.2019.100131
- Peres, R. S., Armelin, E., Moreno-Martínez, J. A., Alemán, C., & Ferreira, C. A. (2015). Transport and antifouling properties of papain-based antifouling coatings. *Appl. Surf. Sci.*, *341*, 75-85. doi:10.1016/j.apsusc.2015.03.004
- Pimpen, P., & Nithiya, R. (2010). Modified starch. Retrieved October 10, 2022, from <https://www.foodnetworksolution.com/wiki/word/0502/modified-starch->

[%E0%B9%81%E0%B8%9B%E0%B9%89%E0%B8%87%E0%B8%94%E0%B8%B1%E0%B8%94%E0%B9%81%E0%B8%9B%E0%B8%A3#disqus_thread](#)

- Qureshi, A., Vyas, J., & Upadhyay, U. (2022). Determination of solubility by gravimetric method: A brief review. *Nat. J. Pharm. Sci.*, 2(1), 01-03.
- Robertson, R., Broers, B., & Harris, M. (2021). Injecting drug use, the skin and vasculature. *Addiction*, 116(7), 1914-1924. doi:10.1111/add.15283
- Sakhnini, N., Al-Zoubi, N., Al-Obaidi, G., & Ardakani, A. (2015). Sustained release matrix tablets prepared from cospray dried mixtures with starch hydrophobic esters. *Pharmazie*, 70(3), 177-182.
- Sangeetha, K., & Abraham, T. E. (2006). Chemical modification of papain for use in alkaline medium. *J. Mol. Catal. B Enzym.*, 38(3-6), 171-177. doi:10.1016/j.molcatb.2006.01.003
- Sasima, K., Na Ayudhya, & Rattanaporn, G. (2011). Pharmacokinetics and Pharmacodynamics. Retrieved October 30, 2022, from [http://www.ns.mahidol.ac.th/english/th/departments/MN/th/doc/km54/เภสัชจลนศาสตร์%20\(Pharmacokinetics\).pdf](http://www.ns.mahidol.ac.th/english/th/departments/MN/th/doc/km54/เภสัชจลนศาสตร์%20(Pharmacokinetics).pdf)
- Schrooyen, P. M., van der Meer, R., & De Kruif, C. G. (2001). Microencapsulation: its application in nutrition. *Proc. Nutr. Soc.*, 60(4), 475-479. doi:10.1079/pns2001112
- Shaji, J., & Patole, V. (2008). Protein and peptide drug delivery: oral approaches. *Indian J. Pharm. Sci.*, 70(3), 269.
- Sharma, M., Sharma, V., Panda, A. K., & Majumdar, D. K. (2011). Development of enteric submicron particle formulation of papain for oral delivery. *Int. J. Nanomedicine*, 6, 2097-2111. doi:10.2147/IJN.S23985
- Sharma, M., Sharma, V., Panda, A. K., & Majumdar, D. K. (2011). Enteric microsphere formulations of papain for oral delivery. *Yakugaku Zasshi*, 131(5), 697-709.
- Shoba, E., Lakra, R., Kiran, M. S., & Korrapati, P. S. (2014). Design and development of papain-urea loaded PVA nanofibers for wound debridement. *RSC Adv.*, 4(104), 60209-60215.
- Shouket, H., Ameen, I., Tursunov, O., Kholikova, K., Pirimov, O., Kurbonov, N., . . . Mukimov, B. (2020). *Study on industrial applications of papain: A succinct review*. Paper presented at the IOP Conference Series: Earth and Environmental Science.
- Squirrels, F. (2023). Clinical Evidence. Retrieved May 20, 2024 from https://www.skincarerebels.com/624250/Clinical_Evidence_Glow-07.12.23.pdf.

- Tacias-Pascacio, V. G., Morellon-Sterling, R., Castaneda-Valbuena, D., Berenguer-Murcia, Á., Kamli, M. R., Tavano, O., & Fernandez-Lafuente, R. (2021). Immobilization of papain: A review. *Int. J. Biol. Macromol.*, *188*, 94-113.
- Tuovinen, L., Peltonen, S., & Jarvinen, K. (2003). Drug release from starch-acetate films. *J. Control Release*, *91*(3), 345-354. doi:10.1016/s0168-3659(03)00259-1
- Wang, Y., & Tan, Y. (2016). Enhanced drug loading capacity of 10-hydroxycamptothecin-loaded nanoparticles prepared by two-step nanoprecipitation method. *J. Drug Deliv. Sci. Technol.*, *36*, 183-191. doi:10.1016/j.jddst.2016.09.012
- Xiao, H., Yang, F., Lin, Q., Zhang, Q., Tang, W., Zhang, L., . . . Liu, G. Q. (2019). Preparation and properties of hydrophobic films based on acetylated broken-rice starch nanocrystals for slow protein delivery. *Int. J. Biol. Macromol.*, *138*, 556-564. doi:10.1016/j.jbiomac.2019.07.121
- Xing, Y., Xu, Q., Ma, Y., Che, Z., Cai, Y., & Jiang, L. (2014). Effect of porous starch concentrations on the microbiological characteristics of microencapsulated *Lactobacillus acidophilus*. *Food Funct.*, *5*(5), 972-983. doi:10.1039/c3fo60438a
- Yang, S., Dai, L., Sun, C., & Gao, Y. (2018). Characterization of curcumin loaded gliadin-lecithin composite nanoparticles fabricated by antisolvent precipitation in different blending sequences. *Food Hydrocoll.*, *85*, 185-194. doi:10.1016/j.foodhyd.2018.07.015
- Ye, C., & Chi, H. (2018). A review of recent progress in drug and protein encapsulation: Approaches, applications and challenges. *Mater. Sci. Eng. C Mater. Biol. Appl.*, *83*, 233-246. doi:10.1016/j.msec.2017.10.003
- Zhou, L., Wang, C., Jiang, Y., & Gao, J. (2013). Immobilization of papain in biosilica matrix and its catalytic property. *Chin. J. Chem. Eng.*, *21*(6), 670-675. doi:10.1016/s1004-9541(13)60528-5
- Zhu, F. (2017). Encapsulation and delivery of food ingredients using starch based systems. *Food Chem.*, *229*, 542-552. doi:10.1016/j.foodchem.2017.02.101



APPENDIX A

SUPPLEMENTARY INFORMATION

A.1 The Focused Beam Reflectance Measurement (FBRM) data to check particles are nano size or micro size

The Focused Beam Reflectance Measurement (FBRM) technique was utilized to determine whether the papain particles obtained through precipitation were at the nano level or micro level. FBRM measures the chord length distribution of particles in real-time, providing a count of particles across different size ranges.

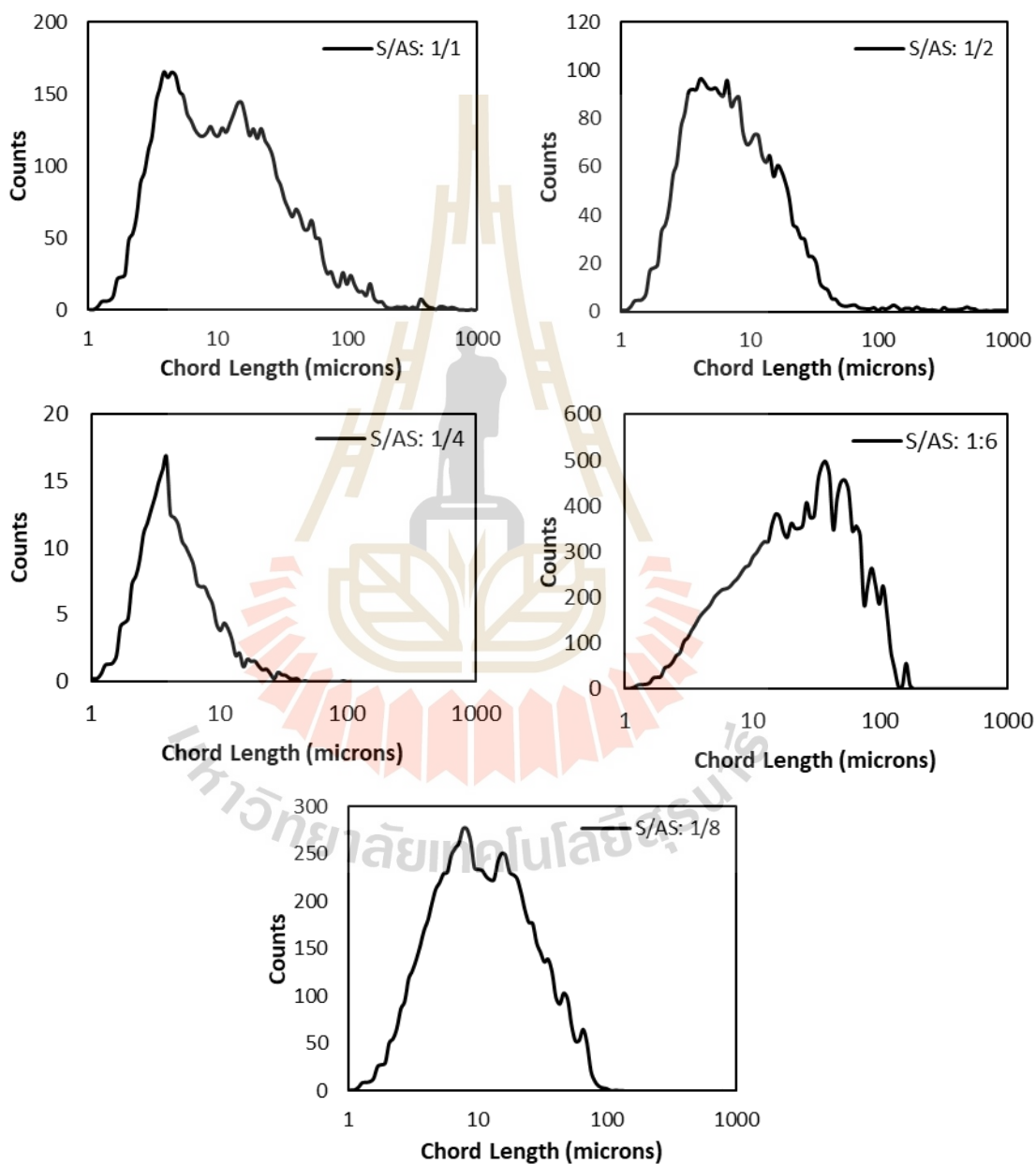


Figure A1 Particle size distribution by FBRM at different solvent-to-anti-solvent volume ratios.

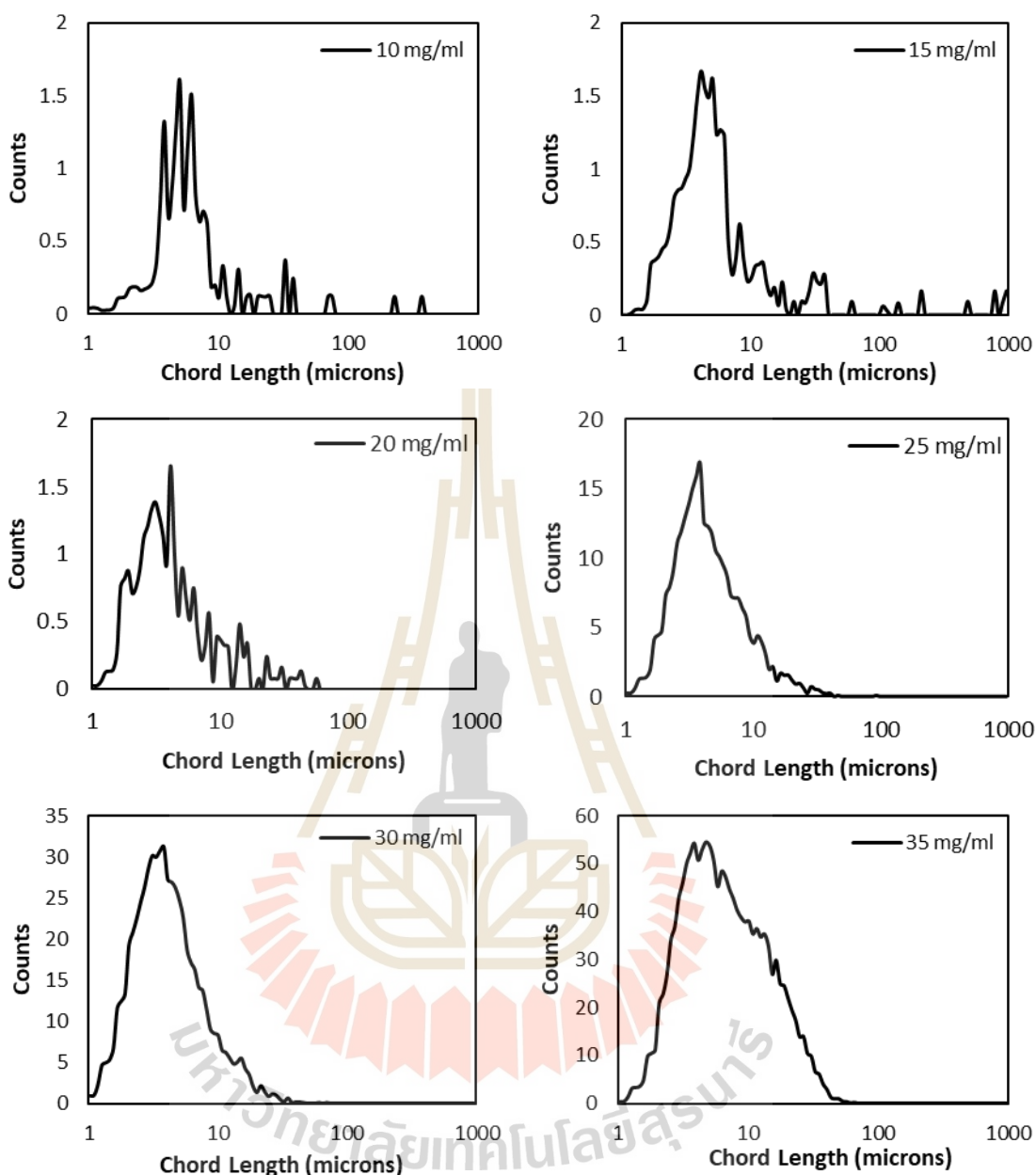


Figure A2 Particle size distribution by FBRM at different papain concentrations.

The counts of particles measured at the micro size level using FBRM was low, which did not correspond to the color of the resulting suspension. The suspension appeared very cloudy, which typically indicates a higher number of particles. This was one of the reasons why the researchers perceived that papain particles obtained by precipitation using this method might be at the nano level.

A.2 SEM images of ACS/Papain composites

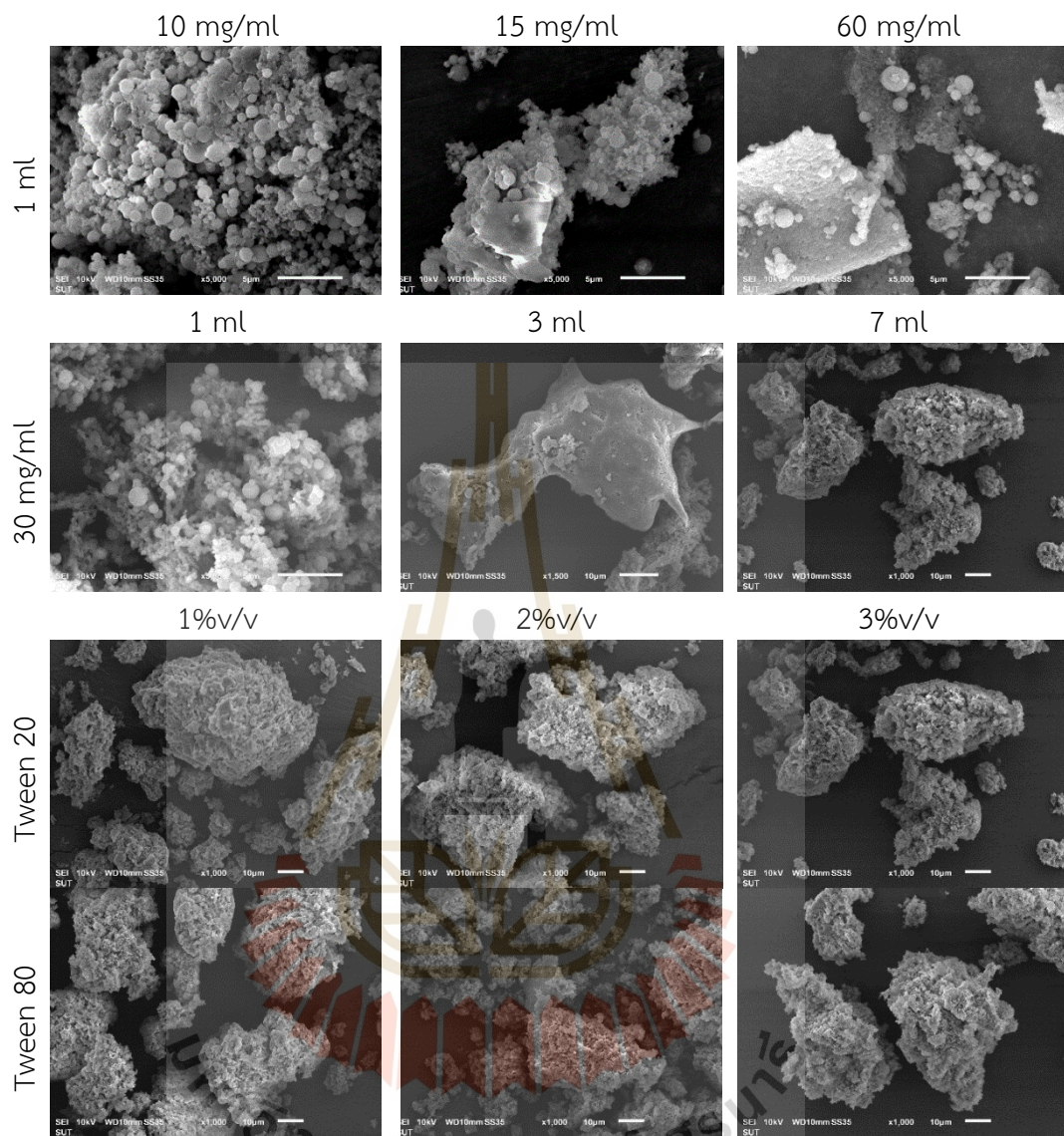


Figure A3 SEM images of ACS/Papain composites at various conditions.

A.3 FTIR Data of papain/ACS mixture

The Fourier Transform Infrared (FTIR) spectroscopy technique was employed to confirm the encapsulation of papain within the acetylated starch (ACS) composites. The FTIR spectra provides detailed information on molecular interactions and validates the successful encapsulation process.

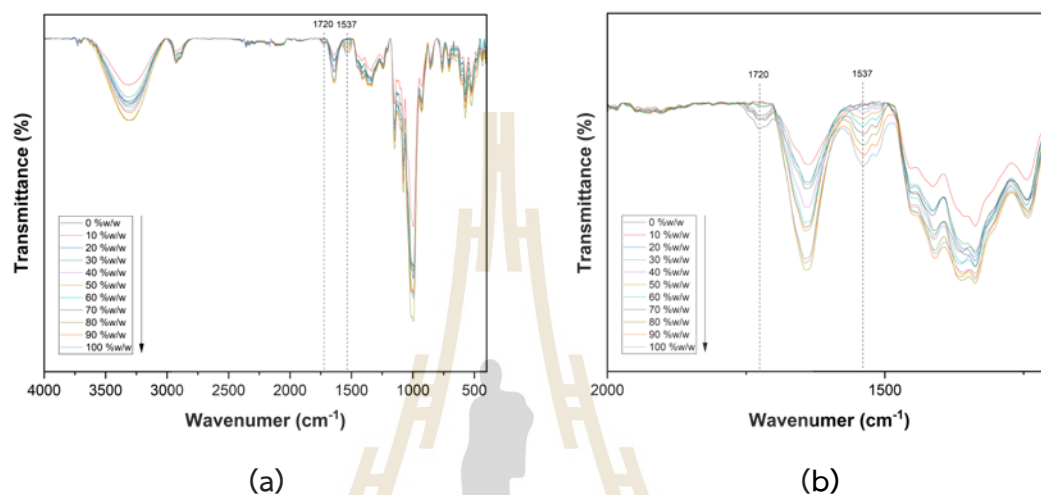


Figure A4 The FTIR spectra of different amount of papain in Papain/ACS mixture (a) 400-4000 cm^{-1} and (b) 1200-2000 cm^{-1}

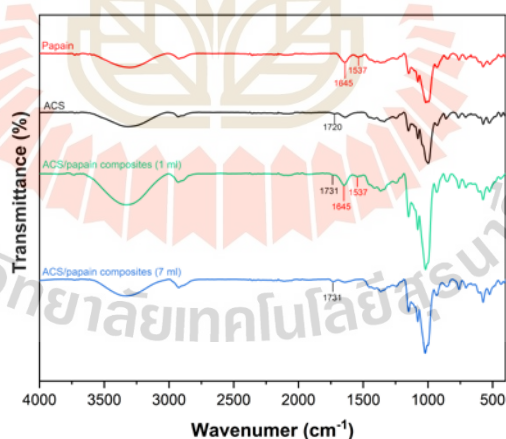


Figure A5 The FTIR spectra of ACS/Papain composites to confirm the presence of papain in solid form.

Key Observations

- **Disappearance of Papain Peaks:** The FTIR spectra of the ACS/papain composites showed that the characteristic peaks of pure papain were absent.

- **Encapsulation Evidence:** The disappearance of papain's characteristic peaks suggests successful encapsulation, with no free papain remaining on the surface or in the solid form.

Analysis

- **Absence of Amide I and Amide II Bands:** The notable amide I (around 1650 cm^{-1}) and amide II (around 1540 cm^{-1}) bands were not present in the spectra of ACS/papain composites, indicating no free papain.

- **Starch Peaks:** The spectra showed peaks corresponding to acetylated starch (around 1730 cm^{-1}), indicating the integration and encapsulation of papain within the starch matrix.

Figure A4 demonstrates the use of FTIR spectra with varying concentrations of papain and acetylated starch to confirm and distinguish the characteristic peaks of papain and acetylated starch. This approach aids in the analysis of encapsulation by providing a clear understanding of which peaks are affected by the presence of papain and which are inherent to the starch.

Figure A5 illustrates the FTIR spectra of ACS/papain composites at different volumes, specifically at 1 ml and 7 ml, to demonstrate the presence or absence of free papain in solid form on the surface of the composites or free particles. At the 1 ml volume, a distinct amide II peak is observed, indicating the presence of free papain in solid form, while the amide I peak, although overlapping with the acetylated starch peak, shows considerable intensity compared to the spectra of pure papain and acetylated starch. In contrast, at the 7 ml volume, the amide II peak is no longer present, suggesting the absence of free papain in solid form. Additionally, a prominent carbonyl C=O stretching vibration peak of acetylated starch at 1731 cm^{-1} confirms successful encapsulation, and the intensity of the amide I peak is significantly reduced, further indicating the absence of free papain. These findings align with the results from the fluorescent spectra discussed in Chapter 4, confirming the successful encapsulation of papain within the ACS matrix at higher volumes.

The logo of Sakon Nakhon Rajabhat University is a large, faint watermark in the background. It features a central figure of a person standing within a stylized, golden, A-shaped structure. Below this is a circular emblem containing a book and a lotus flower. The entire logo is surrounded by a decorative border of red and orange triangles.

APPENDIX B
PUBLICATIONS AND PRESENTATIONS

มหาวิทยาลัยเทคโนโลยีสุรนารี

B.1 List of publications

Sasitorn Boonkerd, Hongxun Hao, and Lek Wantha (2024). **Preparation and Characterization of Acetylated Starch/Papain Composites**. RSC advances (Accepted).

Sasitorn Boonkerd, and Lek Wantha (2023). **Antisolvent Crystallization of Papain**. ChemEngineering, 8(1), 4.



Please do not adjust margins

ARTICLE

Preparation and Characterization of Acetylated Starch/Papain Composites

Sasitorn Boonkerd,^a Hongxun Hao^b and Lek Wantha*^aReceived 10th August 2024,
Accepted 11th November 2024

DOI: 10.1039/x0xx00000x

This research aimed to prepare and characterize of acetylated starch/papain composites by encapsulating papain within acetylated cassava starch with a low degree of substitution (DS = 0.037) through a stepwise antisolvent precipitation method. The effect of starch concentrations, starch solution volumes, and surfactant types and concentrations were examined. Increasing starch concentrations generally enhanced EE, but excessive concentrations led to decreased performance due to starch aggregation. Furthermore, LC decreased as starch concentration increased, while the volume of the starch solution primarily influenced LC. Surfactants were employed to disperse particles and prevent aggregation during encapsulation, with higher concentrations, particularly of Tween 80, improving both EE and LC, but reducing papain activity. Optimal results were achieved with a starch concentration of 30 mg/ml, 7 ml of solution, and 3% v/v Tween 80, resulting in an EE of 96.23% and an LC of 12.40%. However, residual papain activity under these conditions dropped to approximately 56%. In contrast, Tween 20 at 1% v/v preserved higher papain activity (~87%), although it yielded a lower EE of 69.87% and LC of 9.32%. SEM images revealed that the resulting composite particles had rough, indistinct clusters with surfaces featuring clustered starch nanoparticles. Confirmatory analyses via fluorescence spectra and FTIR confirmed successful papain entrapment within acetylated starch with a lower degree of substitution.

1. Introduction

Papain or papaya proteinase I (EC 3.4.22.2), an enzyme that is extracted from papaya (*Carica papaya*), is primarily sourced from the latex of the papaya plant, which can be found in its leaves, stems, and unripe fruits.¹ This enzyme consists of 212 amino acids.² Papain's versatility extends across various industries, including food processing, cosmetics formulation, detergent manufacturing, leather processing, and pharmaceutical production.³ Its enzymatic properties make it valuable in numerous applications, such as wound healing,⁴ anti-inflammatory formulations,⁵ antibacterial treatments⁶ and even exhibits antioxidant properties.⁷ Furthermore, papain has shown promise in cancer therapy⁸ and its role in aiding digestion.⁹ Despite its wide range of benefits, the use of papain in medical or pharmaceutical applications, as well as in food, faces several limitations due to its chemical instability, low bioavailability, and pH instability under acidic conditions (pH below 2.8).^{10,11}

Encapsulation is one of method to produce composite particles which it is a process of enclosing substances within a carrier material to protect them from external factors such as heat, moisture, and oxidation, thereby enhancing their stability and prolonging their shelf life.¹² In the pharmaceutical industry,

encapsulation is commonly used to deliver drugs in a controlled manner, ensuring targeted release and improved efficacy while minimizing side effects.¹³ Similarly, in the food industry, encapsulation can preserve flavors, vitamins, and nutrients, preventing degradation during processing or storage.¹² Overall, encapsulation offers versatile solutions for various applications, ranging from drug delivery and food preservation to cosmetics and agriculture. Therefore, encapsulation is a method that can help improve the chemical stability and oral bioavailability of papain for various applications.

Carrier materials come in various forms, including synthetic polymers, biopolymers, or inorganic porous materials etc.^{10,14,15} The choice of carrier materials is essential to the properties of particles. In the encapsulation of papain, various materials have been used to protect and controlled release of papain, such as chitosan-reinforced alginate,¹⁶ poly(ϵ -caprolactone),² poly(lactic-co-glycolic acid) (PLGA),¹⁰ PVA nanofibers,^{17,18} hydroxypropyl methylcellulose phthalate (HPMCP), Eudragit L 100 and Eudragit S 100¹⁹ etc. However, to our knowledge, no publications have been devoted to the encapsulation of papain using starch as a carrier material.

Starch has gained popularity as an encapsulation material for bioactive compounds in the food and biomedical fields due to its a natural, renewable, biodegradability and biocompatibility.^{20,21} It has been successfully used to encapsulate a range of substances, including curcumin,^{22,23} catechin,²⁴ luteolin,²⁵ diclofenac sodium,²⁶ quercetin,²⁷ zeaxanthin,²¹ ciprofloxacin¹⁵ and bovine serum albumin (BSA).²⁸ Starch's ability to protect and deliver these bioactive compounds while maintaining their stability and functionality

^aSchool of Chemical Engineering, Institute of Engineering, Suranaree University of Technology, Nakhon Ratchasima 30000, Thailand. E-mail: lekwa@g.sut.ac.th

^bNational Engineering Research Center of Industrial Crystallization Technology, School of Chemical Engineering and Technology, Tianjin University, Tianjin 300072, China

Please do not adjust margins

Please do not adjust margins

ARTICLE

Journal Name

has made it an excellent choice for encapsulation. With its numerous benefits, starch has become an increasingly attractive option for encapsulation material in various applications while also protecting it from adverse environmental conditions.

There are various types of starch used for encapsulation, such as native starch,^{21, 27, 28} OSA starch,²⁹ acetylated starch,^{15, 28} oxidized starch,²⁵ cross-linked starch,²⁶ and other type of modified starch.²⁰ Native starch offers several advantages, such as environmental friendliness, biocompatibility, and non-toxicity.^{20, 21} However, it may not be suitable for controlling drug release due to its tendency to rapidly release drugs.^{28, 30} This rapid release is attributed to the high swelling of native starch granules and their susceptibility to enzymatic digestion in biological fluids.^{15, 28} Therefore, if controlling drug release is desired, modified starches are of interest as they offer better control over drug release.²⁸

Acetylated starch is one of the modified starches capable of controlling drug release, as this modification helps reduce swelling and improves resistance to enzymatic digestion compared to native starch.^{22, 28} However, the properties of acetylated starch depend on the degree of substitution (DS).^{15, 28} The higher the DS, the better it inhibits swelling and enzymatic digestion.²⁸ However, most of factories in Thailand can only produce acetylated starch with low DS. To increase its value, this study selected low-DS acetylated starch as the encapsulation material.

The encapsulation of proteins into coating particles can be achieved through various methods, such as emulsion evaporation/extraction, solvent evaporation, interfacial, physical absorption, antisolvent precipitation, and supercritical fluid antisolvent precipitation, among others.³¹⁻³³ In this research, antisolvent precipitation was employed to encapsulate papain with acetylated starch. This method stands out for its simplicity, quickness, and ease of operation, requiring no extended shear or stirring rates, sonication, or very high temperatures. Additionally, it offers high encapsulation efficiency with low power consumption.³⁴

Encapsulation of papain is very important to improve the stability of papain, so the encapsulation process is primarily studied in this research for preparing the acetylated starch/papain composites. This work aimed to design and fabricate a papain delivery system by encapsulating papain with acetylated cassava starch (ACS) with lower DS using a stepwise antisolvent precipitation method and to determine effect of the concentration and volume of the starch solution including type and concentration of surfactant on papain encapsulation. The chosen surfactants, Tween 20 and Tween 80, are both biocompatible and widely used in the food and pharmaceutical industries.³⁵ This selection ensures the safety of the encapsulation process and potential future applications. The analysis focused on evaluating the effect on encapsulation efficiency, enzyme loading capacity, and residual activity of papain. The characterization of ACS/Papain composite utilized diverse techniques: fluorescence spectroscopy, Fourier transform infrared spectroscopy (FTIR), and scanning electron microscopy (SEM). These methodologies aim to ascertain the

success of papain encapsulation within acetylated cassava starch (ACS) at lower DS, providing insights into the effective coating of papain.

2. Materials and methods

2.1 Materials

Papain powder (GRM058, Mw = 23 kDa) and L-cysteine hydrochloride monohydrate (GRM046) were purchased from Himedia (Nashik, India). Acetylated cassava starch (ACS) with low DS (DS = 0.037 and Acetyl content = 0.96%) was supported by Sanguan Wongse Industries Co., Ltd., Nakhon Ratchasima, Thailand. Ethanol was purchased from Duksan (Gyeonggi-do, Korea). Tween 20 (T20) and Tween 80 (T80) were purchased from Loba Chemie™ (Mumbai, India). Na-benzoyl-DL-arginine 4-nitroanilide (BAPNA) was purchased from Sigma-Aldrich (Saint-Louis, Switzerland). Dimethyl sulfoxide, Sodium hydroxide, and ethylenediaminetetraacetic acid were purchased from RCI-Labscan (Bangkok, Thailand). All other chemicals and reagents used were of analytical grade.

2.2 Preparation of Acetylated Cassava Starch (ACS) Solution

The ACS solution was prepared using a two-step process, involving heating/gelatinization and subsequent ultrasonication, following a well-established method.³⁶⁻³⁸ Briefly, acetylated cassava starch, dispersed in DI water at a concentration of 100 mg/ml, underwent gelatinization in a shaking water bath at 90 °C for 30 minutes, with shaking set at 180 rpm. The gelatinized starch paste was then cooled to approximately 60 °C. Following this, a 10-minute ultrasonication process using a kHz ultrasonic processor (Branson SFX250 Digital Sonifier, Branson Ultrasonics, USA) equipped with a probe transducer featuring a flat tip of 1/2" (13 mm). The ultrasonication, conducted at 60% amplitude with a pulse function (5/2s on/off) to minimize heat generation, was used to ensure the homogeneity in the starch solution. Subsequently, this solution was further diluted to concentrations of 10, 15, 30, and 60 mg/mL in preparation for the subsequent encapsulation process.

2.3 Preparation of ACS/Papain Composites

ACS/Papain composites were prepared using the stepwise antisolvent precipitation³⁹ with minor modifications, and ethanol was used as antisolvent. Papain was initially precipitated from a 1 ml aqueous solution with a concentration of 30 mg/ml by adding ethanol solution containing different surfactants (Tween 20 and Tween 80) at various concentrations (1%, 2%, and 3% v/v). This step was carried out at a volume ratio of 1:8 (papain solution to ethanol solution). Subsequently, Acetylated cassava starch (ACS) solutions at varying concentrations (10, 15, 30, and 60 mg/ml) and volumes (1, 3, and 7 ml) were added to the papain suspension. This mixture was stirred for 30 minutes at 500 rpm to achieve a homogenous dispersion. Homogenization using a homogenizer at 8000 rpm for 1 minute was then conducted to facilitate the settling of fine particles in the colloidal suspension in ethanol-water systems.

Please do not adjust margins

Please do not adjust margins

Journal Name

ARTICLE

The resulting sediments were collected by centrifugation (BKC-TH16R11, BIOBASE, China) for 10 minutes at 3000 rpm. They were then washed with ethanol to dehydrate and subsequently filtrated using a 0.25 μm membrane using vacuum pump. After filtration, the ACS/Papain composites were dried in a desiccator to remove any remaining moisture and dry the composite.

2.4 Preparation of Standard Curve of Papain Concentration

Creating a standard curve for papain involved utilizing various concentrations of papain, and subsequently recording the corresponding absorbance values at 278 nm. This approach allows for the establishment of a reliable relationship between the concentration of papain and its absorbance, providing a basis for accurate quantification in subsequent analyses. This calibration curve was previously established and reported in our previous work.⁴⁰

2.5 Encapsulation Efficiency (EE) and Loading Capacity (LC)

The encapsulation efficiency (EE) and loading capacity (LC) of the ACS/papain composites were obtained by measuring the absorbance of free papain in the collected solution at 278 nm by a spectrophotometer (DR6000, Hach, USA). Concurrently, a blank sample, comprising composites without papain but with an identical composition to the test sample, underwent the same procedure as the test sample, mitigating potential contributions from other components to the absorbance. Finally, the papain content was quantified against the standard calibration curve of papain in DI water. EE and LC of papain were computed using the following equations:^{2, 23}

$$\text{EE (\%)} = \frac{\text{initial amount of papain} - \text{amount of free papain}}{\text{initial amount of papain}} \times 100\% \quad (1)$$

$$\text{LC (\%)} = \frac{\text{amount of papain used} - \text{amount of free papain}}{\text{total weight of composites}} \times 100\% \quad (2)$$

The method for determining the amount of free papain (unencapsulated papain) varied depending on the volume of starch solution used in the encapsulation process. For starch solution volumes of 1 and 3 ml, the free papain was quantified by combining free papain in the supernatant with the free papain obtained by twice washing the dried precipitate with an ethanol solution (1:1 water: ethanol with surfactant). Conversely, for a starch solution volume of 7 ml, only the supernatant obtained after centrifugation was used to determine the amount of free papain.

2.6 Enzyme Activity Measurement

The evaluation of enzyme activity, based on Arnon Ruth's methodology (1970),^{17, 41} 1 ml of free-papain solution (1 mg/ml) or papain samples solution were placed into test tubes. A precisely measured 5 ml of the substrate solution (43.5 mg of BAPNA in 1 ml of dimethyl-sulfoxide and the volume was adjusted to 100 ml with 0.05 M Tris buffer, pH 7.5 containing 0.005 M cysteine and 0.002 M EDTA) was added. Following a

25-minute incubation at 298.15 K, the enzymatic reaction was terminated by adding 1 ml of 30% acetic acid. The quantification of liberated p-nitroaniline was then conducted via spectrophotometric analysis at 410 nm (SP-UV 200, Spectrum Instruments, China). Notably, control tubes without enzyme demonstrated the absence of self-hydrolysis.

Units and specific activity: The enzymatic activity of papain was quantified based on substrate hydrolysis. BAPNA activity is defined as the enzyme hydrolyzing 1 micromole of substrate per minute ($E = 8800$). This is calculated using the equation described by I.E. Moreno-Cortez et al.:¹⁷

$$\text{BAPA units } (\mu\text{mol}/\text{min}) = \frac{\Delta A_{410\text{nm}}}{t} \times \frac{3 \times 1000}{8800} \quad (3)$$

where $\Delta A_{410\text{nm}}$ is absorbance at 410 nm, t is the time in minutes, which is the duration of the enzymatic reaction, and $8800 \text{ M}^{-1}\text{cm}^{-1}$ is the p-nitroanilide molar extinction coefficient at 410 nm. Specific activity is expressed as units per milligram of protein.

The residual activity (RA) was determined by comparing the enzyme's activity after the process to its initial activity. This was calculated using the following equation:^{42, 43}

$$\text{Residual Activity (\%)} = \left(\frac{\text{Post-process enzyme specific activity}}{\text{Initial enzyme specific activity}} \right) \times 100\% \quad (4)$$

The specific activity of the enzyme was first measured before the process, and post-process activity was determined under the same conditions. The residual activity is reported to reflect the enzyme's retention of function after the process.

2.7 Particle Characterization

Papain and papain loaded starch particles were analyzed using a fluorescence spectrometer (FP-8300, JASCO Corp., Japan). Fluorescence spectra of pure papain (1 mg papain dissolved in 1 ml of DI water and then mixed with 8 mL ethanol) and ACS/Papain composites dispersions were recorded. Excitation was performed at 280 nm, and the emission spectra were obtained between 290 nm and 450 nm using a quartz cell with a 10 mm path length. Both the excitation and emission bandwidths were set at 5 nm. All data was collected at room temperature.

The morphology of the particles was examined using Scanning Electron Microscopy (SEM) and Field Emission Scanning Electron Microscope (FE-SEM). SEM and FE-SEM analysis were performed using the JEOL JSM-6010LV and JEOL JSM-7800F models (JEOL Ltd, Tokyo, Japan). The observations were conducted at an accelerating voltage of 10 kV and 3 kV for SEM and FE-SEM, respectively. During the analysis, the surface of the samples was sputter-coated with a gold layer for SEM and a carbon layer for FE-SEM to avoid charging.

The Fourier Transform Infrared (FTIR) spectra for papain, ACS, ACS composites and ACS/Papain composites were recorded using a Fourier Transform Spectrophotometer (Tensor 27, Bruker, Germany) with a range of 4000 to 400 cm^{-1} with 2 cm^{-1} resolution. To obtain the baseline adjustment.

Please do not adjust margins

Please do not adjust margins

Journal Name

ARTICLE

papain concentration were examined. The primary role of the antisolvent is to reduce the solubility of papain in the solution, leading to rapid precipitation. The antisolvent induces a high degree of supersaturation, which increases the nucleation rate. This increased nucleation rate leads to the continuous development of small, amorphous particles.^{47, 48} The choice of solvent and antisolvent is very important. Water was used as the solvent because papain has good solubility in water. For the antisolvent, three types of organic solvents were used: acetone, acetonitrile, and ethanol, as papain is sparingly soluble or insoluble in these solvents. Additionally, the solvent and antisolvent must be miscible to ensure effective precipitation of papain.^{1, 40, 48}

The results revealed that ethanol was the most suitable antisolvent for papain precipitation because it maintains the highest enzyme activity compared to the other two organic solvents. Additionally, ethanol offers a safer and more environmentally friendly option, effectively reducing the solubility of papain in water and leading to rapid precipitation with minimal aggregation. The optimal conditions for papain precipitation were found to be at a papain concentration of 30 mg/ml and a solvent-to-antisolvent volume ratios of 1:4 (Fig. 1(a)), where papain maintained its stability at a zeta potential of 35.1 ± 3.6 mV and maintains 100% activity with a particle size of 207.6 ± 2.1 nm.

However, upon further utilization for encapsulation purposes, it was observed that at a 1:4 ratio, the papain precipitates tended to aggregate (Fig. 1(c)). Increasing the ratio to 1:8 (Fig. 1(b)) resulted in smaller (179.1 ± 1.4 nm) and more uniform papain precipitates with reduced aggregation (Fig. 1(d)) and a relatively high zeta potential (43.9 ± 1.9 mV), suggesting that the precipitates were stable and suitable for encapsulation with starch. Despite this, the higher ratio (1:8) at 30 mg/ml of papain also led to the formation of larger particles (more than 1000 nm). Consequently, for the encapsulation experiments, we opted for a papain solution concentration of 30 mg/ml and a solvent-to-antisolvent volume ratio of 1:8 for the initial precipitation step.

3.2 Preparation of ACS/Papain Composites

After identifying the optimal conditions for papain precipitation, papain encapsulation was proceeded to form the ACS/Papain composites. In this section, the effects of starch concentration and starch volume on the process were investigated. Moreover, two surfactants, Tween 20 and Tween 80, at different concentrations were tested.

3.2.1 Effect of Starch Concentrations

The study of starch concentration's effects is crucial in encapsulation processes. This study investigated starch concentrations ranging from 10 mg/ml to 60 mg/ml, using Tween 20 as the surfactant at a concentration of 3% v/v and a starch solution volume of 1 ml. Concentrations beyond this range result in rapid aggregation of starch particles, making effective papain encapsulation difficult.

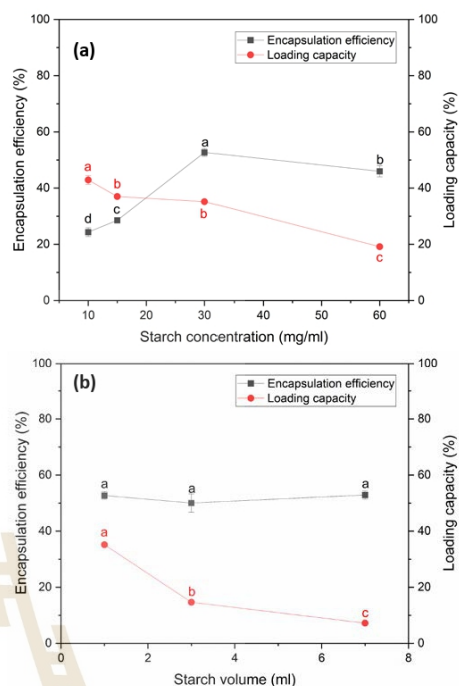


Fig. 2 Encapsulation efficiency and loading capacity of ACS/papain composites as functions of (a) starch concentration with fixed volume of starch solution of 1 ml and Tween 20 concentration of 3%v/v, and (b) starch volume with fixed starch concentration of 30 mg/ml and Tween 20 concentration of 3%v/v.

The results, depicted in Fig. 2(a), illustrate the encapsulation efficiency and loading capacity of ACS/papain composites as a function of starch concentration. From 10 to 30 mg/ml, the encapsulation efficiency rises significantly from 24.33 ± 1.56 to $52.70 \pm 1.38\%$. However, at 60 mg/ml, encapsulation efficiency decreases to $45.99 \pm 1.97\%$. This trend aligns with similar observations in the encapsulation of *Lactobacillus acidophilus* into porous starch.⁴⁹ The decline in encapsulation efficiency at higher starch concentrations is attributed to the increased viscosity of the starch solution at 60 mg/ml, which causes rapid precipitation and aggregation of starch particles. This higher viscosity inhibits diffusion between the starch solution and ethanol, resulting in non-uniform molecular supersaturation and slower nucleation rates. Consequently, larger and more aggregated particles are formed,^{37, 48} reducing the encapsulation efficiency. Even with the addition of surfactant to aid in dispersion, these challenges persist due to the rapid self-aggregation of starch before effective encapsulation of papain can occur.

Meanwhile, the loading capacity (LC) continuously decreases from $42.89 \pm 1.58\%$ at 10 mg/ml to $19.15 \pm 0.67\%$ at 60 mg/ml. The LC values at 15 mg/ml and 30 mg/ml are quite

Please do not adjust margins

similar, at $37.02 \pm 0.60\%$ and $35.18 \pm 0.60\%$, respectively. This continuous reduction is likely due to the increase in the amount of starch as the starch concentration increases, which lowers the amount of papain encapsulated per unit of starch. At higher concentrations, the starch particles tend to aggregate, leading to less effective encapsulation. This aggregation reduces the available surface area for encapsulating papain, as a result, LC greatly decreased from $35.18 \pm 0.60\%$ at 30 mg/ml to $19.15 \pm 0.67\%$ at 60 mg/ml.

Therefore, a starch concentration of 30 mg/ml was selected for subsequent experiments, as it provided the highest encapsulation efficiency and a relatively high loading capacity. While these methods proved effective in encapsulation, the efficiency of encapsulation decreases with higher starch concentrations. Hence, selecting an appropriate starch concentration is crucial in producing composites with the highest encapsulation efficiency towards papain particles.

3.2.2 Effect of Starch Solution Volumes

To find suitable encapsulation efficiency of papain without increasing the starch concentration beyond 30 mg/ml, the volume of starch solution was adjusted. Volumes of 1, 3, and 7 ml were examined, maintaining a starch concentration of 30 mg/ml and using tween 20 at 3% v/v as the surfactant. The results shown in Fig. 2(b) demonstrate the encapsulation efficiency and loading capacity of ACS/papain composites as a function of starch solution volume. Encapsulation efficiency at volumes of 1, 3, and 7 ml are $52.70 \pm 1.38\%$, $50.02 \pm 3.28\%$, and $52.89 \pm 1.47\%$, respectively. These values do not significantly differ from each other, indicating that encapsulation efficiency is relatively stable across different starch volumes. This result suggests that the amount of starch used in these volumes is sufficient to encapsulate the available papain, achieving a saturation point where additional starch does not further enhance encapsulation efficiency.

However, the loading capacity gradually decrease as the volume of starch solution increase. This reduction occurred

because although more starch was used for encapsulation, the amount of papain encapsulated remained the same. A starch volume of 7 ml was chosen as the optimal choice, as it allows any unencapsulated papain to dissolve back into the solution, making it easier to separate from the final product. This simplifies the purification process, as dissolved papain can be easily removed by centrifugation or filtration. In contrast, at volumes of 1 and 3 ml, residual free papain remains in solid form, requiring additional steps for removal, increasing process complexity and waste. These extra washing steps also raise the risk of papain degradation.

Hence, a starch solution volume of 7 ml seemed the most suitable for subsequent experiments, as it balances encapsulation efficiency and loading capacity while simplifying the purification process and minimizing the risk of papain degradation.

3.2.3 Effect of Surfactants

In the process of encapsulating papain with starch, surfactants such as Tween 20 and Tween 80 are employed to aid in dispersing the starch particles effectively, preventing them from aggregating and forming clumps (Fig. 3).⁵⁰ Besides facilitating particle dispersion, Tween surfactants are commonly studied in pharmaceutical applications to ensure protein stability, as demonstrated in research by Duskey et al.,⁵¹ who investigated the influence of different types of Tween—20, 60, and 80—on enzyme activity and stability during the encapsulation process of β -glucosidase (β -Glu) in PLGA nanoparticles. Furthermore, other studies have shown that Tween surfactants can enhance enzyme activity⁵² and protect protein surfaces from denaturation.⁵³ However, it's worth noting that while Tween surfactants can enhance enzyme activity for some enzymes, these may also cause a decrease in activity for others, as observed in studies by Battestin & Macedo⁵⁴ and Kar et al.,⁵⁵ which investigated the impact of four types of Tween—Tween 80, Tween 60, Tween 40, and Tween 20—ranging from 0.025-1 %v/v on tannase activity. The results indicated that Tween caused a reduction in tannase activity. From Fig. 4(c), both Tween 20 and Tween 80 caused a decrease in papain activity as their concentrations increased. This reduction in activity is likely due to the interaction between the surfactants and the papain molecule. The fatty acid tails of the Tween molecules—oleic acid in Tween 80 and lauric acid in Tween 20—can bind to hydrophobic regions on the papain surface, potentially disrupting its conformation and hindering its enzymatic activity.⁵⁴ This effect parallels findings observed with tannase in previous studies.^{54, 55} However, the system with Tween 20 retained slightly higher activity than Tween 80. This difference may be attributed to the varying lengths and saturation levels of the fatty acid tails, with the shorter, more saturated lauric acid in Tween 20 causing less disruption to the papain molecule than the longer oleic acid in Tween 80.⁵⁶

For studying the effect of Tween 20 and Tween 80 on encapsulation efficiency and loading capacity, the concentration of both Tween 20 and Tween 80 was limited to 3% v/v. This restriction was implemented because investigations revealed that papain activity decreased



Fig. 3 Effect of surfactants on starch particle dispersion: (a) Without surfactant and (b) With surfactant.

Please do not adjust margins

Journal Name

ARTICLE

significantly to 50-60% when the surfactant concentration reached 3% v/v after the precipitation process (Fig. 4(c)). The results from Fig. 4(a) and (b) indicate that both encapsulation efficiency and loading capacity were influenced by the type and concentration of the surfactants. With Tween 20, encapsulation efficiency and loading capacity decreased initially within the range of 1 to 2% v/v. This decrease is likely due to Tween 20 molecules interacting with both papain and starch particles, hindering papain encapsulation. At concentrations of 2-3% v/v, encapsulation efficiency and loading capacity remained relatively constant. This result of Tween 20 aligns with the findings of Duskey et al.,⁵¹ where an increase in the concentration of Tween 20 resulted in initially decreased both encapsulation efficiency and loading capacity and was then relatively constant.

Conversely, for Tween 80, both parameters increased as the concentration increased from 1 to 3% v/v. Tween 80 appears to be more effective at dispersing starch particles and promoting papain encapsulation within the particles. This is similar to the findings obtained by Shae MA et al.⁵⁷ This could be due to the longer oleic acid tail in Tween 80, allowing for better interaction with both starch and papain.

For residual activity after the encapsulation process, give an example of the result at 3% v/v Tween 80, the post-encapsulation papain activity remained at $55.70 \pm 7.18\%$. Remarkably, no additional loss in activity was observed after encapsulation compared to the initial precipitation step, where the activity was $53.21 \pm 0.94\%$, indicating no additional activity loss during the final step.

At the highest encapsulation efficiency and loading capacity, Tween 20 achieved $69.87 \pm 2.36\%$ and $8.96 \pm 0.30\%$, respectively, at 1% v/v. In comparison, Tween 80 reached $96.23 \pm 2.06\%$ and $12.40 \pm 0.23\%$, respectively, at 3% v/v.

Interestingly, Tween 20's highest residual activity occurred at the same point as its peak EE and LC, yielding approximately 87%. In contrast, Tween 80's highest residual activity occurred at a concentration of 1% v/v, where it reached approximately 80%, alongside EE and LC values of $75.14 \pm 6.10\%$ and $9.95 \pm 0.73\%$, respectively.

3.3 Particle Characterization

3.3.1 Fluorescent Spectrum

Fluorescence spectroscopy analysis was utilized to confirm the encapsulation process. Fig. 5 illustrates the emission spectra of pure papain and ACS/papain composites dispersions upon excitation at 280 nm. In Fig. 5(d), the maximum emission wavelength of papain is determined to be 322 nm (black spectrum), consistent with a previous report documented at 332 nm.² The fluorescence intensities of ACS/papain composites at varying starch concentrations (1 ml) exhibit distinct values, correlating with the encapsulation efficiency (%EE) (Fig. 5(a)). Specifically, as the %EE increases, indicating a higher degree of successful encapsulation of papain within the carrier material, the intensity tends to decrease. This decrease is attributed to the reduction in the presence of free papain

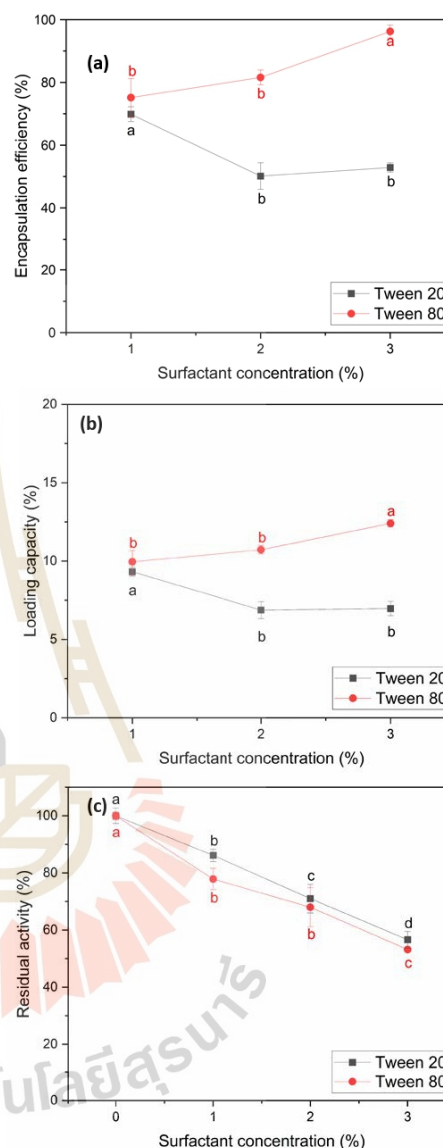


Fig. 4 Encapsulation efficiency (a) and loading capacity (b) with fixed starch concentration of 30 mg/ml and starch solution volume of 7 ml, (c) residual activity after papain precipitation as functions of surfactant concentration (%v/v) and surfactant types.

Please do not adjust margins

Please do not adjust margins

ARTICLE

Journal Name

molecules, unencapsulated papain molecules, which typically contribute to the overall intensity observed in the solution or solid form. This relationship suggests that the ACS encapsulation effectively shields papain, reducing the availability of papain to emit fluorescence in response to excitation. Conversely, lower %EE values correspond to higher fluorescence intensities, reflecting a greater concentration of free papain molecules.

For differing starch volumes (Fig. 5(b)), the intensity values at the maximum wavelength are similar across the conditions, consistent with their respective %EE values, suggesting that altering starch volume does not significantly impact the fluorescence emission, possibly due to uniform encapsulation efficiency across varying starch volumes. In the surfactant results (Fig. 5(c)), the fluorescence intensities at different concentrations of Tween 80 align with the obtained %EE values. However, Tween 20 at 1% v/v, which has the highest %EE, shows higher intensity compared to Tween 20 at 3% v/v, which has a lower %EE. This higher intensity is due to the greater

presence of papain on the composite surface at 1% v/v. Conversely, Tween 80 at a concentration of 3% v/v, with the highest %EE of $97.31 \pm 1.24\%$, did not show an intensity value at the maximum wavelength. Fig. 5(d) indicates that at this highest %EE, no emission maximum is detected (red spectrum), signifying that papain molecules are effectively encapsulated by ACS with minimal free papain remaining. This supports successful papain encapsulation within ACS, consistent with the findings of Budama-Kilinc Y. et al.²

3.3.2 FTIR Analysis

The FTIR spectra of ACS, papain, ACS composites, and ACS/papain composites are summarized in Table 1, while Fig. 6 illustrates these spectra for comparative visualization.

The FTIR spectra of ACS reveal characteristic absorption bands associated with acetylated starch. Peaks at 1150, 1078, and 1012 cm^{-1} corresponds to C-O bond stretching, while additional characteristic absorption bands at 999, 923, 860, 765,

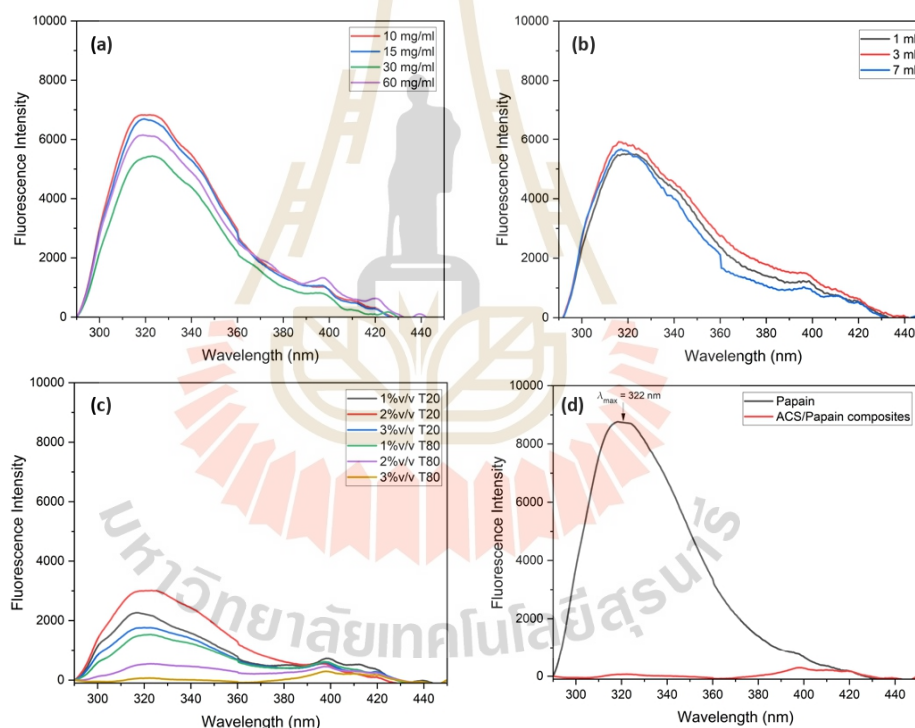


Fig. 5 Fluorescence spectra of ACS/papain composites: (a) at different starch concentrations, (b) at different starch volume, (c) at different surfactant type and concentrations, and (d) at optimum condition (30 mg/ml, 7 ml, and 3% v/v Tween 80) and pure papain.

Please do not adjust margins

Please do not adjust margins

Journal Name

ARTICLE

and 572 cm^{-1} are attributed to the stretching vibrations of the anhydroglucose ring, reflecting the basic structural components of the starch. A peak at 1641 cm^{-1} is assigned to water adsorption, indicating the presence of bound water within the starch. The band at 2931 cm^{-1} corresponds to C-H stretching vibrations, and a broad band around 3300 cm^{-1} corresponds to the O-H stretching vibrations, representing both free and inter-/intramolecularly bound hydroxyl groups, which are crucial to

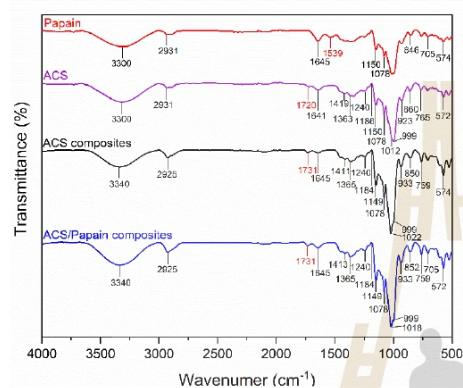


Fig. 6 The FTIR spectra of papain, ACS, ACS composites and ACS/papain composites.

the structure of starch. Furthermore, as the starch used is acetylated starch, additional peaks are observed at 1720 , 1419 , and 1363 cm^{-1} , attributed to carbonyl C=O, CH_3 antisymmetric bending vibration, and CH_3 symmetry bending vibration, respectively. These additional peaks confirm the introduction of acetyl groups into the starch granules.

The FTIR spectra of papain show a broad absorption band at 3300 cm^{-1} , corresponding to N-H stretching of secondary amide bonds, representing the protein backbone. A peak at 2931 cm^{-1} is associated with $-\text{CH}_2-$ asymmetric stretching. The amide-I and amide-II bands are observed at 1645 cm^{-1} and 1539 cm^{-1} , respectively, confirm the protein's secondary structure, reflected in the peptide bond vibrations. Papain also shows characteristic peaks between 1150 , 1078 , 846 cm^{-1} and 705 – 574 cm^{-1} , attributed to sulphide and disulphide ($-\text{CS}$) stretching vibrations. Additionally, the peak observed at 846 cm^{-1} is also attributed to the aromatic residues of tryptophan or tyrosine.

In contrast, the FTIR spectra of ACS composites that have undergone a process without papain loading but with the inclusion of tween 80 show peaks closely aligned with ACS, the raw material. However, noticeable changes in peak intensity and position. Specifically, the carbonyl C=O peak becomes sharper and shifts from 1720 to 1731 cm^{-1} , and the C-O bond stretching peak shifts from 1012 to 1022 cm^{-1} and becomes more pronounced. These changes likely result from the addition of tween 80 and subsequent reprecipitation, which could induce alterations in the structure and properties of ACS. The O-H stretching vibration shifts from 3300 to 3340 cm^{-1} ,

indicating stronger hydrogen bonding within the matrix, possibly due to interactions with the surfactant and cross-linking.

Upon comparing the spectra of papain, ACS composites, and ACS/papain composites, it is observed that many papain peaks overlap with those of ACS composites. However, the distinguishing peaks between ACS composites and papain are the amide-II peak (1537 cm^{-1}) for papain and the carbonyl C=O peak (1731 cm^{-1}) for ACS composites. In the spectra of ACS/papain composites, the amide-II peak of papain is absent, while the carbonyl C=O peak of ACS composites is present. This absence of the amide-II peak suggests that papain has been encapsulated within the ACS without remaining in its free form. Previous studies have reported similar results,^{2, 22, 24, 25} where the peak representing the core material disappears or decrease in intensity, confirming the successful encapsulation. Additionally, the increased intensity of the amide-I peak (1645 cm^{-1}) and the O-H stretching (3340 cm^{-1}) compared to ACS composites indicates interactions between the papain and ACS, likely through hydrogen bonding between the hydroxyl ($-\text{OH}$) and carboxyl groups ($-\text{COOH}$) of ACS and the amide groups of papain. This further confirms the enhanced hydrogen bonding in ACS/papain composites, supporting the successful encapsulation of the enzyme.

Other studies have used starch as a coating material and reported similar encapsulation behavior for active ingredients and starch, where hydrogen bonding between hydroxyl and carboxyl groups facilitated encapsulation.^{15, 22, 58} In this study, the encapsulation of papain with ACS is achieved through similar interactions. The hydroxyl ($-\text{OH}$) and carboxyl ($-\text{COOH}$) groups on ACS form hydrogen bonds with functional groups on papain, such as the amide groups, facilitating the entrapment of papain within the ACS matrix. These hydrogen bonds not only aid in the encapsulation process but also contribute to maintaining the enzyme's structural integrity and activity, enhancing the overall efficacy of the encapsulation.

3.3.3 Morphology of Particles

The morphological images of native papain particles, native ACS particles, and ACS/papain composites under a starch concentration of 30 mg/ml , starch volume of 7 ml , and Tween 80 concentration of $3\%v/v$ are depicted in Fig. 7, obtained using scanning electron microscopy. The native papain particles typically exhibit indistinct shapes (Fig. 7(a)). However, after undergoing precipitation with ethanol, its shape and size transform into spherical and decreases in size from micro to nano levels (Fig. 1). In the case of ACS, the morphological characteristics showed elliptical, kettledrum, or spherical truncated shapes, with some damaged granule particles observed (Fig. 7(b)). On the other hand, the ACS/papain composites appear as rough, indistinct clusters rough, indistinct clusters, with the surface featuring small starch nanoparticles clustered together (Fig. 7(c) and (d)), which is similar to the morphology observed in the work of Li et al.²¹ who encapsulated zeaxanthin with corn starch using a one-step antisolvent precipitation method.

Please do not adjust margins

Table 1. The FTIR spectrum of Papain, ACS and ACS/Papain composite

Assignment of Papain	References		Assignment of ACS		References		This study	
	Papain	ACS/Pap.com.	Papain	ACS/Pap.com.	Papain	ACS/Pap.com.	ACS	ACS/Pap.com.
N-H stretching of secondary amide bond	3300 ⁶¹	3340	3300	3340	3405 ²²	3340	3300	3340
	3289 ²				3388 ²⁸			
	3450-3225 ⁶²				3421 ^{15, 59}			
-CH ₂ -asymmetric stretching	2924 ⁶¹	2925	2931	2925	3404 ²¹			
	2931 ²				3000-3700 ⁶⁰			
					2930 ²²	2925	2931	2925
-CONH amide I	1637 ⁶¹	1645	1645	1645	2930 ¹⁵	1645	1641	1645
	1652 ²				2935 ⁶⁰			
	1645, 2 ⁶²				1644 ²¹	1645	1641	1645
-CONH amide II	1551 ⁶¹	-	1539	-	1655 ⁶⁰			
	1557 ²				1731 ²²	1731	1720	1731
					1754 ²⁸			
CS stretching (sulphide)	1150 ⁶¹	1150	1150	1149	1750 ¹⁵	1240	1240	1240
	1076 ⁶¹	1078	1078	1078	1760 ⁶⁰			
	1080 ²				1754 ⁵⁹			
-CS stretching (disulphide)	852 ⁶¹	846	846	852	1240 ^{59, 60}	1240	1240	1240
	705-570 ¹⁸	705-574	705-574	705-572	1193 ²⁸			
					1435 ^{15, 59}	1419	1411	1413
Aromatic residue of tryptophan or tyrosine	868, 850 ^{18, 19}	846	846	852	1373 ²⁸	1363	1365	1365
					1245 ²⁸			
					1375 ^{15, 59}			
Anhydroglucose ring stretching vibration	992, 930, 862, 763, 574 ¹⁵	992, 930, 862, 763, 574 ¹⁵	992, 930, 862, 763, 574 ¹⁵	992, 930, 862, 763, 574 ¹⁵	1380 ⁶⁰	1186, 1150, 1078, 1012	1184, 1149, 1078, 1022	1184, 1149, 1078, 1018
	935, 855, 767, 577 ⁶⁰	935, 855, 767, 577 ⁶⁰	935, 855, 767, 577 ⁶⁰	935, 855, 767, 577 ⁶⁰	1024 ¹⁵			
	992, 929, 861, 765, 575 ⁵⁹	992, 929, 861, 765, 575 ⁵⁹	992, 929, 861, 765, 575 ⁵⁹	992, 929, 861, 765, 575 ⁵⁹	1155, 1086, 1022 ⁶⁰			

Please do not adjust margins

Journal Name

ARTICLE

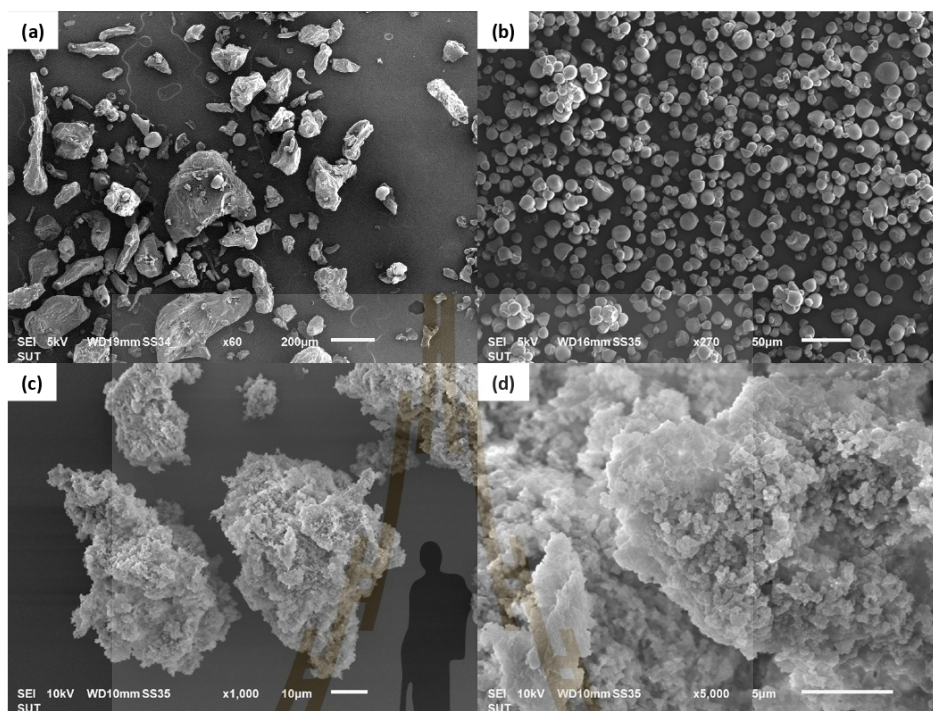


Fig. 7 SEM photomicrographs of (a) native papain particles, (b) native ACS particles, (c) and (d) ACS/papain composites.

4. Conclusion

The preparation of ACS/Papain composites by encapsulation of papain within ACS with a low degree of substitution ($DS = 0.037$) using the stepwise antisolvent precipitation method was achieved. The study of the effect of starch concentration, starch solution volume, and surfactant type and concentration could determine suitable condition to achieve high encapsulation efficiency and loading capacity, with minimal loss of enzyme activity. The findings reveal that while surfactants facilitate encapsulation, their higher concentrations impact enzyme activity. Tween 80, in particular, achieved the highest encapsulation efficiency, although it led to a notable decrease in papain activity. On the other hand, Tween 20 better preserved papain activity compared to Tween 80, though its encapsulation efficiency remained lower. The ACS/Papain composites were successfully confirmed by SEM images, fluorescence spectra, and FTIR spectra.

Although the encapsulation process yielded clear results in terms of efficiency, the decrease in papain activity indicates that surfactant selection and encapsulation conditions should be further investigated to better preserve enzyme functionality.

Future research should investigate different surfactant types and concentrations to improve the enzyme's stability and activity. Furthermore, studying the papain release profile of ACS composites in a physiological setting will help us better understand the protective effect of encapsulation. Exploring different organic solvents and applying this approach to other enzymes could broaden the potential applications of ACS-based composites, providing valuable insights into the encapsulation system's strengths and limitations.

Author contributions

The conceptualization of the study was conducted by S.B. and L.W., with methodology developed by both authors as well. S.B. carried out the investigation and data curation were done by S.B. and L.W. The original draft was prepared by S.B., and the review and editing were performed by S.B., H.H., and L.W. Visualization was also handled by S.B. The project was supervised and administered by L.W., who also acquired the necessary funding. All authors have read and agreed to the published version of the manuscript.

Please do not adjust margins

Please do not adjust margins

ARTICLE

Journal Name

Conflicts of interest

There are no conflicts to declare.

Data availability

All data generated or analyzed during this study are included in this published article.

Acknowledgements

This work was supported by (i) Suranaree University of Technology (SUT), (ii) Thailand Science Research and Innovation (TSRI), and (iii) National Science, Research and Innovation Fund (NSRF) - Grant no. 160346 and 179270. The authors also acknowledge the research funding from the SUT Research and Development Fund. S.B. also wishes to express gratitude to Suranaree University of Technology for generously providing a grant in support of her pursuit of a Master's degree.

References

- E. El-Zalaki, *Alex. J. Fd. Sci. & Technol.*, 2021, **18**, 27-32.
- Y. Budama-Kilinc, R. Cakir-Koc, S. Kecel-Gunduz, T. Zorlu, Y. Kokcu, B. Bicak, Z. Karavelioglu and A. E. Ozel, *J. Fluoresc.*, 2018, **28**, 1127-1142.
- H. Shouket, I. Ameen, O. Tursunov, K. Kholikova, O. Pirimov, N. Kurbonov, I. Ibragimov and B. Mukimov, *IOP Conf. Ser. Earth Environ. Sci.*, 2020.
- R. N. F. Moreira Filho, N. F. Vasconcelos, F. K. Andrade, M. F. Rosa and R. S. Vieira, *Colloids Surf. B Biointerfaces*, 2020, **194**, 111222.
- A. Ezekiel and M. Florence, *Am. J. Biochem. Biotechnol.*, 2012, **8**, 99-104.
- M. M. dos Anjos, A. A. da Silva, I. C. de Pascoli, J. M. G. Mikcha, M. Machinski, R. M. Peralta and B. A. de Abreu Filho, *Int. J. Food Microbiol.*, 2016, **216**, 121-126.
- C. R. da Silva, M. B. Oliveira, E. S. Motta, G. S. de Almeida, L. L. Varanda, M. de Padula, A. C. Leitao and A. Caldeira-de-Araujo, *J. Biomed. Biotechnol.*, 2010, **2010**, 197898.
- S. P. Chandran, K. P. Nachimuthu, S. B. Natarajan, M. G. Inamdar and M. S. B. M. Shahimi, *Curr. Cancer Ther. Rev.*, 2018, **14**, 75-87.
- C. Muss, W. Mosgoeller and T. Ender, *Neuro Endocrinol. Lett.*, 2013, **34**, 38-46.
- C. Chankhampān, J. Manosroi, H. Yamamoto, K. Tahara, W. Manosroi, Y. Kawashima and A. Manosroi, *J. Exp. Nanosci.*, 2012, **9**, 138-151.
- C. Channamade, J. M. Raju, S. B. Vijayaprakash, R. Bora and N. R. Shekhar, *J. Young Pharm.*, 2021, **13**, 87-90.
- N. J. Zuidam and V. Nedovic, *Encapsulation technologies for active food ingredients and food processing*, Springer, 2010.
- I. Klojdova, T. Milota, J. Smetanova and C. Stathopoulos, *Pharmaceuticals*, 2023, **16**.
- L. N. Hassani, F. Hindre, T. Beuvier, B. Calvignac, N. Lautram, A. Gibaud and F. Boury, *J. Mater. Chem. B.*, 2013, **1**, 4011-4019.
- S. H. Mahmoudi Najafi, M. Baghaie and A. Ashori, *Int. J. Biol. Macromol.*, 2016, **87**, 48-54.
- C. I. S. Arisanti, H. Rachmawati, J. S. Pamudji and Y. C. Sumirtapura, *J. Pharm. Sci. Appl.*, 2012, **1**.
- I. E. Moreno-Cortez, J. Romero-Garcia, V. Gonzalez-Gonzalez, D. I. Garcia-Gutierrez, M. A. Garza-Navarro and R. Cruz-Silva, *Mater. Sci. Eng. C Mater. Biol. Appl.*, 2015, **52**, 306-314.
- E. Shoba, R. Lakra, M. S. Kiran and P. S. Korrapati, *RSC Adv.*, 2014, **4**, 60209-60215.
- M. Sharma, V. Sharma, A. K. Panda and D. K. Majumdar, *Yakugaku Zasshi*, 2011, **131**, 697-709.
- F. Zhu, *Food Chem.*, 2017, **229**, 542-552.
- S. Li, D. Feng, E. Li and R. G. Gilbert, *Foods*, 2023, **12**.
- L. Acevedo-Guevara, L. Nieto-Suaza, L. T. Sanchez, M. I. Pinzon and C. C. Villa, *Int. J. Biol. Macromol.*, 2018, **111**, 498-504.
- S. F. Chin, S. N. A. Mohd Yazid and S. C. Pang, *Int. J. Polym. Sci.*, 2014, **2014**, 1-8.
- M. Ahmad, P. Mudgil, A. Gani, F. Hamed, F. A. Masoodi and S. Maqsood, *Food Chem.*, 2019, **270**, 95-104.
- Y. Y. Chen, K. Liu, X. Q. Zha, Q. M. Li, L. H. Pan and J. P. Luo, *Carbohydr. Polym.*, 2021, **273**, 118552.
- M. E. El-Naggar, M. H. El-Rafie, M. A. El-sheikh, G. S. El-Feky and A. Hebeish, *Int. J. Biol. Macromol.*, 2015, **81**, 718-729.
- Y. Farrag, W. Ide, B. Montero, M. Rico, S. Rodriguez-Llamazares, L. Barral and R. Bouza, *Int. J. Biol. Macromol.*, 2018, **114**, 426-433.
- H. Xiao, F. Yang, Q. Lin, Q. Zhang, W. Tang, L. Zhang, D. Xu and G. Q. Liu, *Int. J. Biol. Macromol.*, 2019, **138**, 556-564.
- X. Liu, L. A. Ibarra-Sanchez, M. J. Miller and Y. Lee, *Curr. Res. Food Sci.*, 2022, **5**, 1110-1117.
- L. Tuovinen, S. Peltonen and K. Jarvinen, *J. Control. Release*, 2003, **91**, 345-354.
- C. Ye and H. Chi, *Mater. Sci. Eng. C Mater. Biol. Appl.*, 2018, **83**, 233-246.
- D. J. McClements, *Adv. Colloid Interface Sci.*, 2018, **253**, 1-22.
- B. Mishra, B. B. Patel and S. Tiwari, *Nanomed.: Nanotechnol. Biol. Med.*, 2010, **6**, 9-24.
- F. Y. de Boer, A. Imhof and K. P. Velikov, *Color. Technol.*, 2019, **135**, 183-194.
- F. Rancan, J. Jurisch, C. Gunday, E. Tureli, U. Blume-Peytavi, A. Vogt, C. Schaudinn and N. Gunday-Tureli, *Pharmaceutics*, 2021, **13**.
- Y. Chang, X. Yan, Q. Wang, L. Ren, J. Tong and J. Zhou, *Food Chem.*, 2017, **227**, 369-375.
- H. Dong, L. Chen, Q. Zhang, J. Gao and T. Vasanthan, *Food Hydrocoll.*, 2021, **121**.
- H. Dong, Q. Zhang, J. Gao, L. Chen and T. Vasanthan, *Food Hydrocoll.*, 2022, **122**.
- S. Yang, L. Dai, C. Sun and Y. Gao, *Food Hydrocoll.*, 2018, **85**, 185-194.
- S. Boonkerd and L. Wantha, *ChemEngineering*, 2023, **8**.
- R. Arnon, in *Methods in enzymology*, Elsevier, 1970, vol. 19, pp. 226-244.
- J. Milošević, B. Jančević, R. Prodanović and N. Polović, *Amino Acids*, 2019, **51**, 829-838.
- J. K. Gill, V. Orsat and S. Kermasha, *J. Solgel Sci. Technol.*, 2018, **85**, 657-663.
- M. Morales-Cruz, G. M. Flores-Fernandez, M. Morales-Cruz, E. A. Orellano, J. A. Rodriguez-Martinez, M. Ruiz and K. Griebenow, *Results Pharma. Sci.*, 2012, **2**, 79-85.
- H. Fessi, F. Puisieux, J. P. Devissaguet, N. Ammoury and S. Benita, *Int. J. Pharm.*, 1989, **55**, R1-R4.

Please do not adjust margins

Please do not adjust margins

Journal Name


ARTICLE

46. L. C. Nelemans, M. Buzgo and A. Simaite, presented in part at the The 1st International Electronic Conference on Pharmaceutics, 2020.
47. M.-W. Park* and S.-D. Yeo, *Sep. Sci. Technol.*, 2010, **45**, 1402-1410.
48. I. J. Joye and D. J. McClements, *Trends Food Sci. Technol.*, 2013, **34**, 109-123.
49. Y. Xing, Q. Xu, Y. Ma, Z. Che, Y. Cai and L. Jiang, *Food Funct.*, 2014, **5**, 972-983.
50. X. Bu, X. Wang, L. Dai, N. Ji, L. Xiong and Q. Sun, *Int. J. Biol. Macromol.*, 2020, **163**, 2048-2059.
51. J. T. Duskey, I. Ottonelli, A. Rinaldi, I. Parmeggiani, B. Zambelli, L. Z. Wang, R. K. Prud'homme, M. A. Vandelli, G. Tosi and B. Ruozi, *Nanomaterials*, 2021, **11**.
52. G. Kamande, J. Baah, K.-J. Cheng, T. McAllister and J. Shelford, *J. Dairy Sci.*, 2000, **83**, 536-542.
53. A. Arsiccio, J. McCarty, R. Pisano and J. E. Shea, *J. Phys. Chem. B*, 2018, **122**, 11390-11399.
54. V. Battestin and G. A. Macedo, *Electron. J. Biotechnol.*, 2007, **10**, 0-0.
55. B. Kar, R. Banerjee and B. C. Bhattacharyya, *Process Biochem.*, 2003, **38**, 1285-1293.
56. B. A. Kerwin, *J. Pharm. Sci.*, 2008, **97**, 2924-2935.
57. M. Ali Attia Shafie, *J. Clin. Exp. Ophthalmol.*, 2013, **04**.
58. I. Buljeta, A. Pichler, I. Ivic, J. Simunovic and M. Kopjar, *Molecules*, 2021, **26**.
59. H. Chi, K. Xu, X. Wu, Q. Chen, D. Xue, C. Song, W. Zhang and P. Wang, *Food Chem.*, 2008, **106**, 923-928.
60. N. Sakhnini, N. Al-Zoubi, G. Al-Obaidi and A. Ardakani, *Pharmazie*, 2015, **70**, 177-182.
61. R. S. Peres, E. Armelin, J. A. Moreno-Martínez, C. Alemán and C. A. Ferreira, *Appl. Surf. Sci.*, 2015, **341**, 75-85.
62. M. Sharma, V. Sharma, A. K. Panda and D. K. Majumdar, *Int J Nanomedicine*, 2011, **6**, 2097-2111.

Please do not adjust margins

Article

Antisolvent Crystallization of Papain

Sasitorn Boonkerd ¹ and Lek Wantha ^{1,2,*} 

¹ School of Chemical Engineering, Institute of Engineering, Suranaree University of Technology, Nakhon Ratchasima 30000, Thailand; b6003944@g.sut.ac.th

² Research Unit of Adsorption, Catalysis & Energy Storage, Suranaree University of Technology, Nakhon Ratchasima 30000, Thailand

* Correspondence: lekwa@g.sut.ac.th

Abstract: Protein crystallization plays a crucial role in the food and pharmaceutical industries, enhancing product quality and efficiency by improving purity and controlled particle characteristics. This study focused on the crystallization of the versatile protein papain, extracted from papaya. Antisolvent crystallization was performed. This method is cost-effective and is a simple and energy-efficient approach. Beyond protein crystal production, the antisolvent crystallization process serves as a method for encapsulating active pharmaceutical ingredients (APIs). The study investigated organic solvents like ethanol, acetone, and acetonitrile as potential antisolvents. Additionally, the impact of variables such as the solvent-to-antisolvent (S:AS) volume ratio and papain concentration on particle size, particle size distribution, zeta potential, crystallization yield, and residual activity of papain crystals were examined. Ethanol emerged as the optimal antisolvent, reducing the solubility of papain and preserving papain's crystalline structure with minimal activity loss. Optimal conditions were identified at a 1:4 S:AS volume ratio and a papain concentration of 30 mg/mL, resulting in nanosized spherical crystals with a high yield and preserved activity. This research underscored the crucial role of thoughtful parameter selection in antisolvent crystallization to achieve specific particle characteristics while maintaining the functionality of the crystallized substance.

Keywords: papain; antisolvent crystallization; particle size; papain activity; crystallization yield; zeta potential



Citation: Boonkerd, S.; Wantha, L. Antisolvent Crystallization of Papain. *ChemEngineering* **2024**, *8*, 4. <https://doi.org/10.3390/chemengineering8010004>

Academic Editor: Isabella Nova

Received: 8 November 2023

Revised: 7 December 2023

Accepted: 13 December 2023

Published: 20 December 2023



Copyright: © 2023 by the authors. Licensee MDPI, Basel, Switzerland. This article is an open access article distributed under the terms and conditions of the Creative Commons Attribution (CC BY) license (<https://creativecommons.org/licenses/by/4.0/>).

1. Introduction

Papain is an enzyme extracted from papaya (*Carica papaya*) and is primarily found in papaya latex, such as in leaves, stems, and raw fruits [1]. It is a versatile enzyme consisting of a 212-amino acid peptide chain [2]. Its applications are diverse: it serves as a meat tenderizer, aids in dairy production, acts as a gentle exfoliant in cosmetics, removes tough stains in detergents, and adjusts and conditions leather in the leather processing industry [3]. Moreover, papain contributes to the process of wound healing [4], possesses anti-inflammatory activity [5], can be an antibacterial agent [6], and shows potential as an antioxidant [7]. It aids in digestion [8] and exhibits promising potential for use in cancer therapy [9–11]. Its versatility extends across various industries, establishing it as a valuable and enduring resource.

Protein crystallization plays a crucial role in various industries, with widespread significance in the cosmetic, food, and biopharmaceutical industries [12–14]. This process yields numerous benefits that profoundly affect the quality and efficiency of protein-derived products. One of its primary functions is to enhance protein purity by selectively removing unwanted impurities [14]. Furthermore, protein crystallization enables meticulous control over particle size and morphology, influencing the overall quality and functionality of the obtained proteins [15]. Protein crystals, characterized by improved solubility, become versatile for applications across industries, ranging from pharmaceuticals to biotechnology. Moreover, protein crystallization contributes to the stability and robustness of the crystal

product [12,14], leading to minimized costs and maximized overall efficiency during storage and transportation processes. These multifaceted advantages of protein crystallization extend beyond mere separation, playing a vital role in shaping the characteristics that define the utility of proteins in diverse industrial applications.

Crystallization is a widely employed method for separation and purification in the production of fine particles and for product design. Various techniques, such as the use of antisolvents, evaporation, cooling, and reaction, are utilized to induce crystallization [16]. Antisolvent crystallization, which involves the addition of a dissolving agent (called an antisolvent) to reduce the solubility of the solute in the solvent, is a particularly simple, low-energy, and cost-effective method, making it a viable alternative to energy-intensive evaporation and cooling processes. In addition, its application can be employed without compromising thermally sensitive materials or the biological activity of drugs. Therefore, antisolvent crystallization is commonly used in the crystallization of pharmaceutical compounds for practical applications [17].

The antisolvent crystallization process is a highly effective method for producing drug particles ranging from the micro- to nano-size [18]. The primary role of the antisolvent is to reduce the solubility of a solute in the solution, facilitating rapid crystallization. The antisolvent rapidly induces a high level of supersaturation, resulting in an elevated nucleation rate. This increased nucleation rate leads to the development of small particles [19]. The careful selection of suitable antisolvents is critical in this process. Additionally, key process variables such as the temperature, type of antisolvent, solution concentration, injection rate, stirring speed, ultrasound, and the method of mixing the antisolvent with the solution have a significant impact on the size distribution, particle size, morphology, growth rate, and stability of crystals [18,20].

In addition to being used to produce protein crystals, antisolvent crystallization can also be used as a method for encapsulating proteins, active pharmaceutical ingredients (APIs), food, etc. The encapsulation serves to protect substances from unfavorable environmental conditions, increasing protein stability, and aid in drug delivery within the body to reach specific targets and control release. This approach is characterized by its simplicity, rapidity, and ease of operation, eliminating the need for prolonged shear or high stirring rates, sonication, or very high temperatures. Furthermore, it demonstrates high encapsulation efficiency and low power consumption, making it an efficient and practical method for a variety of applications [21]. Antisolvents used for encapsulation are not only liquids but also gases. There are two types of liquid-based methods: the one-step method, which works well for hydrophobic proteins, and the two-step method, which works well for hydrophilic proteins [22].

The purification process is a crucial step in the extraction of papain from papaya latex, and one employed purification method is antisolvent crystallization [1,23]. Moreover, this crystallization technique plays a role in the papain encapsulation process through a two-step antisolvent method. The first step involves the crystallization of papain, followed by the second step, where the crystallized papain is encapsulated [22,24]. Therefore, in this paper, the antisolvent crystallization of papain was investigated. Organic solvents such as ethanol, acetone, and acetonitrile were used as antisolvents. Additionally, the various variables that significantly impact papain crystallization, such as solvent-to-antisolvent volume ratio and papain concentration, were also investigated. The evaluation of these parameters was conducted through the analysis of particle size, particle size distribution, zeta potential, crystallization yield, and papain activity, aiming to identify the optimal conditions for papain crystallization.

2. Materials and Methods

2.1. Materials

Papain powder (GRM058, Mw = 23 kDa) and L-cysteine hydrochloride monohydrate (GRM046) were purchased from Himedia (Nashik, India). Ethanol was purchased from Duksan (Ansan, Republic of Korea). Acetone and acetonitrile were purchased from Carlo

Erba (Val-de-Reuil, France). α -N-benzoyl-L-arginine ethyl ester hydrochloride (BAEE) was purchased from Alfa Aesar (Heysham, UK). N α -benzoyl-DL-arginine 4-nitroanilide (BAPNA) was purchased from Sigma-Aldrich (Saint-Louis, Switzerland). Dimethyl sulfoxide (DMSO) and ethylenediaminetetraacetic acid (EDTA) were purchased from RCI Labscan Limited (Bangkok, Thailand). Deionized water was used for preparing the solutions. All chemicals and reagents used were of analytical grade and used without any further purification.

2.2. Solubility Measurement

The solubility of papain in water/antisolvent mixtures at mass fractions of antisolvent of 0, 0.2, 0.4, 0.5, 0.6, and 0.8 was determined by using the gravimetric method as described by Kongsamai et al. [25] and Qureshi et al. [26]. Briefly, an excess amount of solid papain was added into 10 g of the binary solvent mixture in a jacket crystallizer with temperature control at 298.15 K by circulating water from a thermostat water bath at a stirring rate of 700 rpm. The suspension equilibrated for at least 24 h. Then, suspension was centrifuged at 8000 rpm for 10 min. The supernatant was kept in a vial, which was then weighed at room temperature. Water and antisolvent were then removed by evaporation of the solution at 378.15 K in hot air oven. The residue solid was weighed until a constant weight was achieved. This investigation was used to consider such parameters as optimal and various mass fractions of antisolvent for selecting suitable solvent-to-antisolvent volume ratio ranges in the effect study.

2.3. Crystallization Experiment

The experimental setup for papain crystallization is illustrated in Figure 1, comprising a jacket crystallizer, a thermostat water bath for temperature control, a burette for antisolvent injection, and a magnetic stirrer. The antisolvent was added to the papain solution at a flow rate of 1.22 ± 0.052 mL/s via a burette with free flow, and the magnetic stirrer operated at 500 rpm to agitate a mixture of papain solution and antisolvent. A constant temperature of 298.15 K was maintained and regulated by circulating water from a thermostat water bath.

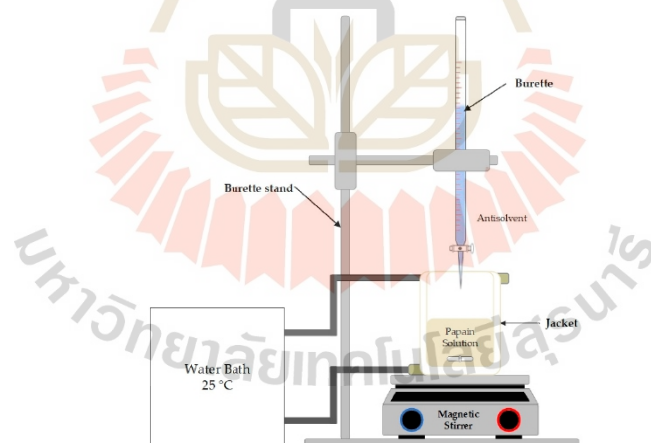


Figure 1. Experimental setup for antisolvent crystallization of papain.

In the papain crystallization experiment, the papain solution was prepared by dissolving papain in deionized water at varying concentrations. Subsequently, 10 mL of the papain solution was placed in the jacket crystallizer (Figure 1). The antisolvent was then added to the papain solution. During this stage, the formation of solid particulates and

subsequent precipitation were noted. Following the addition of the antisolvent, continuous stirring was maintained for 5 min at a temperature of 298.15 K.

The effects of different process variables were investigated, including antisolvent types (acetone, acetonitrile, and ethanol), the solvent/antisolvent (S:AS) volume ratio (1:1, 1:2, 1:4, 1:6, and 1:8), and the papain concentration (10, 15, 20, 25, 30, and 35 mg/mL). Subsequently, the resulting suspension underwent analysis to determine particle size, size distribution, polydispersity index, and zeta potential. Following centrifugation of the suspension, the papain particles were separated from the remaining solution. The papain particles were then characterized to determine the enzyme activity and morphology, while the supernatant was utilized to determine the crystallization yield. This comprehensive approach allowed for a detailed understanding of the effects of different process variables on the crystallization of papain.

2.4. Crystallization Yield

The papain suspension was subjected to centrifugation at 8000 rpm for 10 min (BKC-TH16R11, BIOBASE, Jinan, China). Subsequently, the supernatant was collected, and its absorbance was measured at a wavelength of 278 nm via UV-visible spectroscopy (DR6000, Hach, Ames, IA, USA) to determine the concentration of remaining papain. A prepared calibration curve (Figure 2) at the same wavelength was used to quantify the papain concentration in the supernatant. By determining the amount of papain in the supernatant, the yield of nanoparticle formation could be calculated using the following equation:

$$\text{Crystallization Yield (\%)} = \frac{W_1 - W_2}{W_1} \times 100\% \quad (1)$$

where W_1 is the amount of total papain added and W_2 is the amount of dissolved papain remaining in the supernatant after centrifugation.

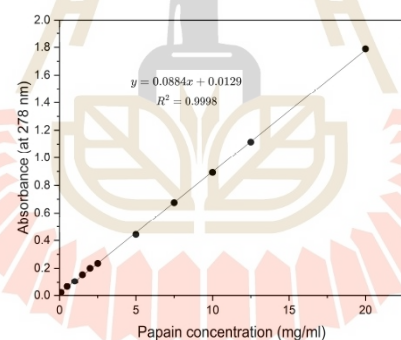


Figure 2. Calibration line for determining the papain concentration.

2.5. Residual Activity

The evaluation of enzyme activity, based on Arnon Ruth's methodology (1970) [27,28], involved the utilization of two distinct substrates: α -N-benzoyl-L-arginine ethyl ester hydrochloride (BAEE) and $N\alpha$ -benzoyl-DL-arginine 4-nitroanilide (BAPNA). The pH-stat method at 298.15 K was employed for the BAEE substrate. The reaction mixture comprised 7 mL of substrate solution (0.08 M BAEE), 1 mL of activators (0.05 M Cysteine and 0.02 M EDTA pH 6.2), and 1 mL of NaCl (3 M) at pH 6.3. Subsequently, 1 mL of either free-papain solution or papain samples solution was added, and the pH was monitored until it reached 6.2. To sustain the pH at 6.2, 20 mM NaOH was introduced, and the time taken for the consumption of 50 μ L of 20 mM NaOH was recorded, repeating the process for approximately 5–10 min. For the BAPNA substrate, 1 mL of free-papain solution

(1 mg/mL) or papain samples solution was placed into test tubes. A precisely measured 5 mL of the substrate solution (43.5 mg of BAPNA in 1 mL of dimethyl-sulfoxide and the volume was adjusted to 100 mL with 0.05 M Tris buffer, pH 7.5, containing 0.005 M cysteine and 0.002 M EDTA) was added. Following a 25 min incubation at 298.15 K, the enzymatic reaction was terminated by adding 1 mL of 30% acetic acid. The quantification of liberated p-nitroaniline was then conducted via spectrophotometric analysis at 410 nm (SP-UV 200, Spectrum Instruments). Notably, control tubes without enzyme addition demonstrated the absence of self-hydrolysis.

Units and specific activity: The enzymatic activity of papain was quantified based on substrate hydrolysis. BAPNA activity is defined as the enzyme hydrolyzing 1 micromole of substrate per minute ($E = 8800$). This is calculated using the following equation:

$$\text{BAPNA units} = \frac{A_{410\text{nm}}}{t} \times \frac{3 \times 1000}{8800} \quad (2)$$

where $A_{410\text{nm}}$ is absorbance at 410 nm; t is the time in minutes, which is the duration of the enzymatic reaction; and $8800 \text{ M}^{-1} \text{ cm}^{-1}$ is the p-nitroanilide molar extinction coefficient at 410 nm.

For the BAPNA substrate, one unit of enzyme activity represents the hydrolysis of 1 micromole of BAEE per minute at 298.15 K. Specific activity is expressed as units per milligram of protein.

2.6. Particle Characterization

Particle size, polydispersity index (PDI), and particle size distribution were determined using dynamic light scattering (DLS) with a Zetasizer (Nano ZS, Malvern Instruments, Worcestershire, UK). Papain particles were directly measured as a suspension in their water/antisolvent mixture. The analysis took place at a scattering angle of 173° in a temperature-regulated cell at 298.15 K. All analyses were conducted on samples appropriately diluted with a water/antisolvent mixture (50 times). For each sample, the mean diameter \pm standard deviation of three determinations was established. Particle size distribution is indicated by PDI values ranging from 0 to 1, where a smaller PDI suggests a narrower size distribution. The zeta potential of the particles in the water/antisolvent mixture was determined in a U-shaped cuvette. All measurements were carried out at 298.15 K in triplicates.

Crystal morphology examination was performed through scanning electron microscopy (SEM) and a microscope. SEM and FE-SEM analysis were executed using the JEOL JSM-6010LV and JEOL JSM-7800F models. The sample underwent a coating process under vacuum conditions through cathodic sputtering with gold and was observed under an accelerating voltage of 10 kV and 3 kV.

3. Results and Discussion

3.1. The Effect of Antisolvent Types

The selection of antisolvent in the crystallization process of papain is a highly crucial step due to its impact on the characteristics of the resulting crystals and the activity of papain. Choosing a suitable antisolvent is essential for controlling the size and morphology of the crystals, as well as ensuring the purity of the obtained papain. Additionally, the choice of antisolvent influences the efficiency and safety of the manufacturing process. Therefore, selecting the appropriate type of antisolvent is the first thing that should be considered. The solubility of papain in water at 298.15 K revealed that papain exhibits high solubility, gradually dissolving until the solution becomes highly viscous. Consequently, water was selected as the solvent for papain crystallization, and three organic solvents, acetone, acetonitrile, and ethanol, were chosen for the antisolvent test. These organic solvents are known for their ability to induce crystallization of proteins, offering a way to effectively separate papain from the solution. In the experiment, antisolvent was added to the papain solution at a papain concentration of 25 mg/mL and a solvent-to-antisolvent

volume ratio of 1:4 using a burette with free flow, followed by stirring for 5 min at 298.15 K. Results indicated that acetonitrile exhibited the highest yield in crystallizing papain from water, followed by acetone and ethanol, respectively (Table 1). From Figure 3b, it is evident that acetonitrile induces a change in color in the crystallized papain, turning it discolored. Furthermore, the crystals become sticky and adhere to the walls of the container, which indicates that the activity could not be determined. As a result, acetone and ethanol are better choices as antisolvents than acetonitrile. Although acetone resulted in more papain crystallization yield than ethanol, it led to sticky crystals with lower residual activity (Table 1). Therefore, ethanol is deemed more suitable for this process compared to the other solvents mentioned because it gives a high crystallization yield and can preserve the enzymatic activity effectively. Additionally, considering environmental impact, ethanol, as an organic solvent, is also more suitable compared to the other solvents mentioned [29].

Table 1. Residual activity of papain precipitate ¹ and crystallization yield (%) at different antisolvent types *.

Antisolvent	Crystallization Yield (%)	Residual Activity (%)
Acetonitrile	98.67 ± 1.15	N/A **
Acetone	89.33 ± 2.31	25.16 ± 5.47
Ethanol	80.10 ± 9.33	82.47 ± 7.00

* Papain concentration: 25 mg/mL; volume ratio of solvent to antisolvent: 1:4. ** Cannot find the value. ¹ Using amidase method (N α -benzoyl-DL-arginine 4-nitroanilide (BAPNA) to subtract).

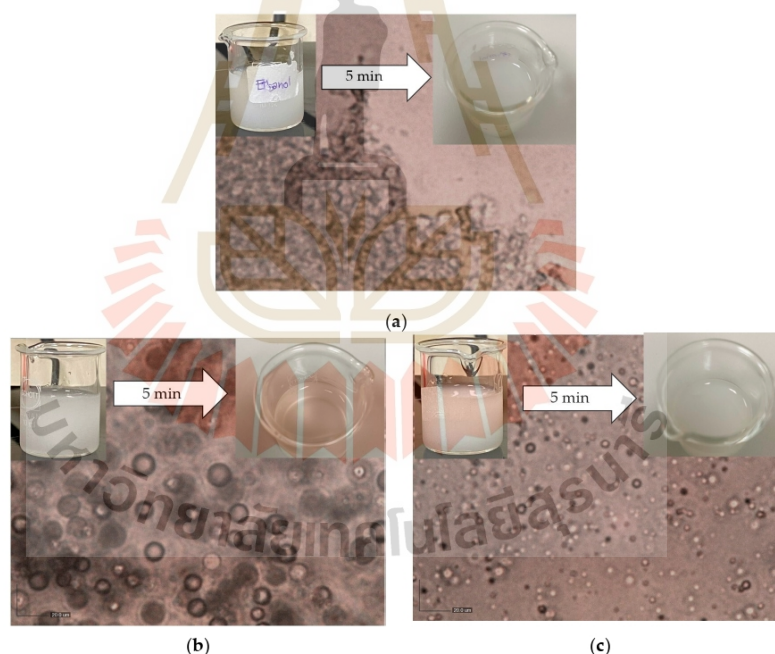


Figure 3. Photomicrographs of papain crystals obtained using different antisolvent types: (a) ethanol, (b) acetonitrile, and (c) acetone.

3.2. The Effect of Solvent-to-Antisolvent Volume Ratios

The experiment investigated the solubility of papain in a water and ethanol mixture (Figure 4), it was observed that an increase in the ethanol content resulted in reduced papain solubility. This confirms that ethanol, as an antisolvent, can reduce the solubility of papain in solution and can be used in an antisolvent crystallization process effectively. However, at mass fractions of 0 and 0.2, solubility was difficult to determine as the papain continued to dissolve, yielding an undesirable viscous and sticky solution. Hence, antisolvent addition at these ratios was considered unsuitable for papain crystallization. Commencing from a mass fraction of 0.4, solubility could be determined, leading the study to focus on mass fractions from 0.4 and above. A mass fraction of 0.4 corresponds to an approximate 1:1 volume ratio of water to ethanol. Various solvent-to-antisolvent volume ratios—1:1, 1:2, 1:4, 1:6, and 1:8—were investigated, representing different added amounts of ethanol to encourage papain crystallization from the solution.

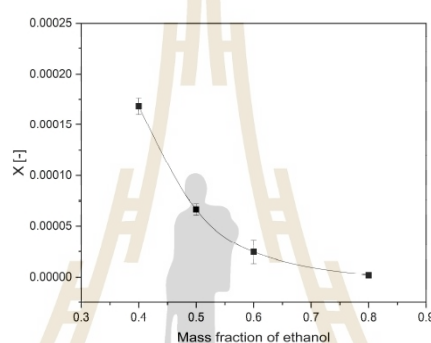


Figure 4. Solubility of papain in water/ethanol mixture at 298.15 K.

The preparation of papain particles involved adding varying volumes of ethanol (acting as the antisolvent) to the papain solution (with a concentration of 25 mg/mL) using a burette with free flow. After the antisolvent addition was completed, continuous stirring was sustained for 5 min at a temperature of 298.15 K. The visual analysis of Figure 5b clearly indicates that varying solvent-to-antisolvent ratios lead to distinctions in the suspended solutions. This change in turbidity is likely attributed to differences in particle number, particle size, and size distribution. Figure 5a,b illustrate that at ratios ranging from 1:1 to 1:4, particles present a uniform dispersion in the suspended solution, devoid of any apparent agglomeration. However, at ratios of 1:6 and 1:8, noticeable particle aggregation occurred, which is confirmed by Figure 5b, and more than one peak was found in Figure 5a, with a small peak indicating the presence of aggregation (larger size). This is likely due to the initial rapid supersaturation of the molecule induced by rapid molecular dehydration under a large solvent-to-antisolvent (S:AS) ratio. In Figure 5d, the S:AS volume ratio influences the zeta potential, that is, as the S:AS volume ratio increases (1:1 to 1:8), the zeta potential also increases (10.8 to 40.1 mV). The zeta potential values are indicative of good colloidal stability in particles. In general, a zeta potential with a magnitude greater than or equal to ± 30 mV is considered suitable for maintaining colloidal stability [30,31]. It is evident that the zeta potential values for ratios of 1:1 and 1:2 are lower than the range associated with stable suspensions. From a ratio of 1:4 onwards, the suspension exhibited higher stability, as indicated by zeta potential values within the stable range. The relationship between the volume of ethanol used and the crystallization yield is evident. With an increase in ethanol volume (from 1:1 to 1:8), the crystallization yield also rises, ranging from 29.33% to 81.83%. Within the ratio range of 1:4 to 1:8, which maintains a stable suspension, the crystallization yield remains consistently high, hovering around 70–80%. The particle sizes

obtained at ratios of 1:1, 1:2, 1:4, 1:6, and 1:8 were in the nanoparticle range, with average sizes of 365.4 nm, 320 nm, 204 nm, 240.3 nm, and 288.3 nm, respectively. Notably, the PDI values, indicative of particle size distribution, were at their lowest (PDI = 0.075) at a ratio of 1:4 (Figure 5c), corresponding with the results shown in Figure 5a. This implies that at a ratio of 1:4, the particle size distribution is narrower and more uniform than at other ratios (Figure 5a,c). Consequently, it can be concluded that papain nanoparticles can be produced using the minimum amount of ethanol at a ratio of 1:4, providing the most suitable conditions for the desired particle characteristics.

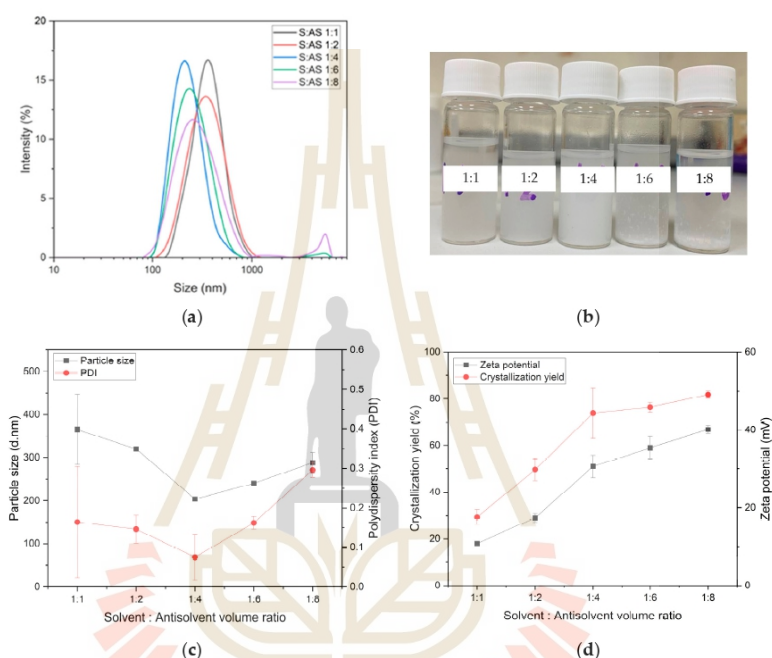


Figure 5. The effect of S:AS volume ratios: (a) particle size distribution, (b) photograph of the suspensions formed after mixing ethanol with papain solution, (c) particle size (back line) and polydispersity index (PDI) (red line), and (d) crystallization yield (red line) and zeta potential (back line) of particles with papain concentration of 25 mg/mL at different S:AS ratios.

3.3. The Effect of Papain Concentration

The concentration of papain is critical in the solution crystallization process. The effect of the concentrations of papain solutions on the particle size, particle size distribution, zeta potential, and crystallization yield were investigated by using six different papain concentrations. Ethanol was added as an antisolvent at a volume ratio of 1:4 S:AS (solvent-antisolvent) to papain solutions with different concentrations (10, 15, 20, 25, 30 and 35 mg/mL) using a burette with free flow at a temperature of 298.15 K. From Figure 6a, it can be observed that an increase in the concentration of papain leads to a significant increase in the average particle size, ranging from 170.3 nm to 184.4 nm, 194.5 nm, 204.0 nm, 207.6 nm, and 211.4 nm, at concentrations of 10, 15, 20, 25, 30, and 35 mg/mL, respectively. This correlation between papain concentration and particle size is in line with the explanation provided earlier. The heightened viscosity resulting from the increased papain concentration interferes with the effective diffusion between the solvent and antisolvent.

This disruption in diffusion leads to non-uniform supersaturation, subsequently slowing down the nucleation rate and promoting particle aggregation, ultimately resulting in larger particle sizes [20].

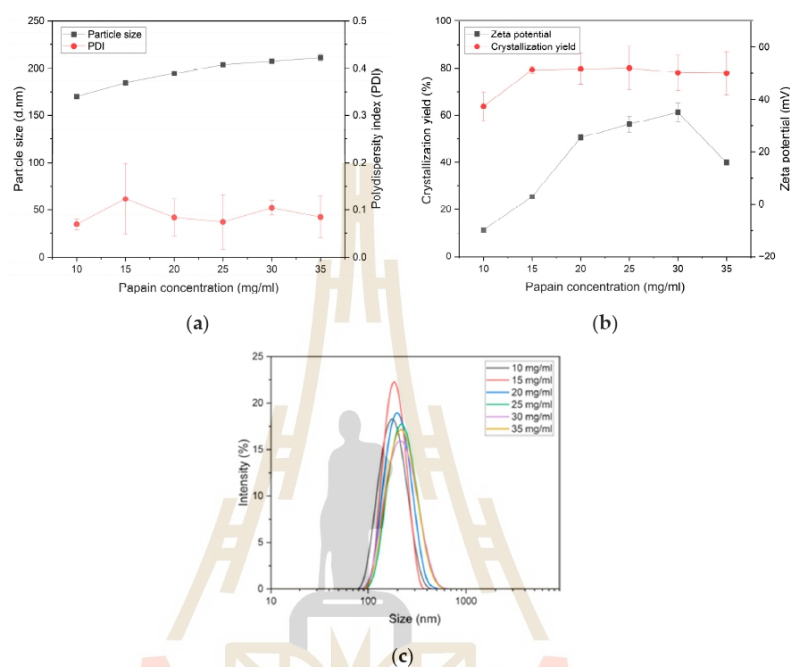


Figure 6. The effect of papain concentrations: (a) particle size (back line) and polydispersity index (PDI) (red line), (b) crystallization yield (red line) and zeta potential (back line), and (c) particle size distribution of particles with papain concentration of 25 mg/mL at different AS:S ratios.

However, regarding particle size distribution (Figure 6a,c), it is evident that at every concentration, there is a narrow size distribution (i.e., low PDI), and these values are within a closely aligned range. This implies that variations in papain concentration do not significantly impact the particle size distribution.

As for crystallization yield, in the initial concentration range of 10–15 mg/mL, an increase in concentration resulted in an increase in yield (63.81 to 79.29%). However, in the concentration range from 15 mg/mL and above, the obtained yield values were relatively constant, hovering around 80%.

Regarding zeta potential (Figure 6b), the concentration of papain influences an increase in zeta potential in the range of 10–30 mg/mL (−9.8 to 35.1 mV) and a decrease at 35 mg/mL (15.9 mV). These values indicate the stability of the formed colloids, as an increase in zeta potential leads to reduced attraction between particles, resulting in lower aggregation [30,31]. Therefore, the concentration of 30 mg/mL appears to be the optimal condition where the suspension exhibits the highest stability, as indicated by the highest zeta potential value (35.1 mV). Moreover, this concentration is also the point where the residual activity is highest (Table 2).

Table 2. Residual activity of papain precipitate at different papain concentrations (25–35 mg/mL)¹.

Concentration (mg/mL)	Residual Activity (%)
25	89.68 ± 0.57
30	100 ± 6.55
35	90.87 ± 2.66

¹ Using titration of the rate of hydrolysis of α -N-benzoyl-L-arginine ethyl ester hydrochloride (BAEE) method.

The optimal conditions (a papain concentration of 30 mg/mL and a solvent-to-antisolvent ratio of 1:4) are further illustrated in Figure 7, showing the morphology of papain particles using Field Emission Scanning Electron Microscopy (FE-SEM). The FE-SEM images reveal that papain particles have a spherical shape, and aggregated papain does not exhibit distinct shapes, while the commercially purchased papain particle (unprocessed) produce crystals with irregular shapes. Figure 7b,c provide additional confirmation that antisolvent crystallization under optimal conditions results in the formation of nanocrystals [18]. Moreover, in comparison with the commercially purchased papain particle (unprocessed), antisolvent crystallization in this study demonstrates an improvement in crystal quality, as the obtained crystals exhibit a perfect spherical shape and retain their enzymatic activity. The use of nanosized spherical crystals with a high yield and preserved activity holds significant implications for practical applications in various industries, particularly in the food and pharmaceutical sectors. The nanosized spherical crystals can enhance the bioavailability, stability, shelf life, and controlled release properties of drug and food products. The high yield and preserved activity imply efficient resource utilization, potentially contributing to cost-effectiveness in production processes.

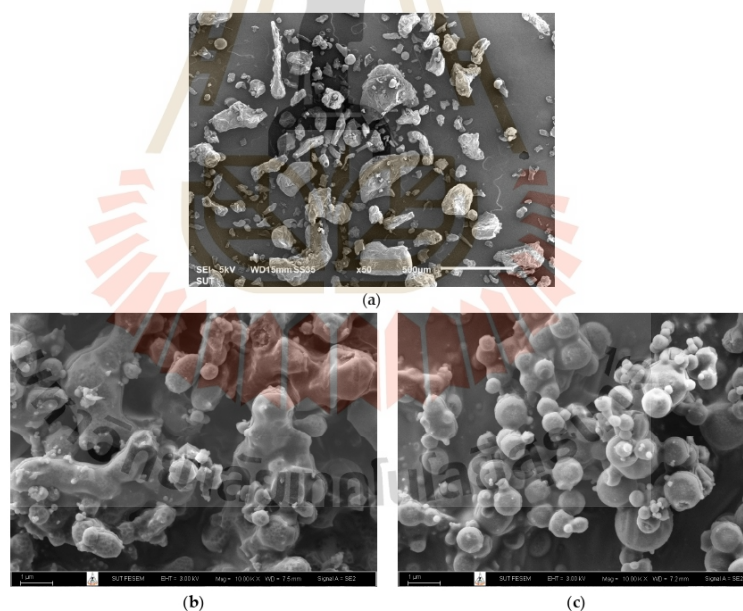


Figure 7. SEM photomicrographs of papain crystals under optimal conditions (papain 30 mg/mL, S:AS 1:4): (a) purchased papain particles (unprocessed), (b) papain aggregation obtained after antisolvent crystallization, and (c) papain nanocrystals obtained after antisolvent crystallization.

4. Conclusions

In this study, the impact of various parameters on the antisolvent crystallization process for preparing papain particles were explored. The different types of antisolvent, solvent-to-antisolvent (S:AS) volume ratios, and papain concentrations were investigated on the crystallization of papain. After careful examination, the optimal conditions were using ethanol as the antisolvent, maintaining an S:AS volume ratio of 1:4 and having a papain concentration of 30 mg/mL. Under these conditions, the precipitated papain was obtained without compromising its activity. The papain crystals obtained under the identified optimal conditions exhibited a spherical shape with an average size of 207.6 nm, and the crystallization yield was approximately 80%. These results underscore the significance of carefully choosing the right parameters in antisolvent crystallization to achieve the intended particle characteristics while preserving the functionality of the precipitated substances. In general, this research represents only the beginning of an itinerary required for papain crystallization for their validation as a potent tool before scaling-up and encapsulation studies.

Author Contributions: Conceptualization, S.B. and L.W.; methodology, S.B. and L.W.; investigation, S.B.; data curation, S.B. and L.W.; writing—original draft preparation, S.B.; writing—review and editing, S.B. and L.W.; visualization, S.B.; supervision, L.W.; project administration, L.W.; funding acquisition, L.W. All authors have read and agreed to the published version of the manuscript.

Funding: The authors acknowledge the research funding from the SUT Research and Development Fund, grant no. IRD7-706-63-12-21.

Data Availability Statement: The data presented in this study are available upon request from the corresponding author.

Acknowledgments: The authors thank the Suranaree University of Technology for providing equipment and facilities.

Conflicts of Interest: The authors declare no conflict of interest.

References

- El-Zalaki, E. Preparation and properties of papain precipitated from fresh latex of papaya fruits (*Carica papaya*). *Alex. J. Food Sci. Technol.* **2021**, *18*, 27–32. [[CrossRef](#)]
- Budama-Kilinc, Y.; Cakir-Koc, R.; Kecel-Gunduz, S.; Zorlu, T.; Kokcu, Y.; Bicak, B.; Karavelioglu, Z.; Ozel, A.E. Papain loaded poly(epsilon-caprolactone) nanoparticles: In-silico and in-vitro studies. *J. Fluoresc.* **2018**, *28*, 1127–1142. [[CrossRef](#)] [[PubMed](#)]
- Shouket, H.; Ameen, I.; Tursunov, O.; Kholikova, K.; Pirimov, O.; Kurbonov, N.; Ibragimov, I.; Mukimov, B. Study on industrial applications of papain: A succinct review. *IOP Conf. Ser. Earth Environ. Sci.* **2020**, *614*, 012171. [[CrossRef](#)]
- Moreira Filho, R.N.F.; Vasconcelos, N.F.; Andrade, F.K.; Rosa, M.F.; Vieira, R.S. Papain immobilized on alginate membrane for wound dressing application. *Colloids Surf. B Biointerfaces* **2020**, *194*, 111222. [[CrossRef](#)] [[PubMed](#)]
- Amri, E.; Mamboya, F. Papain, a plant enzyme of biological importance: A review. *Am. J. Biochem. Biotechnol.* **2012**, *8*, 99–104.
- dos Anjos, M.M.; da Silva, A.A.; de Pascoli, I.C.; Mikcha, J.M.G.; Machinski, M.; Peralta, R.M.; de Abreu Filho, B.A. Antibacterial activity of papain and bromelain on *Alicyclobacillus* spp. *Int. J. Food Microbiol.* **2016**, *216*, 121–126. [[CrossRef](#)] [[PubMed](#)]
- da Silva, C.R.; Oliveira, M.B.; Motta, E.S.; de Almeida, G.S.; Varanda, L.L.; de Padula, M.; Leitao, A.C.; Caldeira-de-Araujo, A. Genotoxic and cytotoxic safety evaluation of papain (*Carica papaya* L.) using in vitro assays. *J. Biomed. Biotech.* **2010**, *2010*, 197898.
- Muss, C.; Mosgoeller, W.; Endler, T. Papaya preparation (Caricol[®]) in digestive disorders. *Neuro Endocrinol. Lett.* **2013**, *34*, 38–46.
- Patel, A.; Cholkar, K.; Mitra, A.K. Recent developments in protein and peptide parenteral delivery approaches. *Ther. Deliv.* **2014**, *5*, 337–365. [[CrossRef](#)]
- Arisanti, C.I.S.; Rachmawati, H.; Pamudji, J.S.; Sumirtapura, Y.C. Chitosan reinforced alginate microcapsules retained the release of papain in simulated gastric fluid. *J. Pharm. Sci. Appl.* **2012**, *1*, 47–61.
- Chandran, S.P.; Nachimuthu, K.P.; Natarajan, S.B.; Inamdar, M.G.; Shahimi, M.S.B.M. Papain loaded solid lipid nanoparticles for colorectal cancer therapy. *Curr. Cancer Ther. Rev.* **2018**, *14*, 75–87. [[CrossRef](#)]
- Basu, S.K.; Govardhan, C.P.; Jung, C.W.; Margolin, A.L. Protein crystals for the delivery of biopharmaceuticals. *Expert Opin. Biol. Ther.* **2004**, *4*, 301–317. [[CrossRef](#)] [[PubMed](#)]
- Wang, G.D.; Mallet, F.P.; Ricard, F.; Heng, J.Y.Y. Pharmaceutical nanocrystals. *Curr. Opin. Chem. Eng.* **2012**, *1*, 102–107. [[CrossRef](#)]
- Hartje, L.F.; Snow, C.D. Protein crystal based materials for nanoscale applications in medicine and biotechnology. *Wiley Interdiscip. Rev. Nanomed. Nanobiotechnol.* **2019**, *11*, e1547. [[CrossRef](#)] [[PubMed](#)]
- Liu, H.; Zhao, Y.; Sun, J. Heterogeneous nucleation in protein crystallization. *Biomimetics* **2023**, *8*, 68. [[CrossRef](#)] [[PubMed](#)]

B.2 List of presentations

Sasitorn Boonkerd, and Lek Wantha (2024). Papain Crystallization and Encapsulation by Anti-Solvent Crystallization Method. **The 4th Thailand Biorefinery Symposium (TBioS-4)**, Khon Kaen, Thailand, June 13-14, 2024, organized by Faculty of Engineering, Khon Kaen University. (Oral presentation)

Sasitorn Boonkerd, and Lek Wantha (2023). Papain Nanoparticle Preparation using Anti-solvent Precipitation Method. **the 6th Asian Crystallization Technology Symposium (ACTS 2023) (Virtual conference)**, Taipei, Taiwan, September 25-26, 2023, organized by National Central University. (Oral presentation)

Sasitorn Boonkerd, and Lek Wantha (2023). Papain Precipitation and Encapsulation by Anti-Solvent Precipitation Method. **The 12th International Symposium on Nano & Supramolecular Chemistry (ISNSC-12) & The 3rd Thailand Biorefinery Symposium (TBioS-3)**, Chiang Mai, Thailand, July 23-26, 2023, organized by Faculty of Science and Technology, Thammasat University. (Oral presentation)

Sasitorn Boonkerd, and Lek Wantha (2023). Papain Precipitation by Anti-solvent. **The 32nd Thai Institute of Chemical Engineering and Applied Chemistry Conference (TICHE2023)**, Nakhon Pathom, Thailand, March 16-17, 2023, organized by The Thai Institute of Chemical Engineering and Applied Chemistry (TICHE) and the Department of Chemical Engineering, Silpakorn University. (Oral presentation)

BIOGRAPHY

Miss Sasitorn Boonkerd was born on July 17, 1998, in Phang Nga, Thailand. She completed her lower secondary education at Thapputwittaya School, Thapput, Phang Nga, in the academic year 2013. She then attended Deebuk Phangnga Wittayayon School, Muang Phang Nga, Phang Nga for her upper secondary education, finishing in the academic year 2016. She pursued a bachelor's degree in chemical engineering at Suranaree University of Technology and graduated in the academic year 2020 with second-class honors. Her undergraduate research focused on studying the properties of bagasse and separating charcoal residues from the burned bagasse. As part of her studies, she completed an internship at Stiebel Eltron Asia Co., Ltd. She continued her education by pursuing a master's degree in mechanical and process system engineering (chemical engineering) at Suranaree University of Technology, starting in 2021. During her master's research, she focused on enzyme encapsulation using modified starches produced in Thailand. Additionally, she has presented her research at various international conferences, delivering oral presentations at the 32nd Thai Institute of Chemical Engineering and Applied Chemistry Conference (TICHE2023), held on March 16-17, 2023 in Nakhon Pathom, Thailand, the 12th International Symposium on Nano & Supramolecular Chemistry (ISNSC-12) & the 3rd Thailand Biorefinery Symposium (TBioS-3) on July 23-25, 2023 in Chiang Mai, Thailand, the 6th Asian Crystallization Technology Symposium (ACTS 2023), a virtual conference on September 25-26, 2023, hosted from Taipei, Taiwan, and the 4th Thailand Biorefinery Symposium (TBioS-4), held on June 13-14, 2024 in Khon Kaen, Thailand. Furthermore, she was a teaching assistant, contributing to knowledge enhancement and research development.